Research Square

Preprints are preliminary reports that have not undergone peer review.
They should not be considered conclusive, used to inform clinical practice,
or referenced by the media as validated information.

Precision Limits of Hamiltonian Learning for Quantum Processors under Calibration Uncertainty

Yi Pan
University of Georgia https://orcid.org/0009-0001-2938-7646
Meng Hsiu Tsai
University of Tennessee at Chattanooga https://orcid.org/0009-0001-7752-0253
Hanqi Jiang
University of Georgia https://orcid.org/0009-0007-2778-959X
Junhao Chen
University of Georgia https://orcid.org/0009-0008-5888-129X
Wei Zhang
Augusta University https://orcid.org/0000-0001-6508-8144
Isaac Lyngaas
Oak Ridge National Laboratory https://orcid.org/0000-0002-1682-4309
Yingfeng Wang
yingfeng-wang@utc.edu
University of Tennessee at Chattanooga https://orcid.org/0000-0002-3715-5124
Tianming Liu
tliu@uga.edu
University of Georgia https://orcid.org/0000-0002-8132-9048

Research Article

Keywords:

Posted Date: November 12th, 2026

DOI: https://doi.org/10.21203/rs.3.rs-11695581/v1

License: This work is licensed under a Creative Commons Attribution 4.0 International License.
Read Full License

Additional Declarations: The authors declare no competing interests.

Precision Limits of Hamiltonian Learning for Quantum Processors under Calibration Uncertainty

Yi Pan,[1,*] Meng Hsiu Tsai,[2,*] Hanqi Jiang,[1,*] Junhao Chen,[1] Wei Zhang,[3] Isaac Lyngaas,[4] Yingfeng Wang,[2,†] and Tianming Liu[1,†]

[1] *School of Computing, University of Georgia, Athens, Georgia 30602, USA*
[2] *Department of Computer Science and Engineering, University of Tennessee at Chattanooga, Chattanooga, Tennessee 37403, USA*
[3] *School of Computer and Cyber Sciences, Augusta University, Augusta, Georgia 30912, USA*
[4] *National Center for Computational Sciences, Oak Ridge National Laboratory, Oak Ridge, Tennessee 37830, USA*

Learning the Hamiltonian of a quantum processor is important for controlling and certifying quantum devices, but the state preparation and measurement used to probe it are themselves imperfect. Even when exact data identify an interaction uniquely, identifiability alone does not determine finite-data precision. Here we show, for n-qubit Markovian dynamics under geometric regularity conditions, that the local uncertainty of a Hamiltonian coefficient scales either linearly or as the square root of the entrywise error in the generator matrix in the readout gauge. Square-root scaling occurs exactly when a gauge transformation moves the coefficient at first order while noise positivity can be restored at second order, and real noise correlations drive this first-order change. As a consequence, under suitable dynamical and readout conditions, square-root scaling forces uniformly valid confidence intervals from N shots to have expected length $\Omega(N^{-1/4})$, even for adaptive local experiments. Under a common generator norm bound, estimating this matrix attains this rate up to logarithmic factors. Experiments on three superconducting processors show that additional measurement bases increase the visibility of injected rotations at a matched number of shots. Whether a coupling admits the usual $N^{-1/2}$ scaling is therefore set by how noise correlations and positivity constrain its gauge directions.

I. INTRODUCTION

Much of the trust placed in quantum processors and simulators rests on knowing the dynamics they actually implement. Learning their Hamiltonian and noise is therefore a basic task in controlling, benchmarking, and certifying quantum devices [1–3]. Coherent couplings are a central example: they enable entangling operations [4–6], and when unwanted they produce crosstalk, which dedicated protocols aim to detect and characterize [7, 8]. Correlated errors induced by crosstalk are especially harmful to quantum error correction [8]. Estimating a coupling, however, requires separating its contribution to the measured dynamics from dissipation and calibration error, because state preparation and measurement (SPAM) are imperfectly calibrated. How precisely this separation can be made therefore affects both how accurately an interaction can be controlled or compensated and how many measurements a characterization experiment needs.

A wide range of learning methods addresses this task. Hamiltonian learning extracts couplings from eigenstate and thermal-state correlations, time traces, short-time and continuous measurements, or trusted quantum simulation [9–17], and reaches efficient or Heisenberg-limited estimation [18–21]. Lindblad generators are learned from steady states and from quench and digital-simulation records [22–24], and Pauli-noise learning characterizes structured and correlated noise [25–30]. However, these guarantees rest on calibration, control, and model assumptions. For instance, Lindblad tomography calibrates preparation and measurement with ideal fiducial rotations before fitting a positive Lindblad matrix [31], while other approaches use robust fitting, local time-series data, or observables that cancel SPAM errors [32–34]. When preparation and measurement are unknown, a prior question is which parameters the data determine at all.

Unknown SPAM thus makes coupling estimation a problem of physical identification as well as statistics. System identification determines which dynamical parameters can be inferred from given controls and observations [35, 36]. Self-consistent tomography estimates preparation, measurement, and gates together [37–39], operational representations express predictions through observable probabilities [40], and in Pauli-noise learning only gauge-invariant parameter combinations are learnable [41–43]. In particular, with trusted single-qubit controls, exact data leave a gauge freedom: gauge transformations that commute with these controls rescale the subspaces of fixed Pauli support without changing any outcome probability (Sec. II). Recently, Flammia, Sinha, and Tong showed that positivity can remove this freedom for a Hamiltonian coefficient at the positivity boundary of an n-qubit Lindbladian's Kossakowski matrix [44]. They asked how efficiently such boundary invariants can be learned, and how learning guarantees degrade away from the boundary. Exact identification, however, does not settle precision: with preparation and readout unknown within a prescribed error budget, finite data still permit nearby physical models with different values of a canonical Hamiltonian coefficient.

* These authors contributed equally to this work.
† Corresponding authors: yingfeng-wang@utc.edu; tliu@uga.edu.

What determines how rapidly this ambiguity shrinks as measurements become more precise?

Here, we answer this question by finding the gauge directions that change the target coefficient and asking how physical noise constrains them. The key observation is that near the positivity boundary, a gauge transformation can move the target at first order without changing the block on the reference kernel at first order. A second-order noise correction then restores positivity, so an error δ in the matrix elements of the generator admits target changes of order $\sqrt{\delta}$. Under geometric regularity conditions on the reference model, we prove that such a direction exists precisely when the target has square-root stability, and that its stability is otherwise linear (Sec. III). For these geometrically regular references, our dichotomy answers the question of Ref. [44] about learning near the positivity boundary quantitatively, in terms of local precision. In contrast, single-qubit coefficients are gauge invariant and have exactly linear stability at every reference. We derive a selection rule that traces square-root stability to real correlations between anticommuting Pauli fluctuations with different supports whose product is the target up to phase. Building on this rule, we construct physical models with this behavior on two qubits, on a pair embedded in a larger register, and for every many-body target $Z_1 \cdots Z_w$, $w \geq 3$, including zero reference coupling in the many-body case (Sec. IV).

The same geometry sets the statistical cost and guides measurement choice. Specifically, we show that square-root stability forces uniformly valid confidence intervals to have expected length $\Omega(N^{-1/4})$, including for adaptive experiments at arbitrary interrogation times, whenever the reference is mixing: unital, uniformly mixing under all allowed controls, and with outcome probabilities bounded below by a positive constant. Conversely, by estimating all matrix elements of the generator under a common norm bound, we attain this rate up to logarithmic factors and obtain expected length $\widetilde{O}(N^{-1/2})$ on the linear branch, where $\widetilde{O}$ suppresses logarithmic factors (Sec. V). While boundary constraints and singular information are known to change likelihood asymptotics [45–49], and continuity moduli govern the length of uniformly valid confidence intervals [50–52], here we find that positivity of the Kossakowski matrix and gauge freedom determine which rate applies. Finally, we show that measuring additional matrix elements that constrain this gauge direction changes the rate. In an explicit two-qubit family, four additional matrix elements detect a noise correlation absent from the original 23 and constrain the relevant gauge direction at unchanged diagonal noise strengths and Kossakowski rank. For fixed nonzero correlation η, they give expected length $\widetilde{O}(N^{-1/2})$ once the error in the matrix elements is at most of order η^2 in the reference rate units (Sec. VI). Moreover, for two-local generators these pair results are independent of register size when the summed norms of the terms acting on each qubit are bounded.

We test response selection on three superconducting quantum processors (Sec. VII). For nine neighboring pairs, our Ramsey experiments with the control prepared in $|0\rangle$ or $|1\rangle$ resolve kilohertz conditional frequency shifts while the target-qubit populations depend little on the control preparation, and the dependence of the fitted frequencies on processing shows why assigning a signal to a Hamiltonian coefficient also requires physical constraints. In experiments with injected rotations on three- and four-qubit registers, we find that additional measurement bases increase visibility at a matched number of shots and that, under the specified preparation and rotation model, signed responses recover the programmed angles across 66 estimates.

II. PHYSICAL MODEL AND INFERENCE PROBLEM

This section fixes the dynamics, the allowed experiments, and the notion of precision used throughout. We first define the canonical target and the experiment class, then identify what the measured data determine and how confidence intervals are assessed.

A. Canonical dynamics and experimental resources

We consider n qubits, $d = 2^n$, and use the canonical Gorini–Kossakowski–Sudarshan–Lindblad (GKSL) representation [53–55] in the unnormalized Hermitian Pauli basis P_a, $a \in \{I, X, Y, Z\}^n$:

$$\mathcal{L}(X) = -i[H, X] + \sum_{a,b \neq I} C_{ab} \left(P_a X P_b - \tfrac{1}{2}\{P_b P_a, X\} \right), \qquad (1)$$

$$H = \tfrac{1}{2} \sum_{a \neq I} h_a P_a, \qquad C = C^\dagger \succeq 0.$$

Throughout, we assume time-independent Markovian dynamics. The distinction from dynamics with memory is reviewed in Refs. [56, 57]. Identity jump labels are excluded and H is traceless. These conventions make H and the $(4^n - 1) \times (4^n - 1)$ Kossakowski matrix C unique, and we call its entries C_{ab} Kossakowski coefficients. The target is the canonical coefficient h_P of a fixed nonidentity Pauli label P in the effective Markovian generator, and on two qubits it is h_{ZZ}. Certifying h_{ZZ}, for instance, separates the coherent interaction, which unitary compensation can cancel, from dissipative contributions that also shift individual conditional-phase responses (Sec. II C). Other Hamiltonian coefficients and complex off-diagonal Kossakowski coefficients are allowed in the inference class.

We allow adaptive protocols with local control in which every shot starts from a new preparation. A shot prepares an ideal product state, passes it through a fixed unknown preparation channel A, evolves under $\mathcal{L}$ with any finite sequence of instantaneous trusted single-qubit unitaries, and passes through a fixed unknown readout channel B before an ideal rank-one projective product measurement.

Trusted single-qubit controls are also available immediately after the preparation channel and before the readout channel, and settings may depend on preceding shots. The experiment class excludes intermediate measurement or reset, coherent memory between shots, trusted entangling control, and environment measurement.

The SPAM channels obey the unhalved diamond-norm budget

$$\|A - \mathrm{id}\|_\diamond + \|B - \mathrm{id}\|_\diamond \le \varepsilon, \qquad 0 < \varepsilon < 1. \tag{2}$$

Both are completely positive and trace preserving (CPTP), and invertible as linear maps. Their inverses enter only algebraically. Bounds uniform in register size below keep this global budget ε fixed. The exact data are the complete set of exact outcome probabilities for the allowed experiments, including zero-duration calibration sequences. Note that equality of exact data is stronger than agreement of one Ramsey trace.

We use three model classes. The unrestricted class (U) contains every physical canonical generator, with arbitrary Hamiltonian and complex Kossakowski matrix, together with every pair of SPAM channels obeying Eq. (2). The product class (P) has the same generators and restricts A and B to tensor products over qubits. The two-local class (L2) has SPAM channels as in (U) and two-local generators, that is, sums of physical single- and two-qubit GKSL terms. In addition, upper bounds obtained from measurements impose a common norm bound admitting the reference and the constructed physical paths (Appendix C). Unless stated otherwise, results refer to class (U).

B. Observable responses and confidence intervals

Data from twirled experiments directly determine the generator G in the readout gauge. For a map $\mathcal{X}$ on dimension d, its transfer matrix is $X_{R,Q} = d^{-1}\,\mathrm{Tr}[R\mathcal{X}(Q)]$, and in particular L is the transfer matrix of $\mathcal{L}$. Independent physical twirling of preparation and readout by single-qubit Cliffords gives twirled SPAM channels $\bar{A}, \bar{B}$, which act as a scalar on each of the $2^n - 1$ subspaces of fixed nonempty Pauli support. Their gains a_Q, b_Q obey, with $l = 1 - \varepsilon$,

$$l \le a_Q, b_Q \le 1, \qquad q_Q = a_Q b_Q \ge l. \tag{3}$$

These data determine

$$T(t) = \bar{B} e^{tL} \bar{A}, \qquad G = T'(0)T(0)^{-1} = \bar{B} L \bar{B}^{-1}. \tag{4}$$

The $4^n \times 4^n$ matrix G is determined by the data, whereas L is the canonical physical generator. Two models give the same exact data exactly when they are related by a gauge transformation (SLS^{-1}, SA, BS^{-1}), as in gate-set tomography [38, 39] and Ref. [44]. Here S acts as a positive scalar on each subspace of fixed Pauli support and therefore commutes with the trusted single-qubit controls. For product SPAM channels these scalars factor over qubits. Appendix A proves the twirl, equivalence, and positivity statements.

For N shots and $0 < \alpha < 1$, an interval I_N is uniformly valid at confidence $1 - \alpha$ over a specified physical class if

$$\inf_{M} \Pr_{M}\{h_P(M) \in I_N\} \ge 1 - \alpha. \tag{5}$$

Our risk is the expected length at a specified reference, $\mathbb{E}_0|I_N|$. Coverage is uniform over the class, and all rates for confidence intervals below refer to this pointwise expected length. Finite-data analysis treats reference zeros as boundary points within the class in Eq. (5), which also includes nearby models with small positive rates. Table I collects the notation and standing assumptions.

Two sets of conditions recur below. A reference is *geometrically regular* (regular for short) if it satisfies the geometric conditions (i)–(iii) of Sec. III, and *mixing* if its generator is unital, every allowed controlled reference evolution of duration T contracts traceless operators in Hilbert–Schmidt norm by e^{-gT} for a common $g > 0$, and every outcome has reference probability at least a common $\mu > 0$ (Corollary 1). Rates refer to the shot number N at fixed n and reference, and $\widetilde{O}(\cdot)$ suppresses polylogarithmic factors in N.

C. From responses to physical attribution

A response frequency need not equal the canonical coupling. For commuting two-qubit dephasing with $H = (\omega_1 ZI + \omega_2 IZ + hZZ)/2$ and $C_{ZI,IZ} = a + ib$, half of the signed difference between the two conditional frequencies is $h - 2b$ for one choice of probe qubit and $h + 2b$ for the other. Their mean isolates h under that model, and correlated-dephasing spectroscopy exploits such relations [58]. Here, however, inference permits arbitrary complex Kossakowski matrices and fixed SPAM channels within the budget, so no such model-specific relation is available.

Positivity can identify the target despite the gauge freedom. For example, a Kossakowski diagonal supported entirely on local Pauli labels forces every other row to vanish and identifies the two-qubit interaction (Appendix A). Exact identification fixes the target for identical exact data. Local precision, in contrast, depends on how far the targets can differ when the data are close, and Section III turns this question into a criterion.

III. A CRITERION FOR LOCAL PRECISION

We first identify the gauge directions that limit precision, then express their target motion in terms of physical noise correlations.

TABLE I. Notation and standing assumptions. Upper bounds from finite-time measurements additionally use the applicable norm bound.

Symbol	Meaning
n; d; P	Number of qubits; $d = 2^n$; nonidentity target Pauli label
h_P; $h = h_{ZZ}$	Canonical Hamiltonian coefficient of P in $\mathcal{L}$, the inference target; its two-qubit case
C; $\ker C$	Canonical Kossakowski matrix, Eq. (1); its kernel
A, B; ε	Unknown SPAM channels; their diamond-norm budget, Eq. (2)
G; d_{23}, d_{27}; δ	Generator in the readout gauge, Eq. (4); two-qubit/pair maximum distance over the 15 nonidentity diagonal entries and both orientations of Eq. (13), or with Eq. (27) added; entrywise error in G
N; $1-\alpha$; I_N	Number of shots; confidence level; uniformly valid confidence interval, Eq. (5)
γ; γ_{tot}	Bound on the summed norms of the terms acting on each qubit (pair measurements); bound on the completely bounded norm of the Heisenberg generator $\mathcal{L}^\dagger$ (estimation of all entries of G)
h_0, λ, m, k	Reference coupling and Kossakowski coefficients, Eq. (14)
θ; q	Parameter of the gauge transformation S_θ; strength of the depolarizing noise added to restore positivity
η	Reference correlation $C_{IX,YZ}$ of Sec. VI
ψ	Programmed angle of injected rotations (Sec. VII)
Assumption	**Content**
Experiment class	Adaptive shots, each with a new product preparation, rank-one projective product measurement, and trusted single-qubit unitaries at arbitrary times; settings may adapt to earlier outcomes
Model classes	(U) canonical generators with complex Kossakowski matrix and fixed physical SPAM channels obeying Eq. (2); (P) the same with product SPAM channels; (L2) sums of physical single- and two-qubit terms
Coverage and risk	Coverage uniform over the model class; expected length at a specified reference
Geometrically regular; mixing	Conditions (i)–(iii) of Sec. III; unital reference, uniform mixing under allowed controls, and outcome probabilities bounded below (Corollary 1)
Rates	In N at fixed n and reference; $\widetilde{O}$ suppresses polylogarithmic factors

A. A local precision dichotomy

The precision law is governed by how gauge directions meet the kernel of the Kossakowski matrix. To make this precise, fix a reference $M_0 = (L_0, A_0, B_0)$ with canonical Kossakowski matrix C_0, target $h_{P,0}$ and generator $G_0 = \bar{B}_0 L_0 \bar{B}_0^{-1}$ in the readout gauge. For $x \in \mathbb{R}^{2^n-1}$, indexed by the nonempty qubit supports s, let $W(x)$ multiply every Pauli coordinate of support s by x_s and annihilate I. The gauge transformation $S_x = e^{W(x)}$ multiplies these coordinates by e^{x_s} and commutes with all single-qubit controls.

We now expand the canonical Hamiltonian and Kossakowski coefficients along these gauge transformations. Directions with $[W(x), L_0] = 0$ leave L_0 unchanged, and we work on a fixed complement V of them with the norm $|x| = \max_s |x_s|$. Let $\widetilde{C}(x)$ and $\widetilde{h}_P(x)$ be the canonical Kossakowski matrix and target of $S_x L_0 S_x^{-1}$, and let Π project onto $\ker C_0$. Write $\widetilde{C}(x) = C_0 + C_1(x) + C_2(x) + O(|x|^3)$, with C_1 linear and C_2 quadratic, and let $\ell_P(x)$ be the first-order target change. The kernel block $D(x) = \Pi C_1(x) \Pi$ is linear in x, and the decisive conditions are

$$D(x) = 0, \qquad \ell_P(x) \neq 0. \tag{6}$$

To state the second-order condition, define

$$\begin{aligned} \mathcal{B}(x) &= (I - \Pi) C_1(x) \Pi, \\ Q_2(x) &= \Pi C_2(x) \Pi - \mathcal{B}(x)^\dagger C_0^+ \mathcal{B}(x). \end{aligned} \tag{7}$$

where C_0^+ is the inverse on the range of C_0, extended by zero on the kernel. We call a reference (L_0, A_0, B_0) geometrically regular, or regular for short, if:

(i) When Eq. (6) has a solution, it has a solution $u \in V$ with $|u| = 1$ and a representative $\hat{u}$, differing from u by a direction that leaves L_0 unchanged, such that $S_{\theta\hat{u}} A_0$ and $B_0 S_{\theta\hat{u}}^{-1}$ form an admissible pair for $0 \leq \theta \leq \theta_{\mathrm{adm}}$, $\theta_{\mathrm{adm}} > 0$.

(ii) L_0 is the only physical generator of the form $S L_0 S^{-1}$ with S a gauge transformation whose scalars on the subspaces of fixed Pauli support lie in $[l, l^{-1}]$.

(iii) $D(x) \succeq 0$ only when $D(x) = 0$, and every unit $u \in \ker D$ satisfies

$$\sup_{v \in V} \lambda_{\min}[D(v) + Q_2(u)] < 0, \tag{8}$$

with eigenvalues taken on $\ker C_0$.

Each condition has a direct physical meaning. First, condition (i) permits the gauge transformation within the SPAM budget. Second, condition (ii) isolates the

entire generator, a stronger property than uniqueness of h_P, and it confines nearby compatible generators to the local geometry. Finally, in (iii), v allows a curved path $x = \theta u + \theta^2 v$: even after this adjustment, positivity is lost at second order. In particular, when the kernel is spanned by Pauli labels, the first part of (iii) is automatic, and the second follows if $\mathcal{B}(u) \neq 0$ for every nonzero $u \in \ker D$ (Appendix D). The following theorem shows that, at regular references, the linear system $D(x) = 0$ and the derivative ℓ_P decide the precision law, and we prove it in Appendix D.

Theorem 1 (Local precision dichotomy)**.** *Let $P \neq I$ and let the reference be regular in class (U). Let $\omega_P(\delta)$ be the supremum of $|h_P(M) - h_{P,0}|$ over models M of the class with $\|G_M - G_0\|_{\max} \leq \delta$, where $\|X\|_{\max} = \max_{R,Q} |X_{R,Q}|$. Then, as $\delta \to 0$, $\omega_P(\delta) = \Theta(\sqrt{\delta})$ if Eq. (6) has a solution, and $\omega_P(\delta) = \Theta(\delta)$ otherwise, with constants depending on the reference and ε. Always $\omega_P(\delta) \geq l\delta$; in the first case, for the witness u of (i),*

$$\omega_P(\delta) \geq \frac{|\ell_P(u)|}{2^{n+1}\sqrt{\Lambda}}\sqrt{\delta}, \qquad 0 < \delta \leq 4^n \Lambda \theta_*^2, \tag{9}$$

with $\Lambda \geq 1$ and $\theta_* > 0$ given in Appendix D. The same conclusions hold in class (P), with x restricted to additive directions $x_s = \sum_{j \in s} y_j$ and conditions (i)–(iii) read on that subspace.

In words, a regular reference has square-root stability exactly when some gauge direction moves the target at first order without a first-order change in the kernel block. The Schur complement explains the two rates (Appendix D). Specifically, along a direction in $\ker D$, a change of size θ leaves the kernel block unchanged at first order, but coupling $\ker C_0$ to the range of C_0 can produce a negative eigenvalue at order θ^2. Adding positive noise of that same order restores a physical generator. The accompanying change of the SPAM channels compensates the gauge transformation, leaving an observable discrepancy of order θ^2 while the target changes by $\theta \ell_P(u) + O(\theta^2)$. Thus an entrywise error δ in G permits target changes of order $\sqrt{\delta}$. Conversely, if ℓ_P vanishes on $\ker D$, the target has no first-order motion along directions requiring a second-order correction, and its variation is instead bounded by order δ. In practice, this gives a concrete use of the criterion: determine $\ker C_0$, solve the linear system $D(x) = 0$, and evaluate the target derivative on its solutions. The global isolation and second-order conditions certify that this local test controls the full physical neighborhood. Single-qubit targets need none of these conditions.

Proposition 1 (Single-qubit targets)**.** *If P has weight one, then $\omega_P(\delta) = \delta$ for every $\delta \geq 0$ at every reference in class (U) or (P).*

For a single-qubit label, every Pauli pair coupled by the commutator with P joins two Pauli coordinates with the same support, so h_P is read directly from G, and the perturbation $L_0 + \delta A_P$, with A_P the transfer matrix of $-i[P/2, \cdot]$, attains the bound (Appendix D).

B. Which noise correlations move the target

Theorem 1 reduces the precision law to the linear functional ℓ_P, and a single family of noise correlations determines it. Call an unordered pair $\{a, b\}$ of nonidentity labels a P-pair if $P_a P_b = i\tau_{ab} P$ with $\tau_{ab} = \pm 1$. Its labels anticommute, and there are 4^{n-1} such pairs. For $S \subseteq [n]$, define the signed sum of real Kossakowski coefficients

$$\Upsilon_S^P = \sum_{\operatorname{supp} b = S} \tau_{ab} \operatorname{Re} C_{ab} - \sum_{\operatorname{supp} a = S} \tau_{ab} \operatorname{Re} C_{ab}, \tag{10}$$

with both sums over P-pairs, each counted once. Exchanging a and b reverses τ_{ab} and the two sums, so Υ^P does not depend on the orientation. The active pairs of P are the 4^{n-1} unordered pairs $\{Q, R\}$ of Pauli labels with $\{P_Q, P\} = 0$ and $P_R \propto P P_Q$. We orient each by $(A_P)_{R,Q} = +1$, where A_P is the transfer matrix of $-i[P/2, \cdot]$, and write $M_{RQ} = [(L_0)_{R,Q} + (L_0)_{Q,R}]/2$ for its symmetric part. The following proposition expresses ℓ_P through these sums and is proved in Appendix E.

Proposition 2 (Noise correlations and the target derivative)**.** *Let $P \neq I$, and let L_0 be a canonical generator with arbitrary Hamiltonian and complex Kossakowski matrix C, allowing nonunital dynamics. With $w_Q = x_{\operatorname{supp} Q}$, $x_\varnothing = 0$, and $\widehat{w}(S) = \sum_{s \neq \varnothing} x_s 3^{|s \setminus S|} (-1)^{|s \cap S|}$,*

$$\ell_P(x) = \frac{4}{d^2} \sum_{\{Q,R\}} (w_R - w_Q) M_{RQ} = \frac{4}{d^2} \sum_{S \subseteq [n]} \Upsilon_S^P \, \widehat{w}(S). \tag{11}$$

(i) ℓ_P vanishes identically on $\mathbb{R}^{2^n - 1}$ if and only if $\Upsilon^P = 0$.
(ii) On additive directions $x_s = \sum_{j \in s} y_j$, $\ell_P = \sum_j y_j \Upsilon_j^P$ with $\Upsilon_j^P = -\Upsilon_{\{j\}}^P$. If $\operatorname{wt} P \geq 2$, then Υ_j^P is the sum of $\tau_{ab} \operatorname{Re} C_{ab}$ over the P-pairs oriented so that a acts on qubit j alone, and each such partner b has support $\operatorname{supp} P$.
(iii) For $n = 2$ and $P = ZZ$, the P-pairs are (XI, YZ), (YI, XZ), (IX, ZY), (IY, ZX) with $\tau = (1, -1, 1, -1)$, and Eq. (11) becomes Eq. (12); in particular $\Upsilon_1^{ZZ} = U_1 - U_2$ and $\Upsilon_2^{ZZ} = U_3 - U_4$.

Equation (11) is a selection rule: only the signed sums of real Kossakowski coefficients between different supports change the target to first order. In particular, coherent couplings, imaginary Kossakowski coefficients, correlations with another product, and correlations within one support contribute no such motion. Hence, single-qubit targets have no eligible pair. For product gauge transformations, which act independently on each qubit, these sums reduce to one signed sum of Kossakowski coefficients per qubit.

However, at a regular reference, the branch is decided by the restriction of ℓ_P to $\ker D$. Eligible correlations

can cancel there, so their presence alone does not imply square-root stability. The explicit constructions of Sec. IV supply directions on which this restriction is nonzero. For two qubits, the target derivative takes the form

$$\ell(W) = (U_3 - U_4)\,\dot{\alpha}_g + (U_1 - U_2)\,\dot{\beta}_g, \tag{12}$$

with $U_1, \ldots, U_4$ the real Kossakowski coefficients on (XI, YZ), (YI, XZ), (IX, ZY), (IY, ZX) and $\dot{\alpha}_g, \dot{\beta}_g$ the rates of the coordinates of Eq. (15). Thus, the coupling moves to first order only if noise correlates a local transverse fluctuation with a conditional one in a different quadrature.

IV. PHYSICAL REALIZATIONS

We now show that the square-root branch occurs in physical noise models. Section IV A constructs regular references for targets of every weight at least three, and Sec. IV B gives a two-qubit reference with explicit constants and matching statistical bounds.

A. Many-body interactions

The selection rule picks a correlation between X_1 and $Y_1 Z_2 \cdots Z_w$, coupling a local fluctuation to one spanning the target support.

Proposition 3 (Many-body reference)**.** *Let $n \geq w \geq 3$, $P = Z_1 \cdots Z_w$, $a = X_1$, and $b = Y_1 Z_2 \cdots Z_w$. Let $H_0 = hP/2$, with $h \in \mathbb{R}$, and let C_0 have diagonal $\lambda > 0$ on each single-qubit label, diagonal $m_0 > 0$ on b, and $C_{ab} = C_{ba} = k \neq 0$, where $\lambda m_0 > k^2$; all other entries vanish. For $A_0 = B_0 = \mathcal{D}_r^{(1)} \otimes \mathrm{id}$, $r = 1 - \varepsilon/3$, the reference is regular in class (U) for every real h, and*

$$\omega_P(\delta) = \Theta(\sqrt{\delta}) \qquad (\delta \downarrow 0).$$

Here $\mathcal{D}_r^{(1)}(X) = rX + (1-r)\,\mathrm{Tr}(X)I/2$ acts on qubit 1. The direction $q_s = \mathbf{1}\{1 \in s\}$ satisfies $D(q) = 0$ and $\ell_P(q) = k$.

Here the target itself acts on w qubits, and the correlated noise spans those same qubits. The two selected labels obey $P_a P_b = iP$: a local transverse fluctuation and a conditional transverse fluctuation therefore contribute to precisely the Hamiltonian sector being inferred. The inequality $\lambda m_0 > k^2$ makes their Kossakowski block positive definite. Because the entire Kossakowski matrix is real and positive semidefinite, its spectral factors give Hermitian Lindblad jump operators, so the correlation is part of a physical Markovian noise model.

Physically, the gauge direction q rescales every Pauli coordinate that involves qubit 1. Its target derivative is k, so the amount and sign of the initial target motion are set directly by the noise correlation. The depolarizing SPAM channels on that qubit provide room for the compensating change, while $\ker C_0$ makes the required positive correction quadratic. The kernel of C_0 and conditions (i) and (ii) are proved in Appendix F. The construction remains regular at $h = 0$: along q, the derivative of the Kossakowski coefficient $\widetilde{C}_{Z_1, Z_2 \cdots Z_w}$ is $ik/2$, independent of h. Since $w \geq 3$, $Z_2 \cdots Z_w$ lies in $\ker C_0$ while Z_1 lies in its range. Hence, their nonzero first-order coupling supplies the second-order positivity cost even when the coherent reference interaction vanishes. Moreover, when these references are also mixing, Corollary 1 converts their square-root moduli into lower bounds $\Omega(N^{-1/4})$ on the expected confidence-interval length for adaptive experiments.

B. An explicit pair and 23 matrix elements

A two-qubit reference realizes the square-root branch with an explicit physical path and a matching upper bound from 23 matrix elements of G. We first specify the reference and show that the exact data identify its coupling, then state the resulting bounds on confidence-interval length and construct the path behind them. For the two-qubit target, the finite-precision upper bound uses 23 entries of G: the 15 nonidentity diagonal entries and both orientations of

$$(R_i, Q_i) = (YZ, XI), (XZ, YI), (ZY, IX), (ZX, IY). \tag{13}$$

Write $d_{23}(G, G_0)$ for their maximum absolute difference. The diagonal entries recover all 15 diagonal Kossakowski coefficients, and the entries with exchanged indices constrain the target Hamiltonian coefficient. These 23 entries support the upper bound. In contrast, the lower bound is established for the complete exact data, so it applies to experiments beyond these entries.

We now specify the reference. On two qubits, set $h_0 = 1/10$ and $H_0 = h_0 ZZ/2$. The Kossakowski matrix has diagonal $\lambda = 1/10$ on all six single-qubit labels, diagonal $m = 1/50$ on YZ, and a single real off-diagonal pair

$$(C_0)_{XI,YZ} = (C_0)_{YZ,XI} = k = 1/100. \tag{14}$$

All other entries vanish, so C_0 has rank seven and a positive definite nonzero block. Rates in this reference family use a fixed inverse-time unit, and times use its reciprocal. The real off-diagonal entry describes correlated XI and YZ Hamiltonian fluctuations, while inference still permits complex alternatives. Set $A_0 = B_0 = \mathcal{D}_r = r\mathrm{id} + (1-r)\mathcal{D}$, where $\mathcal{D}(X) = \mathrm{Tr}(X)I/4$ and $r = 1 - \varepsilon/8$. These SPAM channels use at most $\varepsilon/2$ of the diamond-norm budget. Exact identification follows from positivity. An exactly compatible generator is SL_0S^{-1}, with positive scalars s_1, s_2, s_{12} on the subspaces of fixed Pauli support. For $\alpha_g = \log(s_{12}/s_1)$ and $\beta_g = \log(s_{12}/s_2)$, its gauge-

invariant diagonal Kossakowski coefficients and canonical decomposition give

$$\begin{aligned} \widetilde{h} &= \tfrac{h_0}{2}(\cosh\alpha_g + \cosh\beta_g) + k\sinh\beta_g, \\ \operatorname{Im}\widetilde{C}_{XX,YY} &= -\tfrac{k}{2}\sinh\alpha_g, \\ \operatorname{Re}\widetilde{C}_{YI,XZ} &= \tfrac{k}{2}(\cosh\alpha_g - \cosh\beta_g) - \tfrac{h_0}{4}\sinh\beta_g. \end{aligned} \tag{15}$$

Positivity forces rows with zero diagonal to vanish, hence $\alpha_g = \beta_g = 0$ since $h_0 > 2k$. Thus $\widetilde{h} = h_0$ (Appendix G).

Theorem 2 (Confidence-interval length at an identifiable reference)**.** *For the reference in Eq. (14), fixed $0 < \varepsilon < 1$, and the experiment class of Sec. II, the exact data identify $h_{ZZ} = h_0$. Nevertheless, for every adaptive protocol and every interval uniformly valid over the surrounding physical class,*

$$\mathbb{E}_0|I_N| \geq \frac{3/4 - 2\alpha}{200}\min\left\{\frac{\varepsilon}{100}, (8K_{\mathrm{stat}}N)^{-1/4}\right\}, \tag{16}$$

where $0 < \alpha < 3/8$ and $K_{\mathrm{stat}} = 26.2144/\varepsilon$. Under a common norm bound that admits this reference and its constructed neighborhood, a uniformly valid procedure has

$$\mathbb{E}_0|I_N| = O_{\varepsilon,\gamma,\alpha}\left(N^{-1/4}(\log N)^{5/4}\right). \tag{17}$$

Here γ is the local norm bound of Table I, with the operator-norm convention of Appendix C; it controls response derivatives and the target range when simultaneous estimation fails. These are pointwise bounds on the expected length at the identifiable reference.

Thus, exact identification does not protect precision: the exact data fix h_{ZZ}, yet the expected lengths of uniformly valid intervals cannot shrink faster than $N^{-1/4}$ at this reference, and under a common norm bound this rate is attained up to logarithmic factors.

We build the path from a gauge transformation followed by added depolarizing noise that restores positivity [Fig. 1(a)]. Let S_θ multiply only IX, IY, IZ by e^θ and leave the other Pauli labels fixed. Its compensated generator is

$$L_\theta = S_\theta L_0 S_\theta^{-1} + 16q_\theta(\mathcal{D} - \mathrm{id}), \qquad q_\theta = 0.01\theta^2. \tag{18}$$

The target is

$$h_\theta = \frac{1+\cosh\theta}{20} - \frac{\sinh\theta}{100} = h_0 - k\theta + O(\theta^2). \tag{19}$$

The gauge transformation couples the range of C_0 to its kernel, producing a negative eigenvalue $-h_0^2\theta^2/(16\lambda) + O(\theta^3)$. The positive correction $q_\theta I_{15}$ restores positivity for both signs throughout $|\theta| \leq 0.01$ (Appendix G). Complete positivity is also imposed on the actual SPAM channels,

$$A_\theta = S_\theta\mathcal{D}_r, \qquad B_\theta = \mathcal{D}_r S_\theta^{-1}. \tag{20}$$

For $|\theta| \leq \varepsilon/100$, these are fixed physical channels obeying the budget, and their product $\mathcal{D}_r^2$ leaves zero-time calibration unchanged.

Along this path, the target moves linearly while the data change only quadratically [Fig. 1(b)]. After SPAM compensation, the only observational change in Eq. (18) is the added global depolarization. Moreover, it commutes with every allowed local control and with the unital reference evolution. For any controlled sequence of total duration T, its complete observed channel therefore obeys

$$\mathcal{R}_\theta = \mathcal{D}_r\mathcal{P}_0\mathcal{D}_{e^{-16q_\theta T}}\mathcal{D}_r, \tag{21}$$

where $\mathcal{P}_0$ is the corresponding controlled reference evolution. Local Pauli noise gives a controlled Hilbert–Schmidt mixing rate at least $1/5$. Together with the factor $Te^{-T/5}$, it bounds every outcome change uniformly in duration and controls:

$$|p_\theta - p_0| \leq 32K\theta^2, \qquad K = 0.01. \tag{22}$$

Finally, the positive lower bound $\varepsilon/64$ on outcome probabilities yields per-shot relative entropy at most $K_{\mathrm{stat}}\theta^4$, and the adaptive chain rule (Appendix B) gives $NK_{\mathrm{stat}}\theta^4$. Taking $\theta \propto N^{-1/4}$ keeps the data close while separating their targets, proving Eq. (16) (Appendix H).

For the upper bound, the 23 matrix elements give a matching local statement:

$$\sup_{M:\, d_{23}(G_M, G_0)\leq\delta} |h(M) - h_0| = \Theta_\varepsilon(\sqrt{\delta}) \quad (\delta \downarrow 0). \tag{23}$$

For the lower side, Eq. (21) implies exactly $G_\theta - G_0 = -16K\theta^2\Pi_0$, where $\Pi_0 = \mathrm{id} - \mathcal{D}$, while the target moves linearly. For the upper side, recovering C_{aa} from the diagonal entries of G bounds each formerly zero diagonal coefficient by δ. Positivity then bounds its off-diagonal Kossakowski coefficient with a single-qubit label of nonzero diagonal by $\sqrt{(0.1+\delta)\delta}$. Entries with exchanged indices constrain the two unknown readout gain ratios and hence the canonical target. Appendix I derives explicit inequalities over the stated class with complex Kossakowski matrices. Finite-time measurements (Sec. V) estimate these entries with simultaneous error $\widetilde{O}(N^{-1/2})$, and the smallest interval containing all compatible targets then yields Eq. (17).

A noise prior, moreover, can change precision, as Fig. 1(c) shows. Requiring only $\operatorname{Im} C_{ZI,IZ} = 0$ in every candidate already restores a linear modulus (Appendix J), so a wholly real Kossakowski matrix is sufficient. Indeed, the reference's real correlation moves the target to first order, while the allowed imaginary Kossakowski coefficients in the alternatives let that motion remain hidden to first order.

Remark 1 (Zero reference coupling). Keeping the same Kossakowski matrix and SPAM channels but setting $h_0 = 0$ preserves exact identification. Along S_θ, however, the target is $-k\sinh\theta$ and the positivity defect is $-k^2\theta^4/(16\lambda) + O(\theta^6)$. This gives lower bounds $\omega_{ZZ}(\delta) = \Omega(\delta^{1/4})$ and $\mathbb{E}_0|I_N| = \Omega(N^{-1/8})$ for uniformly valid intervals with $0 < \alpha < 1/2$ (Appendix G 4). The second-order condition fails here; the many-body references of Proposition 3 remain regular at zero coupling.

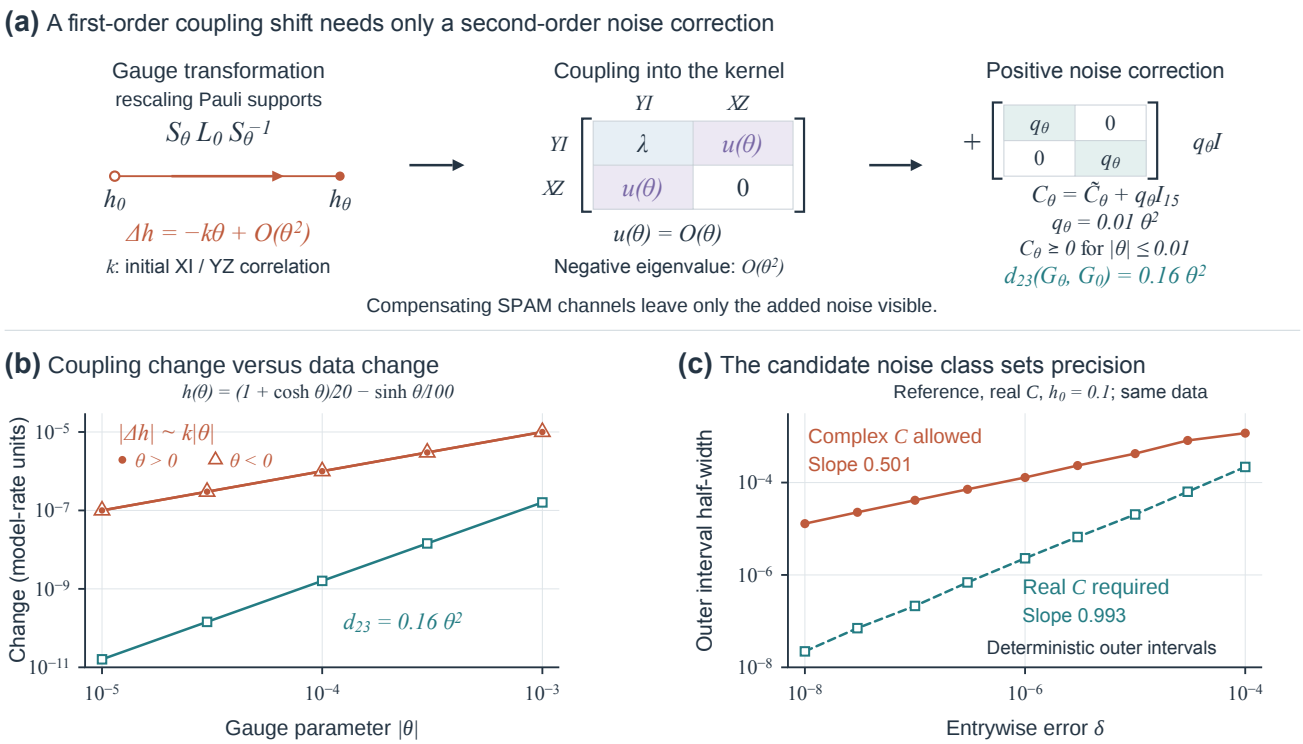


FIG. 1. Physical origin of square-root local uncertainty at the two-qubit reference. (a) A gauge transformation changes the canonical coupling at first order and couples the range and kernel of C_0. Adding $q_\theta I_{15}$, with $q_\theta = 0.01\theta^2$, restores positivity of C for $|\theta| \leq 0.01$. With compensating physical SPAM channels in the admissible range $|\theta| \leq \varepsilon/100$, the maximum entrywise difference is $d_{23}(G_\theta, G_0) = 0.16\theta^2$. (b) Changes of the coupling and of the data for $\varepsilon = 0.1$ along both signs of the physical path. Filled circles and open triangles denote positive and negative θ, respectively. The coupling branches nearly coincide at this scale. (c) Half-widths of deterministic outer intervals for the same reference and data, with candidates allowed complex Kossakowski matrices or constrained to real ones. The fitted logarithmic slopes are 0.501 and 0.993, respectively. Appendix M 3 documents the calculations.

These constructions fix the local geometry of the square-root branch, and Section V turns it into statistical rates at general references.

V. STATISTICAL BOUNDS AND MEASUREMENT PROCEDURES

The stability criterion determines statistical precision through two arguments. A physical path bounds the information available to any allowed protocol, and estimating the required entries of G gives a confidence interval.

A. A lower bound for adaptive experiments

To convert Theorem 1 from entrywise errors in G into a bound in terms of the number of shots, the added noise along the witness path must remain hard to detect for every allowed protocol, including adaptive ones. The following corollary shows that this holds at mixing references.

Corollary 1 (Expected confidence-interval length)**.** *In the first case of Theorem 1, let L_0 be unital, let every allowed controlled reference evolution of duration T contract traceless operators in Hilbert–Schmidt norm by e^{-gT}, $g > 0$, and let every outcome have reference probability at least $\mu > 0$. Then for $0 < \alpha < 1/2$, $\tau = (1 - 2\alpha)/2$ and*

$$\beta_n = \frac{4^n \Lambda \|B_0\|_{2\to 2}\sqrt{1 - 2^{-n}}}{eg},$$
$$\theta_N = \min\left\{\theta_*, \sqrt{\frac{\mu}{2\beta_n}}, \left(\frac{\tau^2\mu}{\beta_n^2 N}\right)^{1/4}\right\}, \tag{24}$$

every interval uniformly valid at level $1 - \alpha$ over a class containing the witness path of Appendix D obeys $\mathbb{E}_0|I_N| \geq (1 - 2\alpha)|\ell_P(u)|\theta_N/4 = \Omega(N^{-1/4})$ under adaptive experiments.

Unitality lets the added depolarizing noise commute through the controlled evolution, and mixing bounds its effect uniformly in duration. The lower bound on outcome probabilities then gives per-shot relative entropy of order θ^4 for target separation of order θ. The adaptive chain rule produces the $N^{-1/4}$ scale (Appendix D).

B. Estimating the generator and confidence-interval length

For the matching upper bound, we estimate the generator directly. We obtain bounded response estimators from SPAM twirling, product preparations, and local measurements. We estimate entries of G by polynomial differentiation and zero-time normalization. Under a known bound γ_{tot} on the completely bounded norm of the Heisenberg generator $\mathcal{L}^\dagger$, we estimate $4^n(4^n-1)$ potentially nonzero entries of G and 4^n-1 calibration quantities, for $K_n = 16^n - 1$ estimated means in total. At fixed n, these estimates have simultaneous error

$$\delta_N = O_{\varepsilon,\gamma_{\mathrm{tot}},\alpha,n}\Big(N^{-1/2}(\log N)^{5/2}\Big). \tag{25}$$

The norm bound controls differentiation bias and the target range when simultaneous estimation fails, and Hoeffding concentration controls sampling error [59]. Note that all measurements count toward N.

The smallest interval containing all target values compatible with these estimates satisfies

$$\mathbb{E}_0|I_N| \le 2\omega_P(2\delta_N) + 2\gamma_{\mathrm{tot}}\zeta_N, \qquad \zeta_N = \min\{\alpha, N^{-1}\}, \tag{26}$$

where ω_P is the full-G modulus of Theorem 1. Corollary 3 in Appendix C proves coverage and bounds the contribution when simultaneous estimation fails. Therefore, the square-root and linear branches give expected lengths $O(N^{-1/4}(\log N)^{5/4})$ and $O(N^{-1/2}(\log N)^{5/2})$. In particular, at mixing references, the square-root upper bound matches the lower exponent of Corollary 1 for any common model class that satisfies the norm bound and contains the constructed physical path.

C. Measuring a pair inside a larger register

We next embed the explicit pair in a larger register, where the same bounds on confidence-interval length hold at the lifted reference. Appendix L embeds the reference on a pair A of n qubits, with arbitrary single- and two-qubit dynamics on the spectators E and SPAM channels $\mathcal{D}_r \otimes A_{\mathsf{E}}$, $\mathcal{D}_r \otimes B_{\mathsf{E}}$, where $r = 1 - \varepsilon_{\mathsf{A}}/8$ and $\|A_{\mathsf{E}} - \mathrm{id}\|_\diamond + \|B_{\mathsf{E}} - \mathrm{id}\|_\diamond \le \varepsilon - \varepsilon_{\mathsf{A}}$.

Corollary 2 (Lift to n qubits)**.** *Fix $n \ge 2$ and $0 < \varepsilon_{\mathsf{A}} \le \varepsilon < 1$, and let $\mathfrak{M}^{\mathrm{L2}}_\varepsilon$ be the n-qubit models with SPAM budget ε whose generators are sums of physical single- and two-qubit terms. At the lifted reference, the 23 pair entries of G identify $h_{ZZ\otimes I_{\mathsf{E}}} = h_0$ over $\mathfrak{M}^{\mathrm{L2}}_\varepsilon$. Every adaptive protocol and every interval uniformly valid over a class containing the lifted reference and its physical path obey Eq. (16) with ε replaced by ε_{A}. Under an n-independent bound γ on the summed norms of the terms acting on each qubit that admits the lifted reference and its path, for instance any $\gamma \ge 6$ that bounds the spectator terms, a uniformly valid procedure over the class satisfying this norm bound attains Eq. (17). All constants are independent of n; for $n = 2$ and $\varepsilon_{\mathsf{A}} = \varepsilon$, this is Theorem 2.*

For two-local generators, the canonical coefficient of the reduced pair generator equals the global coefficient $h_{ZZ\otimes I_{\mathsf{E}}}$. The 23 derivatives and 15 calibrations, or 27 derivatives for Sec. VI, can then be estimated with constants independent of n under this local norm bound γ (Appendix L). In addition, preparing and randomizing the spectator qubits uses $O(n)$ local operations per shot. The interval-length bound uses the modulus for the measured metric, d_{23} or d_{27}, and the contribution when simultaneous estimation fails is at most $4\gamma\zeta_N$. For computation, Appendix M constructs outer intervals from necessary physical constraints and proves that they contain every compatible target whenever simultaneous estimation succeeds. Finally, known systematic and timing errors add to the error bound on the entries of G (Appendix C).

VI. FOUR MATRIX ELEMENTS THAT IMPROVE PRECISION

Having shown that the 23 matrix elements leave a square-root modulus, we now ask which additional matrix elements of G restore linear precision at nonzero reference correlation. We answer it with a second noise correlation that fixes the relevant gauge direction [Fig. 2(a)]. To this end, we add a real Kossakowski coefficient $(C_\eta)_{IX,YZ} = (C_\eta)_{YZ,IX} = \eta$ to Eq. (14), with $|\eta| \le 0.01$. The reference remains rank seven, with exactly the same diagonal profile and ZZ Hamiltonian. Its 23 matrix elements are identical for every η, because the new dissipator couples Pauli labels whose product is proportional to YY, although higher-order finite-time responses may distinguish these references. Here η indexes the reference models, whereas inference uses the full surrounding class with complex Kossakowski matrices and unknown SPAM channels. We then add four ordered entries,

$$(YZ, IX),\ (IX, YZ),\ (YX, IZ),\ (IZ, YX), \tag{27}$$

and write d_{27} for the maximum distance over all 27 entries. Unlike the original 23 entries, these four shift with η [Fig. 2(b)]. These entries are measured with product preparations, local rotations and readout, signed parity processing, and zero-time normalization (Sec. V).

The key step is that a combination of these four entries isolates the sum of two imaginary Kossakowski coefficients. For every canonical two-qubit generator, including nonunital ones, Pauli multiplication gives

$$\begin{aligned}\Phi(L) &:= \mathrm{Im}\, C_{XX,ZZ} + \mathrm{Im}\, C_{XZ,ZX} \\ &= \tfrac{1}{8}(L_{YZ,IX} + L_{YX,IZ} - L_{IX,YZ} - L_{IZ,YX}).\end{aligned} \tag{28}$$

This combination of four entries cancels unrelated canonical contributions and probes correlations between directions in $\ker C_\eta$. Their diagonal Kossakowski coefficients vanish at every C_η. With an entrywise error bound δ, recovering C_{aa} from the diagonal entries of G bounds these four diagonal coefficients of a physical candidate by δ, and

positive two-by-two minors of C give $|\Phi(L)| \le 2\delta$. An imbalance in the readout gains of the entries with exchanged indices would instead produce a term proportional to η times that imbalance. Deconvolving each candidate's unknown gains and comparing to the reference yields

$$|\eta \sinh \beta_g| \le \left(2 + \frac{1}{2l}\right)\delta. \tag{29}$$

Thus a nonzero correlation constrains the same gauge direction that moved the ZZ target.

Theorem 3 (Correlation-dependent local crossover)**.** *At fixed $0 < \varepsilon_{\mathsf{A}} \le \varepsilon < 1$, for the references C_η embedded on a pair of $n \ge 2$ qubits as in Corollary 2 and the unchanged surrounding class with complex Kossakowski matrices $\mathfrak{M}_\varepsilon^{\mathrm{L2}}$, with $h = h_{ZZ\otimes I_{\mathsf{E}}}$ and d_{27} evaluated on the pair entries,*

$$\begin{aligned}\omega_\eta(\delta) &:= \sup_{M:\, d_{27}(G_M, G_\eta)\le\delta} |h(M) - h_0| \\ &= \Theta_{\varepsilon,\varepsilon_{\mathsf{A}}}\left(\min\left\{\sqrt{\delta}, \frac{\delta}{|\eta|}\right\}\right),\end{aligned} \tag{30}$$

uniformly for $|\eta| \le 0.01$ and sufficiently small δ, with constants independent of n. Interpret the second branch as infinite at $\eta = 0$. The same order holds for the maximum distance over all entries of G; the 23 matrix elements alone retain their square-root modulus. The lower-bound construction applies throughout $0 < \delta \le 9.6(\varepsilon_{\mathsf{A}}/100)^2$.

We show the physical models behind the lower bound in Fig. 2(c,d). The positive correction $q_{\eta,\theta} = 0.6(\theta^2 + |\eta\theta|)$ gives a maximum entrywise difference $16q_{\eta,\theta}$ in G after SPAM compensation. The correlation creates Kossakowski coefficients in the kernel of order $\eta\theta$, requiring a linear contribution to the positive correction in addition to the quadratic one. Since the target moves by order $|\theta|$, this yields both branches. Appendix K proves the matching upper bound.

In terms of the number of shots, the same mixing argument applies for $0 < \alpha < 1/2$: for every adaptive protocol and every interval uniformly valid over a class containing the constructed alternatives, the expected length at the reference is at least of order

$$\min\{\varepsilon_{\mathsf{A}}, N^{-1/4}, N^{-1/2}/|\eta|\}, \tag{31}$$

with constants depending only on ε_{A} and α. With a common norm bound fixed independently of n, N, and η, estimating 27 derivatives and 15 calibration quantities gives matching upper bounds on the expected length up to logarithmic factors. In the fixed model units of Eq. (14), the crossover occurs at entry precision $\delta \asymp \eta^2$, or number of shots $N \asymp |\eta|^{-4}$ up to constants and logarithmic factors, when the transition lies inside the local domain.

VII. MEASUREMENT CHOICE AND RECOVERY ON QUANTUM PROCESSORS

Calibration protocols and effective-Hamiltonian analyses characterize coherent interactions in superconducting devices [60–62]. We use measurements on `ibm_boston`, `ibm_kingston`, and `ibm_pittsburgh` to test how response selection affects visibility and parameter recovery. Section VII A asks whether target populations alone reveal a conditional coupling, Sec. VII B whether additional measurement bases improve visibility and the recovery of a programmed parameter, and Sec. VII C what is needed to assign a recovered response to a Hamiltonian coefficient. Appendix N gives the acquisition and processing methods, and Table II collects the sampling settings.

A. Idle evolution: target populations and Ramsey response

The largest observed total-variation distance (TV) between the target's outcome distributions for the two neighbor preparations is 6.0×10^{-4} across the 90 pair–time comparisons [Fig. 3(c)]. For nine neighboring pairs selected for resolvable coupling, we prepare the target in $|0\rangle$ and measure it in Z after ten idle times between 0 and 47 μs, with its neighbor prepared in either computational state [Fig. 3(a)]. A Ramsey experiment on the same pairs, in contrast, resolves conditional frequency shifts of magnitude 3.871–7.243 kHz [Fig. 3(b)]. It prepares the target in a superposition, with the control in $|0\rangle$ or $|1\rangle$, and records X and Y responses. We analyze these data with postselection on the final control outcome matching its preparation and with readout error mitigation (Appendix N).

B. Injected rotations: visibility and parameter recovery

Injected rotations provide a controlled test of the relation between measurement choice and parameter recovery at $n = 3, 4$. The dependence of coherent-rotation sign identification on the measured Pauli settings was studied in Ref. [63]. Here, we apply single-qubit rotations generated by X_0 and X_j, with $j = 1$ or 2, with equal or opposite signs at a matched magnitude. For the ideal diagonal input and these rotations on distinct qubits, computational-basis populations are even in each angle, whereas an additional Y_0Y_1 or Y_0Y_2 measurement distinguishes the relative sign.

Additional bases increase visibility at a matched number of shots. Random subsamples within each preparation match the number of shots in the additional basis to that in the computational basis. Across all 18 combinations of device, qubit number, rotation pair, and angle, the median TV in the additional basis is 2.8–14.1 times that in the computational basis [Fig. 4(a,b)].

The signed response, moreover, supports angle recovery. Let ψ denote the programmed angle. For the specified diagonal preparation and rotations on distinct qubits,

$$\Delta\langle Y_j\rangle = -2\langle Z_j\rangle_{\mathrm{in}} \sin\psi, \qquad \langle Z_j\rangle_{\mathrm{in}} = \sum_u r_u(-1)^{u_j}, \tag{32}$$

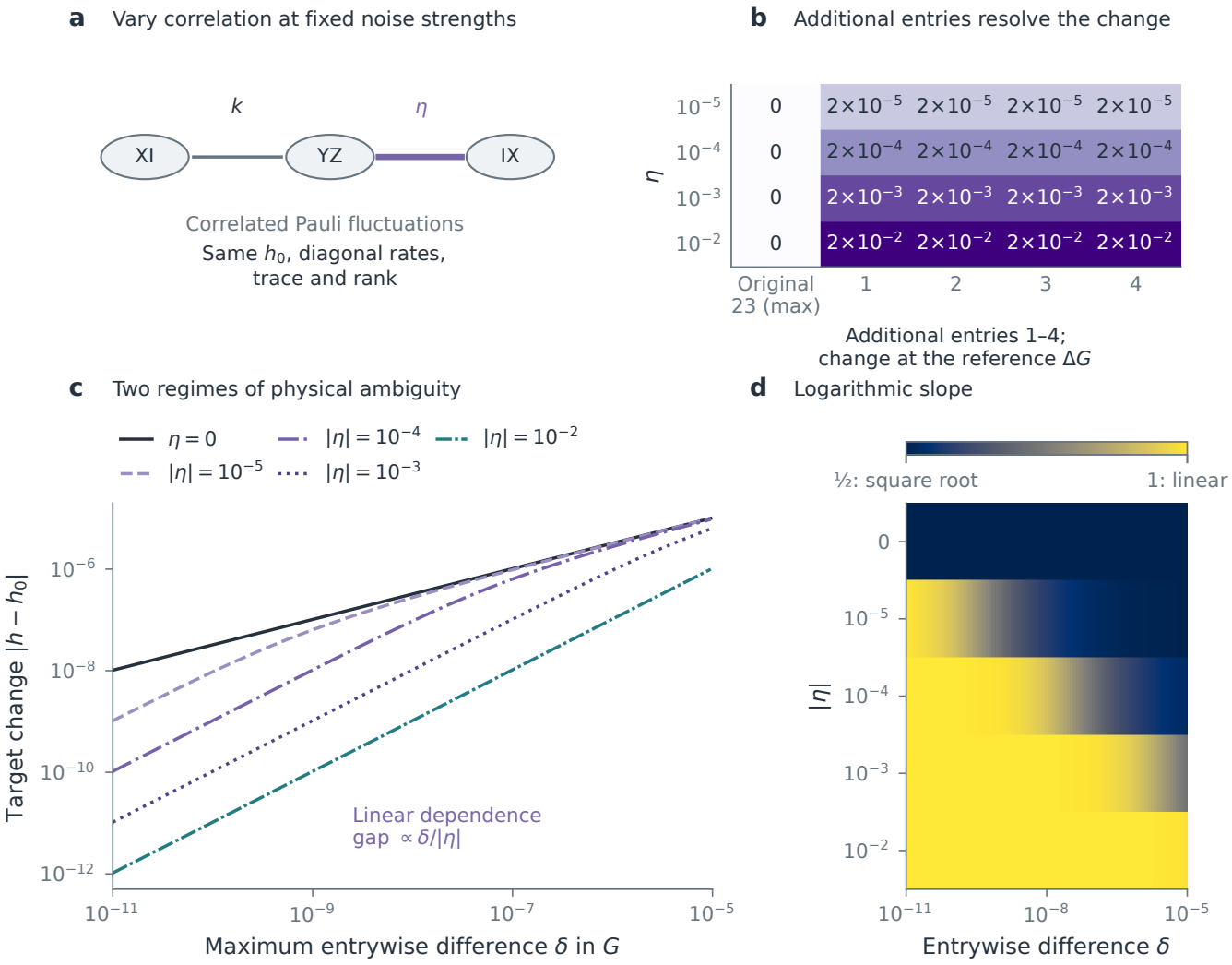


FIG. 2. Correlation-dependent precision. (a) Varied Kossakowski coefficient $C_{IX,YZ} = \eta$ and fixed $C_{XI,YZ} = k$. (b) The original 23 entries are unchanged, whereas the four additional entries shift by $2|\eta|$ in magnitude relative to the $\eta = 0$ reference. Entries 1–4 follow the order in Eq. (27). (c) Physical models constructed with positive correction $q = 0.6(\theta^2 + |\eta\theta|)$ and maximum entrywise difference $16q$ in G. (d) Their logarithmic slopes approach one for $\theta \ll |\eta|$ and one-half for $|\eta| \ll \theta$. These constructions give the lower bound, and Theorem 3 provides the matching upper bound. Model units follow Eq. (14), and Appendix M 3 gives the checks.

where $\Delta\langle Y_j\rangle$ subtracts the response for opposite-sign rotations from that for same-sign rotations, and j labels the qubit whose rotation is reversed. The preparation weights r_u fix the nominal polarization $\langle Z_j\rangle_{\text{in}}$. Table III gives its values and the sampling allocation. Inverting this relation, we obtain 66 estimates across devices, qubit numbers, rotation pairs, and angles. The pooled slope of a weighted linear fit of $\sin\hat{\psi}$ against $\sin\psi$ through the origin is 0.982 ± 0.014 (one standard error), and the median absolute angle error is 0.018 rad. Figure 4(c) shows all 66 angle errors grouped by acquisition.

C. Physical interpretation of the recovered response

However, assigning a recovered response to a Hamiltonian coefficient requires a processing and dynamical model, and the frequency estimate depends on both. For example, postselection on the final control outcome changes fitted frequencies by approximately 0.25–1.48 kHz relative to using all shots across the nine pairs, exceeding the bootstrap standard error on every pair. Moreover, joint fits to probe and calibration counts give deviances above those of all corresponding parametric-bootstrap refits, in-

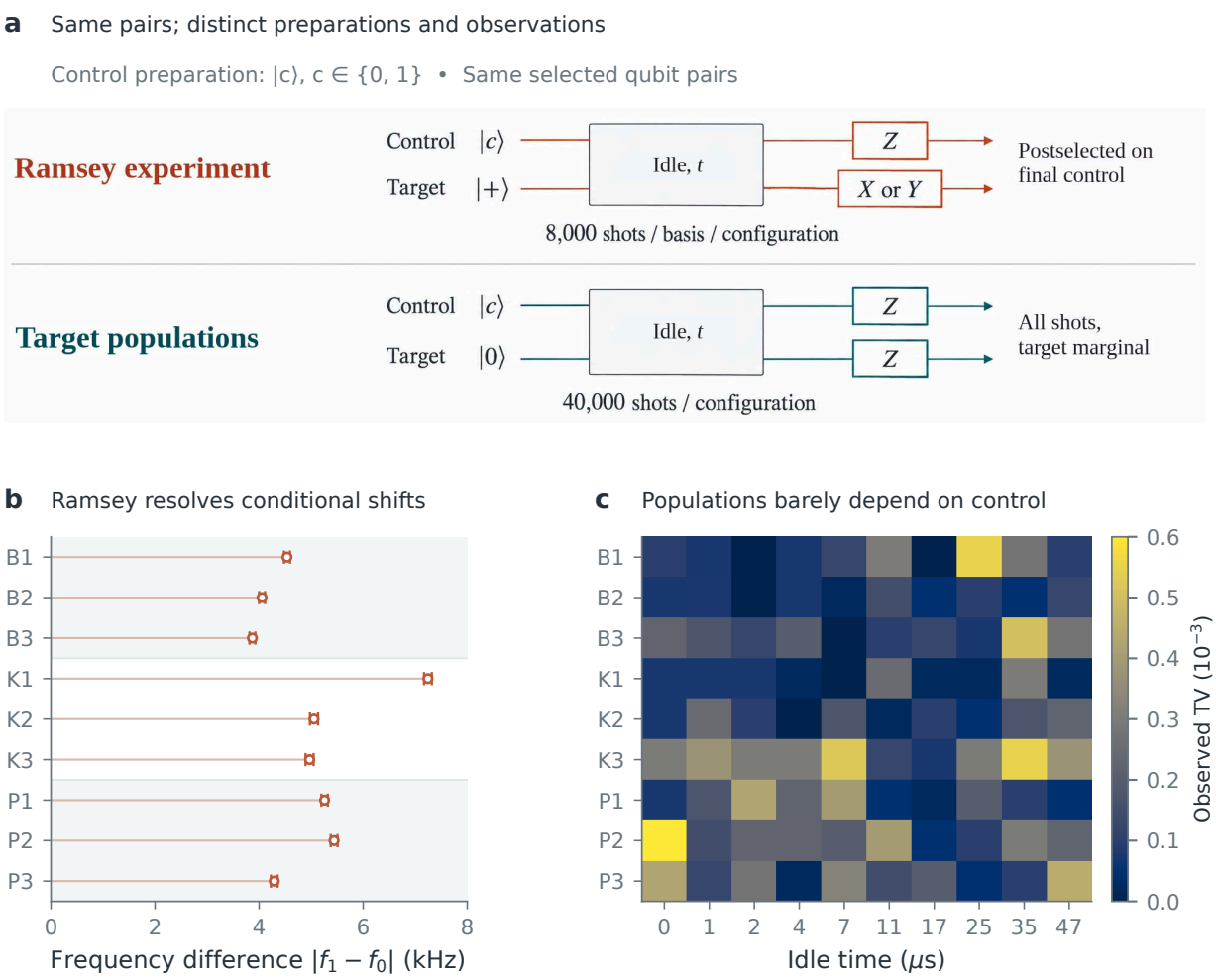


FIG. 3. Population and Ramsey responses during idle evolution. (a) Protocols on the same selected pairs, with the control prepared in either computational state. Preparations, measurement bases, and numbers of shots differ as shown. (b) Magnitudes of conditional frequency shifts from Ramsey experiments. Bars show one bootstrap standard error (0.06–0.08 kHz, comparable to the marker size) with the fitted readout mitigation and retained shot totals held fixed. B, K, and P denote Boston, Kingston, and Pittsburgh, and indices identify the three pairs on each device. (c) The 90 observed total-variation distances $|\hat{p}_1^{(0)} - \hat{p}_1^{(1)}|$ between target-qubit Z-outcome distributions, where $\hat{p}_1^{(c)}$ is the fraction of target outcomes equal to 1 for control preparation $|c\rangle$. These distances use all raw shots without postselection or readout error mitigation.

dicating mismatch with the tested model. Appendix O presents these diagnostics.

For the restricted protocols of Appendix N 2, with control inputs diagonal in the computational basis and no intermediate operations that create control coherence, the dephasing evolution depends on h and $b = \mathrm{Im}\, C_{ZI,IZ}$ through $h + 2b$. Hence, at positive target dephasing, distinct physical couplings can share these restricted data, whereas probes with the control in a superposition distinguish the constructed alternatives. The general theory of Secs. III–VI identifies the additional calibration and physical constraints needed to turn measured responses into intervals for the canonical interaction coefficient.

VIII. DISCUSSION

We have shown that the precision of an identified Hamiltonian coefficient depends on how gauge freedom meets the positivity boundary of C. At geometrically regular n-qubit references, the kernel criterion distinguishes linear from square-root dependence on the entrywise error in G, and single-qubit coefficients have exactly linear stability at every reference. For interactions, real noise correlations determine the first-order change under gauge transformations, and the kernel condition determines whether restoring positivity requires noise of first or second order. Both can be evaluated from the reference generator and target coefficient, and together they identify the gauge directions that limit precision. On hardware, we found

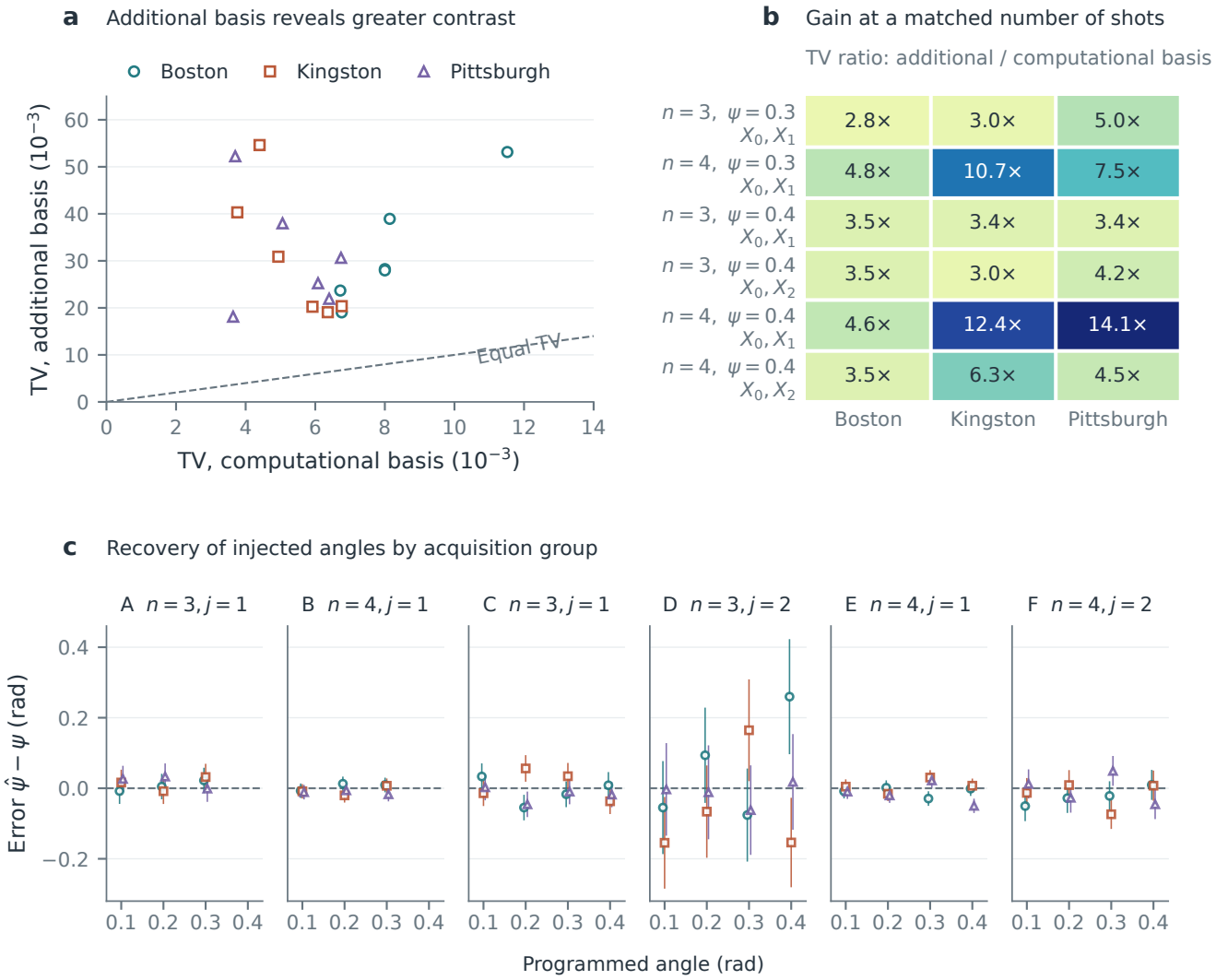


FIG. 4. Visibility and recovery of injected rotations. (a) Each point pairs the total-variation distance (TV) in the computational basis with the median TV in the additional basis over random subsamples within each preparation. TV compares the outcome distributions of equal- and opposite-sign rotations at the same magnitude. Shapes and colors identify devices, and the dashed line denotes equal TV. (b) Median TV in the additional basis divided by TV in the computational basis, for all 18 comparisons. Row labels give n, programmed angle ψ in radians, and rotation generators. Panels (a,b) use 1000 random subsamples with matched totals of 25,000 shots per configuration at $n = 3$ and 50,000 at $n = 4$. (c) All 66 angle-estimation errors $\hat{\psi} - \psi$, grouped by the six acquisitions in Table III, with common axis scales. A/C and B/E are separate acquisitions with overlapping programmed angles. Bars give one standard error from 4000 resamples within each preparation, conditional on the injection and preparation model. Horizontal offsets of at most 0.004 rad distinguish devices, and the zero line denotes exact recovery.

that additional measurement bases increase the visibility of injected rotations and permit angle recovery under the specified preparation and rotation model. Moreover, Ramsey experiments resolve conditional frequency shifts, and their dependence on processing and on the tested dynamical model shows that assigning a response to an interaction requires physical constraints.

For regular references, our results answer the question of Ref. [44] about learning near the positivity boundary in terms of local precision. Specifically, at mixing references, the square-root branch forces uniformly valid intervals to have expected length $\Omega(N^{-1/4})$, even for adaptive local protocols, and generator estimation attains this rate up to logarithmic factors, whereas the linear branch attains $\widetilde{O}(N^{-1/2})$. Moreover, our explicit many-body constructions show that the mechanism extends beyond a single pair.

Our measurement principle is to identify the gauge directions that change the target and to measure responses that constrain them. Noise correlations enter both steps: they cause the target derivative, but a correlation detected by other entries of G can constrain the same gauge

direction, as our four additional matrix elements show. Related methods already measure such correlations: noise spectroscopy reconstructs cross correlations in dephasing environments using tailored control sequences [64–66]. Our results suggest using these methods, together with learning of sparse noise correlations and protocols using single-qubit operations [58, 67], to measure the noise correlations that constrain gauge directions changing the target in self-consistent inference [42, 43].

These results point to several directions. First, positive noise backgrounds can remove exact identification: adding ξI_{15} to the two-qubit reference C_0 lets sufficiently small gauge transformations remain physical without an additional observable correction. For a fixed SPAM budget and sufficiently small $\xi > 0$, models with identical exact data then differ in h_{ZZ} by order $\sqrt{\xi}$, so no amount of data distinguishes them (Appendix G 4). Which minimal additional calibration or noise constraints suffice to restore identification remains open. Second, at the two-qubit reference with zero coupling, uniformly valid intervals have expected length $\Omega(N^{-1/8})$, and sharp precision rates beyond regular references are yet to be classified. Finally, combining the criterion with learning of structured noise [28, 29] could identify which of the $16^n - 1$ quantities estimated by our full-generator acquisition suffice to characterize couplings and crosstalk in large registers.

ACKNOWLEDGMENTS

This research used resources of the Oak Ridge Leadership Computing Facility, which is a DOE Office of Science User Facility supported under Contract DE-AC05-00OR22725. This research was supported by the UTC Applied AI & Industry Partnerships Initiative, funded through the Center of Excellence in Applied Computational Science and Engineering (CEACSE). This study was also funded by the College of Engineering and Computer Science of UTC. The funders played no role in study design, data collection, analysis and interpretation of data, or the writing of this manuscript.

Appendix A: Observation equivalence and canonical quantities

We prove observation equivalence and canonical inversion, and show how depolarizing noise restores positivity. Appendix B gives statistical comparisons and confidence intervals, and Appendix C estimates the entries of G at finite times. Appendix D proves the general classification and statistical lower bound, and Appendices E and F give its physical interpretation and many-body realization. Appendices G–J establish the explicit pair, its local modulus and its SPAM channels. The application with four additional matrix elements and its embedding in larger registers appear in Appendices K and L. The remaining appendices document computed intervals and processor analyses.

1. Equivalence of complete observation records

Let $d = 2^n$, $m = d^2 - 1$, $P_0 = I$ and $\mathrm{Tr}(P_a P_b) = d\delta_{ab}$, and write $a \oplus b$ for the phase-free product label and $\chi_a(Q) = \pm 1$ for $P_a P_Q P_a = \chi_a(Q) P_Q$. The states $(I \pm \sigma)/2$, $\sigma \in \{X, Y, Z\}$, span the single-qubit operators, so product-state inputs and rank-one product effects span the operator space. Thus equality of all their probabilities is equality of the corresponding transfer maps. If (L, A, B) and (L', A', B') have identical exact data, zero-time, control-only, and uncontrolled-evolution experiments give, for every product-unitary channel U and $t \geq 0$,

$$BA = B'A', \qquad BUA = B'UA',$$
$$Be^{tL}A = B'e^{tL'}A'. \tag{A1}$$

The budget $\varepsilon < 1$ makes each boundary invertible by the Neumann series $A^{-1} = \sum_k (\mathrm{id} - A)^k$. Set $S = B'^{-1}B = A'A^{-1}$. Cancellation and differentiation at zero show

$$A' = SA, \quad B' = BS^{-1}, \quad L' = SLS^{-1}, \quad SU = US. \tag{A2}$$

The inverse of an invertible Hermiticity-preserving, trace-preserving map has those same properties, so S is real in the Hermitian basis and trace preserving.

Commutation with Pauli conjugations forces S to be diagonal: for $R \neq Q$, the label $r \oplus q$ has a nonidentity factor at some qubit, and a single-qubit Pauli there that anticommutes with this factor has different characters on R and Q, so $(\chi_b(R) - \chi_b(Q))S_{R,Q} = 0$ gives $S_{R,Q} = 0$. Single-qubit Cliffords permute X, Y, Z on each occupied qubit up to sign and act transitively on the labels of each support, which forces one scalar per support sector,

$$S(P_a) = s_{\mathrm{supp}(a)} P_a, \qquad s_\varnothing = 1, \tag{A3}$$

the last value by trace preservation. Conversely, every such map commutes with all product unitaries, since those preserve the identity and traceless spaces of each qubit and hence every support sector.

Substitution of Eq. (A2) into every sequence cancels the intermediate gauge transformations, so every fixed-setting outcome probability agrees. For adaptive policies, conditioning on a common history and induction over shots give equal joint laws. This proves complete observational equivalence whenever both endpoints are physical. The map S is unital, though it need not be positive; its sector scalars are positive, as proved below.

2. Boundary twirling and positive gains

Finite unitary designs and randomized noise tailoring use group averages to simplify channel descriptions [68, 69]. Here independent local averages act on the

preparation and readout channels. Choose independent uniformly random single-qubit Cliffords on every qubit, with product channels U, V. Preparing $U^{-1}(\rho)$ and applying trusted U immediately after A implements, on average, $\bar{A} = \mathbb{E}_U UAU^{-1}$. Applying trusted V immediately before B and rotating the rank-one product effect implements $\bar{B} = \mathbb{E}_V V^{-1}BV$. The averaged experiment is $\bar{B}e^{tL}\bar{A}$. Both averages are completely positive and commute with all local Cliffords, so the commutant argument makes them support scalars.

Write $\varepsilon_A = \|A - \mathrm{id}\|_\diamond$ and similarly for B. Convexity and unitary invariance give $\|\bar{A} - \mathrm{id}\|_\diamond \le \varepsilon_A$. Applying this to a Hermitian Pauli gives $|1 - a_Q| \le \varepsilon_A$; trace-norm contractivity of positive trace-preserving maps on Hermitian operators gives $|a_Q| \le 1$. Thus $1-\varepsilon_A \le a_Q \le 1$ on each of the 2^n-1 nonempty sectors, with the analogous bound for b_Q, and

$$q_Q = a_Q b_Q \ge (1-\varepsilon_A)(1-\varepsilon_B) \ge 1 - \varepsilon = l. \tag{A4}$$

Consequently $T(0) = \bar{B}\bar{A}$ is invertible and Eq. (4) is observable. For equivalent models, twirling $B' = BS^{-1}$ gives $b'_Q = b_Q/s_Q$. Both gains are positive, so $s_Q > 0$. For each candidate, the ratio b_R/b_Q lies in $[l, l^{-1}]$. This follows from the SPAM budget.

If $A = \bigotimes_j A_j$ and $B = \bigotimes_j B_j$ are products over qubits, independence of the local twirls gives $\bar{A} = \bigotimes_j \bar{A}_j$, and each single-qubit twirl fixes I and has one gain on traceless operators. Hence $a_s = \prod_{j\in s} a_{\{j\}}$ and $b_s = \prod_{j\in s} b_{\{j\}}$. For two models with product SPAM channels, the readout ratio $\bar{B}^{-1}\bar{B}_0$, and in particular the gauge transformation relating two equivalent models, therefore has logarithmic sector scalars $\sum_{j\in s} y_j$ with $y_j = \log(b_{0,\{j\}}/b_{\{j\}})$.

3. Canonical projection, diagonal recovery, and norm bounds

For nonidentity Pauli labels P, define the Hamiltonian superoperator $\mathcal{A}_P = -i[P/2, \cdot]$ and its real transfer matrix A_P. Since $\{P_a/\sqrt{d}\}$ is orthonormal, the Frobenius pairing of transfer matrices equals the Hilbert–Schmidt pairing of superoperators, and

$$\langle A_P, A_Q\rangle = \frac{d^2}{2}\delta_{P,Q}, \qquad h_P = \frac{2}{d^2}\langle A_P, L\rangle. \tag{A5}$$

The Hamiltonian part of L is $\sum_Q h_Q A_Q$. Given the first identity, the second follows for arbitrary complex Kossakowski matrices if each canonical dissipator is orthogonal to A_P. For the left and right multiplication superoperators $\mathcal{L}_F(X) = FX$ and $\mathcal{R}_G(X) = XG$, the superoperator trace obeys $\mathrm{Tr}_{\mathrm{op}}(\mathcal{L}_F\mathcal{R}_G) = \mathrm{Tr}(F)\,\mathrm{Tr}(G)$. Pairing $\mathcal{A}_P$ with a jump map $\mathcal{L}_{P_a}\mathcal{R}_{P_b}$ gives zero because both jump labels are traceless. The remaining anticommutator map $-\frac{1}{2}\{\Gamma, \cdot\}$, with $\Gamma = \sum_{a,b} C_{ab}P_bP_a = \Gamma^\dagger$ because $C = C^\dagger$, is self-adjoint in Hilbert–Schmidt inner product, whereas $\mathcal{A}_P$ is skew-adjoint. Their real transfer matrices are respectively symmetric and antisymmetric, so their pairing vanishes.

Expanding the two commutators with $\mathrm{Tr}_{\mathrm{op}}(\mathcal{L}_F) = \mathrm{Tr}_{\mathrm{op}}(\mathcal{R}_F) = d\,\mathrm{Tr}\,F$ gives $\langle A_P, A_Q\rangle = \frac{1}{4}[2d\,\mathrm{Tr}(PQ) - 2\,\mathrm{Tr}\,P\,\mathrm{Tr}\,Q]$, the first identity. This proves Eq. (A5) for complex Kossakowski matrices and nonunital noise. Antisymmetric transfer entries can also contain dissipative contributions.

The maps $\rho \mapsto P_a\rho P_b$, over all labels including I, are d^4 pairwise orthogonal superoperators of squared Hilbert–Schmidt norm $\mathrm{Tr}(P_aP_a)\,\mathrm{Tr}(P_bP_b) = d^2$, hence a basis. A Hermiticity-preserving, trace-annihilating map $\mathcal{X}$ with transfer matrix X therefore has a unique expansion $\mathcal{X}(\rho) = \sum_{a,b}\eta_{ab}P_a\rho P_b$, and comparing $\mathcal{X}(\rho)$ with $\mathcal{X}(\rho^\dagger)^\dagger$ gives $\eta_{ba} = \overline{\eta_{ab}}$. Put $C = (\eta_{ab})_{a,b\neq I}$, $\Gamma = \sum_{a,b\neq I} C_{ab}P_bP_a$ and $F = \frac{1}{2}\eta_{II}I + \sum_{a\neq I}\eta_{aI}P_a$, so that $\mathcal{X}(\rho) = \sum_{a,b\neq I} C_{ab}P_a\rho P_b + F\rho + \rho F^\dagger$. Trace annihilation gives $\mathrm{Tr}[(\Gamma + F + F^\dagger)\rho] = 0$ for all ρ, so $F + F^\dagger = -\Gamma$; hence $H = (F^\dagger - F)/(2i)$ is Hermitian, traceless because $\mathrm{Tr}\,F = d\eta_{II}/2$ is real, and $F = -\Gamma/2 - iH$. This is Eq. (1) with a Hermitian, possibly indefinite C.

Every canonical representation of $\mathcal{X}$ is such an expansion, so uniqueness of the coefficients makes (H, C) unique, and the map generates a completely positive semigroup exactly when $C \succeq 0$ [53, 54]. The canonical Kossakowski matrix is the coefficient array on $a, b \neq I$.

As the maps $\mathcal{K}_{ab} : \rho \mapsto P_a\rho P_b$ are self-adjoint and orthogonal with squared norm d^2, $\eta_{ab} = d^{-2}\,\mathrm{Tr}_{\mathrm{op}}(\mathcal{K}_{ab}\mathcal{X}) = d^{-3}\sum_Q \mathrm{Tr}[P_bQP_a\mathcal{X}(Q)]$, and the expansion $\mathcal{X}(Q) = \sum_R X_{R,Q}R$ with cyclicity gives

$$\mathrm{CanCov}(X)_{ab} = \frac{1}{d^3}\sum_{R,Q}\mathrm{Tr}(P_aRP_bQ)X_{R,Q}, \qquad a, b \neq I, \tag{A6}$$

and we write $\mathrm{CanH}_P(X) = h_P$ for its canonical Hamiltonian coefficient. Both maps are real-linear. For fixed (a, b, Q) exactly one R gives a nonzero trace in Eq. (A6), of modulus d, so $|\mathrm{CanCov}(X)_{ab}| \le \|X\|_{\max} = \max_{R,Q}|X_{R,Q}|$. Orthogonality of the basis gives $\|X\|_F^2 = d^2\sum_{a,b}|\eta_{ab}|^2$ for the full coefficient array η, so, with unsubscripted matrix norms denoting operator norms,

$$\|\mathrm{CanCov}(X)\| \le \|\mathrm{CanCov}(X)\|_F \le \frac{\|X\|_F}{d} \le 2^n\|X\|_{\max}, \tag{A7}$$

the last step because X has d^4 entries. Half of all labels anticommute with P, since multiplication by one anticommuting label exchanges the commuting and anticommuting sets, and for an anticommuting Q, $\mathcal{A}_P(Q) = -iPQ$ is a signed Pauli. Thus A_P has $d^2/2$ nonzero entries, each ± 1, and Eq. (A5) gives

$$|\mathrm{CanH}_P(X)| \le \|X\|_{\max}, \qquad \mathrm{CanH}_P(A_P) = 1, \tag{A8}$$

with absolute weights $2|(A_P)_{R,Q}|/d^2$ summing to one.

Set $c_a = C_{aa}$ for $a \neq I$. The Hamiltonian diagonal vanishes by cyclicity, and $d^{-1}\,\mathrm{Tr}(QP_aQP_b) = \chi_a(Q)\delta_{ab}$ and $(2d)^{-1}\,\mathrm{Tr}(Q\{P_bP_a, Q\}) = \delta_{ab}$, so Pauli orthogonality

eliminates off-diagonal Kossakowski terms from diagonal transfer entries:

$$L_{Q,Q} = \sum_{a \neq I} c_a(\chi_a(Q) - 1), \tag{A9}$$

where $\chi_a(Q) = 1$ for commuting labels and -1 otherwise. Character orthogonality, $\sum_Q \chi_a(Q)\chi_b(Q) = d^2\delta_{ab}$ since $\chi_a\chi_b = \chi_{a\oplus b}$ and $\sum_Q \chi_e(Q) = 0$ for $e \neq I$, then gives

$$c_a = \frac{1}{d^2}\sum_Q \chi_a(Q) G_{Q,Q}, \quad a \neq I. \tag{A10}$$

Here a diagonal gauge transformation leaves $G_{Q,Q} = L_{Q,Q}$, and trace preservation gives $G_{I,I} = 0$. Each recovered rate has error at most $(1 - 4^{-n})\delta \leq \delta$ if all $4^n - 1$ nonidentity diagonal entries have error at most δ. The identity Fourier coefficient is $d^{-2}\sum_Q G_{Q,Q} = -\sum_{a\neq I} c_a$; it represents the sum of nonidentity rates rather than an identity jump rate.

4. Restoring positivity and preserving product-label sectors

With $\mathcal{D}(X) = \mathrm{Tr}(X)I/d$, the expansion $X = d^{-1}\sum_Q \mathrm{Tr}(P_Q X)P_Q$ and the character sums give $\sum_a P_a X P_a = d\,\mathrm{Tr}(X)I$, hence

$$\sum_{a\neq I}(P_a X P_a - X) = d\,\mathrm{Tr}(X)I - d^2 X = 4^n(\mathcal{D} - \mathrm{id})(X). \tag{A11}$$

Since $P_a^2 = I$, for $t \geq 0$ the canonical generator with Kossakowski matrix tI_m and zero Hamiltonian is $4^n t(\mathcal{D} - \mathrm{id})$, whose transfer matrix is $4^n t\,\mathrm{diag}(0, -1, \ldots, -1)$. It commutes with every support scalar, which fixes I and preserves trace. Replacing L by $L + 4^n t(\mathcal{D} - \mathrm{id})$ at fixed SPAM channels therefore replaces G by $G + 4^n t(\mathcal{D} - \mathrm{id})$, an entry change of exactly $4^n t$. This holds for both unital and nonunital generators.

An invertible support scalar S acts entrywise, $(SLS^{-1})_{R,Q} = (s_R/s_Q)L_{R,Q}$. The trace in Eq. (A6) vanishes unless $r \oplus q = a \oplus b$. A Hamiltonian term with label p has transfer entries only where $r \oplus q = p$, and for a jump pair (a', b') each of $P_{a'}QP_{b'}$, $P_{b'}P_{a'}Q$ and $QP_{b'}P_{a'}$ has label $a' \oplus b' \oplus q$. Transfer entries with $r \oplus q = p$ therefore depend only on h_p, for $p \neq I$, and on the $C_{a'b'}$ with $a' \oplus b' = p$. Consequently $\mathrm{CanCov}(SLS^{-1})_{ab}$ depends only on the canonical coefficients of L in the product-label sector $a \oplus b$, and $\mathrm{CanH}_P(SLS^{-1})$ only on its sector-p data, since every nonzero entry of A_P has $r \oplus q = p$.

5. An exact attribution bound for a Hamiltonian coefficient

For a pair (R, Q) contributing to target P, that is, $(A_P)_{R,Q} \neq 0$, set $K = (L_{R,Q} - L_{Q,R})/2$ and $M = (L_{R,Q} + L_{Q,R})/2$. A gauge transformation with positive sector scalars and $\Delta = \log(s_R/s_Q)$ gives

$$\begin{aligned} K' &= K\cosh\Delta + M\sinh\Delta, \\ M' &= M\cosh\Delta + K\sinh\Delta, \\ K' - K &= \tanh(\Delta/2)(M' + M). \end{aligned} \tag{A12}$$

Define

$$\xi_P = \sum_{a:\{P_a,P\}=0} \sqrt{c_a c_{a\oplus p}}. \tag{A13}$$

Each unordered pair occurs twice. On an active pair, R, Q anticommute and RQ has product label P. The Hamiltonian transfer matrix is antisymmetric and cancels in M, and anticommutator terms give zero trace because $\{R, Q\} = 0$. A jump trace $T_{ab}(R, Q) = d^{-1}\,\mathrm{Tr}(RP_aQP_b)$ is nonzero only for $a \oplus b = p$ and then has unit magnitude. As $R \propto PQ$, $QP_aPQ = -\chi_a(Q)P_aP$ and $PQP_aQ = \chi_a(Q)PP_a$ and $P_aP = \chi_a(P)PP_a$ give $T_{ab}(Q, R) = -\chi_a(P)T_{ab}(R, Q)$, so $M = \sum_{a:\{P_a,P\}=0} C_{a,a\oplus p}T_{a,a\oplus p}(R, Q)$. Positivity gives $|C_{ab}| \leq \sqrt{c_a c_b}$, so $|M| \leq \xi_P$. Both physical endpoints have the same diagonal profile by Eq. (A10).

For equivalent models $s_Q = b_Q/b'_Q \in [l, l^{-1}]$, hence $|\Delta| \leq 2w$, with $w = -\log l$. Equations (A5) and (A12) imply

$$|h'_P - h_P| \leq 2\tanh(w)\xi_P. \tag{A14}$$

Indeed the absolute weights in the canonical Hamiltonian projection sum to one. If the diagonal profile is supported on single-qubit labels and P has weight at least two, a single-qubit label a anticommuting with P sits on a qubit of $\mathrm{supp}\,P$, and $a \oplus p$ has the full support of P and hence zero rate. Thus $\xi_P = 0$ and the target is exactly identified. Finite-shot rates also require the estimation analysis below.

Appendix B: From response errors to confidence intervals

The following lemmas bound the expected length of confidence intervals for physical models using all entries of G or a specified subset of them, with the corresponding metric. Lemma 1 gives the lower bounds on the expected length of Corollary 1 and Eq. (16) of Theorem 2, and Lemma 2 the upper bounds of Eq. (17), Proposition 5, and Corollary 3.

Lemma 1 (Adaptive comparison)**.** *For two models M_0, M_1, suppose every allowed setting has outcome laws p_0, p_1 with $p_{1,j} \geq \mu > 0$ and $\sum_j (p_{0,j} - p_{1,j})^2 \leq v^2$. For any common adaptive policy using N shots, their joint laws satisfy*

$$D_{\mathrm{KL}}(P_0^{(N)} \| P_1^{(N)}) \leq Nv^2/\mu, \qquad \|P_0^{(N)} - P_1^{(N)}\|_{\mathrm{TV}} \leq \tau, \tag{B1}$$

where $\tau = \sqrt{Nv^2/(2\mu)}$. If an interval covers the target with probability at least $1-\alpha$ at each model, then

$$\mathbb{E}_0|I_N| \geq (1-2\alpha-\tau)_+|h(M_1)-h(M_0)|, \tag{B2}$$

where $(z)_+ = \max\{z,0\}$; common randomization of the returned interval is allowed.

Proof. The inequality $\log z \leq z-1$, summed against p_0, gives $D_{\mathrm{KL}}(p_0\|p_1) \leq \sum_j (p_{0,j}-p_{1,j})^2/p_{1,j} \leq v^2/\mu$, since both probability vectors sum to one. Conditional on a common history H_{i-1}, the next-setting kernel $\pi_i(ds \mid \mathsf{H}_{i-1})$ is the same under both models. The chain rule therefore gives

$$\begin{aligned} &D_{\mathrm{KL}}(P_0^{(N)}\|P_1^{(N)}) \\ &\quad= \sum_{i=1}^{N} \mathbb{E}_0 \int \pi_i(ds \mid \mathsf{H}_{i-1}) D_{\mathrm{KL}}(p_0(\cdot \mid s)\|p_1(\cdot \mid s)) \\ &\quad\leq Nv^2/\mu. \end{aligned}$$

Shots with new preparations give these conditional outcome laws. Pinsker's inequality yields the stated total variation, which cannot increase under a common output kernel. Transferring the event $h(M_1) \in I_N$ to P_0 and intersecting it with $h(M_0) \in I_N$ gives probability at least $1-2\alpha-\tau$. On that event the interval contains both targets and has length at least their separation; nonnegativity gives Eq. (B2). □

Lemma 2 (Interval of compatible target values)**.** *Let a model class $\mathfrak{M}$ have target bound $|h(M)| \leq H$. Suppose a finite-valued response estimate $\widehat{g}$ obeys $\Pr_M\{d(\widehat{g}, g(M)) \leq \delta\} \geq 1-\zeta$ uniformly over the class, where d is a metric. Return the smallest closed interval containing*

$$\{h(M) : M \in \mathfrak{M},\ d(g(M),\widehat{g}) \leq \delta\},$$

or $[-H,H]$ if the set is empty. This interval has coverage at least $1-\zeta$ throughout $\mathfrak{M}$. At a reference $M_0 \in \mathfrak{M}$, if $\omega(t)$ bounds $|h(M)-h(M_0)|$ for all class members with $d(g(M),g(M_0)) \leq t$, then

$$\mathbb{E}_0|I| \leq 2\omega(2\delta) + 2H\zeta. \tag{B3}$$

Proof. The hull is contained in $[-H,H]$, and its endpoints are measurable because $\widehat{g}$ takes finitely many values. When the estimate satisfies its error bound, the true model is a candidate, proving coverage. At M_0, the triangle inequality places each candidate within 2δ of $g(M_0)$, so every retained target lies in $[h(M_0)-\omega(2\delta), h(M_0)+\omega(2\delta)]$. The hull has length at most $2\omega(2\delta)$ on that event and at most $2H$ otherwise. Splitting its expectation proves the bound. A modulus over a larger model class also bounds the retained targets and can be used in the same inequality. □

Appendix C: Estimating the matrix elements of the generator at finite times

This appendix specifies the norm bound of Theorem 2 and constructs the finite-time estimator of the entries of G behind its upper bound, Eq. (17), and behind Proposition 5. Appendix C 7 extends the estimator to all entries of G (Theorem 4).

1. Physical assumptions and the pair observable

Let a time-independent global GKSL generator on n qubits admit a decomposition into physical terms

$$\begin{aligned} \mathcal{L} &= \sum_Z \mathcal{L}_Z, \qquad |Z| \leq k_{\mathrm{loc}}, \\ \sup_i \sum_{Z \ni i} g_Z &\leq \gamma, \end{aligned} \tag{C1}$$

where $\mathcal{L}_Z^\dagger(I) = 0$ and the induced observable operator norm obeys $\|\mathcal{L}_Z^\dagger \otimes \mathrm{id}_F\|_{\infty\to\infty} \leq g_Z$ for every additional register F. The bound $\gamma > 0$ on the summed norms of the terms acting on each qubit is known before inference. The explicit constants below use $k_{\mathrm{loc}} = 2$. Here k_{loc} denotes support size, independently of the reference Kossakowski coefficient $k = 0.01$. We also assume that all nonzero global canonical jump labels have Pauli weight at most two. This support assumption preserves the target under pair reduction, while Eq. (C1) controls physical strength.

Fix a target pair A and let E denote its spectators, with dimensions 4 and $d_{\mathsf{E}} = 2^{n-2}$. Write $d = 2^n$ and $\iota(Q) = Q \otimes I_{\mathsf{E}}$. After the prescribed boundary averages, product-state preparations and local measurements give the response

$$f_{R,Q}(t) = \frac{a_Q b_R}{d} \operatorname{Tr}\left[\iota(Q) e^{t\mathcal{L}^\dagger}(\iota(R))\right]. \tag{C2}$$

It is the mean of a signed binary outcome obtained using product-state preparations and local measurements. Write $\iota(Q) = \bigotimes_j Q_j$, and put $\sigma_j = Q_j$ if $Q_j \neq I$ and $\sigma_j = Z$ otherwise. One explicit preparation chooses independent uniform signs $s_j = \pm 1$, prepares $\bigotimes_j [(I + s_j\sigma_j)/2]$, measures the product Pauli R at the end, and multiplies its outcome by the input sign product $\prod_{j:Q_j\neq I} s_j$. By independence, the signed input average is $\bigotimes_j (Q_j/2) = \iota(Q)/d$; every site with $Q_j = I$, including all spectators, receives a maximally mixed input. The independent boundary twirls supply the fixed scalar factors a_Q, b_R. Thus this construction realizes Eq. (C2) using fresh product preparations.

The n-qubit SPAM channels obey Eq. (2). By Appendix A, with $l = 1-\varepsilon$, the twirled zero-time gains obey

$$q_Q = f_{Q,Q}(0) = a_Q b_Q \in [l,1], \qquad a_Q b_R \leq 1. \tag{C3}$$

The entries of G restricted to the pair are

$$G^{\mathsf{A}}_{R,Q} = f'_{R,Q}(0)/q_Q. \tag{C4}$$

The SPAM channels, generator, and their gains are fixed in time. Every shot independently redraws the time index, product-input signs, and both boundary randomizations. The mixture concentration argument therefore uses fresh random settings across shots.

2. Why the reduced target is the global pair coefficient

The derivative in Eq. (C4) comes from the global channel. To relate it to a physical pair generator, define

$$\begin{aligned}\mathcal{E}_{\mathsf{A}}(X) &= X \otimes I_{\mathsf{E}}/d_{\mathsf{E}},\\ \mathcal{R}_{\mathsf{A}}(X) &= \mathrm{Tr}_{\mathsf{E}}\, X,\\ \mathcal{L}_{\mathsf{A}} &= \mathcal{R}_{\mathsf{A}}\mathcal{L}\mathcal{E}_{\mathsf{A}}.\end{aligned} \tag{C5}$$

Expand global Paulis as $F_{a,s} = P_a \otimes S_s$, allowing the identity indices $a = 0, s = 0$, and extend the global Kossakowski matrix by a zero row and column for the global identity. Orthogonality of spectator Paulis gives

$$\begin{aligned}\mathcal{R}_{\mathsf{A}}\big[F_{a,s}\mathcal{E}_{\mathsf{A}}(X)F_{b,t}\big] &= \delta_{st}P_aXP_b,\\ \mathcal{R}_{\mathsf{A}}\big[\{F_{b,t}F_{a,s}, \mathcal{E}_{\mathsf{A}}(X)\}\big] &= \delta_{st}\{P_bP_a, X\}.\end{aligned} \tag{C6}$$

Set $J_{ab} = \sum_s C_{(a,s),(b,s)}$. For each fixed s the summand is a principal submatrix of the extended Kossakowski matrix; consequently $J \succeq 0$. With $\overline{H}_{\mathsf{A}} = \mathrm{Tr}_{\mathsf{E}}\, H/d_{\mathsf{E}}$, the reduced generator has the dissipative expression with Kossakowski matrix J and Hamiltonian $\overline{H}_{\mathsf{A}}$. The J_{00} term vanishes. The terms containing exactly one local identity obey

$$\tfrac{1}{2}(J_{p0} - J_{0p})[P_p, X] = -i[\mathrm{Im}\, J_{0p}\, P_p, X]. \tag{C7}$$

Its canonical coefficients in traceless Pauli coordinates are therefore

$$\begin{aligned}C^{\mathsf{A}} &= (J_{ab})_{a,b\neq 0} \succeq 0,\\ H^{\mathrm{can}}_{\mathsf{A}} &= \overline{H}_{\mathsf{A}} + \sum_{p\neq 0} \mathrm{Im}\, J_{0p} P_p.\end{aligned} \tag{C8}$$

The positive Kossakowski matrix C^{A} and the traceless Hamiltonian in Eq. (C8) are canonical by the uniqueness proof in Appendix A. Factoring C^{A} into traceless Lindblad jumps proves physicality.

For a pair Pauli P_p of weight two,

$$h^{\mathsf{A}}_p = h_{(p,0)} + 2\,\mathrm{Im}\sum_s C_{(0,s),(p,s)} = h_{(p,0)}. \tag{C9}$$

At $s = 0$ the first Kossakowski index is the excluded global identity. At $s \neq 0$ the second label has weight $2 + \mathrm{wt}(S_s) \geq 3$, so the canonical-support assumption makes that term zero. This proves the last equality. One-body Hamiltonian corrections in Eq. (C8) are allowed nuisance parameters and leave the pair target unchanged.

The actual marginal channel $\Phi_{\mathsf{A}}(t) = \mathcal{R}_{\mathsf{A}}e^{t\mathcal{L}}\mathcal{E}_{\mathsf{A}}$ satisfies $\Phi_{\mathsf{A}}(0) = \mathrm{id}$ and $\Phi'_{\mathsf{A}}(0) = \mathcal{L}_{\mathsf{A}}$. Since $(\mathcal{L}_{\mathsf{A}})_{R,Q} = d^{-1}\,\mathrm{Tr}[\iota(R)\mathcal{L}(\iota(Q))]$, Eq. (C2) gives $f'_{R,Q}(0) = a_Qb_R(\mathcal{L}_{\mathsf{A}})_{R,Q}$, and zero-time division yields $G^{\mathsf{A}}_{R,Q} = (b_R/b_Q)(\mathcal{L}_{\mathsf{A}})_{R,Q}$. Thus $G^{\mathsf{A}} = \overline{B}_{\mathsf{A}}\mathcal{L}_{\mathsf{A}}\overline{B}_{\mathsf{A}}^{-1}$, where $\overline{B}_{\mathsf{A}} = \mathcal{R}_{\mathsf{A}}\overline{B}\mathcal{E}_{\mathsf{A}}$ acts as $\overline{B}_{\mathsf{A}}(Q) = b_QQ$ and is invertible because $b_Q \geq l$. Its fifteen diagonals and the eight positions of Eq. (13) obey the reciprocal and Kossakowski matrix identities of Appendix I, with the target in Eq. (C9).

3. All-time derivative bounds from physical locality

Lemma 3 (Derivative bound from support growth)**.** *If R has support at most two, then for every integer $p \geq 1$ and $u \geq 0$,*

$$\begin{aligned}|f^{(p)}_{R,Q}(u)| &\leq M_p,\\ M_p &= \gamma^p \prod_{j=0}^{p-1}[2 + j(k_{\mathrm{loc}} - 1)].\end{aligned} \tag{C10}$$

For physical terms on at most two sites, $M_p = (p+1)!\gamma^p$.

Proof of Lemma 3. Expand $(\mathcal{L}^\dagger)^p(\iota(R))$ into ordered applications of local terms. Retain a separate support S_j for each summand after j applications. A term disjoint from S_j annihilates that summand, because its adjoint annihilates the identity. An intersecting term enlarges the support by at most $k_{\mathrm{loc}} - 1$, so $|S_j| \leq 2 + j(k_{\mathrm{loc}} - 1)$. At each branch of the expansion,

$$\sum_{Z:Z\cap S_j\neq\varnothing} g_Z \leq \sum_{i\in S_j}\sum_{Z\ni i} g_Z \leq [2 + j(k_{\mathrm{loc}} - 1)]\gamma. \tag{C11}$$

Each $\mathcal{L}^\dagger_Z$ acts as $\mathcal{L}^\dagger_Z \otimes \mathrm{id}_F$ on the remaining qubits, and $\|\iota(R)\|_\infty = 1$. The triangle inequality therefore gives

$$\|(\mathcal{L}^\dagger)^p(\iota(R))\|_\infty \leq \sum_{Z_1,\ldots,Z_p}\prod_{r=1}^{p} g_{Z_r} \leq M_p, \tag{C12}$$

where the sum runs over ordered branches with $Z_{j+1} \cap S_j \neq \varnothing$. The last inequality follows by summing over $Z_p, Z_{p-1}, \ldots, Z_1$ in turn, using the preceding bound for each S_j. Counting a term several times when it meets several sites only increases this bound; the branching sum already counts the order of applications, so no further permutation factor occurs.

Differentiating the global exponential at $u \geq 0$ gives

$$f^{(p)}_{R,Q}(u) = \frac{a_Qb_R}{d}\,\mathrm{Tr}\Big[\iota(Q)e^{u\mathcal{L}^\dagger}(\mathcal{L}^\dagger)^p(\iota(R))\Big]. \tag{C13}$$

The differentiated observable is Hermitian. The adjoint of a CPTP map is unital and positive, hence contracts its operator norm. Finally $\|\iota(Q)/d\|_1 = 1$ and $a_Qb_R \leq 1$, giving Eq. (C10). At $k_{\mathrm{loc}} = 2$ the product is $2 \cdot 3 \cdots (p+1) = (p+1)!$. The global expansion controls the spectator dynamics and all required higher derivatives, with bounds independent of register size. □

4. Weighted endpoint differentiation and its bias bound

Differentiating an interpolation polynomial expresses a derivative as a weighted sum of function values [70]. We use this construction at zero time and bound its bias using the physical derivative estimates above.

Choose distinct nodes $0 = t_0 < t_1 < \cdots < t_p = T$ before collecting the inference sample, with integer $p \geq 1$. Let

$$\begin{aligned} \ell_j(t) &= \prod_{m \neq j} \frac{t - t_m}{t_j - t_m}, \\ w_j &= \ell_j'(0), \\ W &= \sum_{j=0}^{p} |w_j|, \\ d_f &= \sum_{j=0}^{p} w_j f(t_j). \end{aligned} \tag{C14}$$

Differentiating the Lagrange products at zero gives

$$\begin{aligned} w_0 &= -\sum_{m=1}^{p} \frac{1}{t_m}, \\ w_j &= \frac{1}{t_j} \prod_{m \geq 1,\, m \neq j} \frac{t_m}{t_m - t_j} \quad (j \geq 1). \end{aligned} \tag{C15}$$

The last product has $j - 1$ negative factors, so $\operatorname{sgn}(w_j) = (-1)^{j+1}$ for every j; no weight vanishes. Interpolation makes this functional exact for the derivative at zero of every polynomial of degree at most p. Its deterministic bias satisfies

$$\begin{aligned} |f'(0) - d_f| &\leq \beta_p, \\ \beta_p &:= \frac{M_{p+1}}{(p+1)!} \prod_{j=1}^{p} t_j \\ &= (p+2)\gamma^{p+1} \prod_{j=1}^{p} t_j \quad (k_{\mathrm{loc}} = 2). \end{aligned} \tag{C16}$$

To prove it, let $\tilde{f} = \sum_j f(t_j)\ell_j$ be the interpolant. For $0 < t < t_1$, the ordinary interpolation remainder and Eq. (C10) imply

$$\frac{|f(t) - \tilde{f}(t)|}{t} \leq \frac{M_{p+1}}{(p+1)!} \prod_{j=1}^{p} |t - t_j|. \tag{C17}$$

Since $f(0) = \tilde{f}(0)$, taking the right limit at zero proves Eq. (C16).

For each shot of a given response, independently draw $J \in \{0, \ldots, p\}$ with probability $|w_J|/W$, and acquire the signed binary product outcome Y at time t_J, with all other randomizations independently redrawn. Since $\mathbb{E}[Y \mid J = j] = f(t_j)$,

$$\begin{aligned} Z &= \operatorname{sgn}(w_J) Y \in \{-1, 1\}, \\ \mathbb{E}Z &= \sum_{j=0}^{p} \frac{|w_j|}{W} \operatorname{sgn}(w_j) f(t_j) = \frac{d_f}{W}, \\ \widehat{d}_f &= \frac{W}{N_D} \sum_{i=1}^{N_D} Z_i, \qquad \mathbb{E}\widehat{d}_f = d_f. \end{aligned} \tag{C18}$$

For $s_D > 0$, Hoeffding's inequality for the independent Z_i, which lie in an interval of length two, gives [59]

$$\Pr\{|\widehat{d}_f - d_f| > s_D\} \leq 2 \exp\left(-\frac{N_D s_D^2}{2W^2}\right). \tag{C19}$$

This concentrates the mixture estimator over all N_D shots. Equivalently, the count of $Z_i = 1$ is exactly binomial with success probability $(1 + d_f/W)/2$.

Acquire the 23 derivative responses and the fifteen zero-time diagonal calibration means separately. For $s_D, s_0 > 0$ and $0 < \alpha < 1$, sufficient counts per response are

$$\begin{aligned} N_D &= \left\lceil \frac{2W^2}{s_D^2} \log \frac{76}{\alpha} \right\rceil, \\ N_0 &= \left\lceil \frac{2}{s_0^2} \log \frac{76}{\alpha} \right\rceil, \end{aligned} \tag{C20}$$

$$N_{\mathrm{total}} = 23 N_D + 15 N_0. \tag{C21}$$

Equation (C19) bounds each derivative failure probability by $2e^{-\log(76/\alpha)} = \alpha/38$. Each calibration mean $\widehat{q}_Q$ averages N_0 independent signed outcomes in $\{-1, 1\}$ with mean q_Q, so Hoeffding's inequality gives $\Pr\{|\widehat{q}_Q - q_Q| > s_0\} \leq 2e^{-N_0 s_0^2/2} \leq \alpha/38$. A union bound over these 38 estimates supplies a common event of probability at least $1 - \alpha$ on which all derivative errors relative to d_f are at most s_D and all calibration errors are at most s_0. Zero-time draws in the derivative mixtures are included in N_D, and the calibration term counts additional preparations. There are at most $23(p+1) + 15$ response–time settings, or $p+1$ distinct evolution times. Merging coincident zero-time response settings leaves $23(p+1)$ distinct response–time pairs. The separate calibration and derivative sample counts are retained even when such settings coincide. These setting counts exclude the individual realizations of the product signs and boundary twirls.

5. Calibration, Kossakowski bounds, and interval inclusion

Clip the estimated diagonal calibration mean to $\widetilde{q}_Q \in [l, 1]$ and set $\widehat{G}^{\mathsf{A}}_{R,Q} = \widehat{d}_f / \widetilde{q}_Q$. Projection onto this interval

cannot increase the error because $q_Q \in [l, 1]$. On the common event, the decomposition

$$\frac{\widehat{d}_f}{\widetilde{q}_Q} - \frac{f'(0)}{q_Q} = \frac{\widehat{d}_f - f'(0)}{\widetilde{q}_Q} + f'(0)\frac{q_Q - \widetilde{q}_Q}{q_Q \widetilde{q}_Q} \tag{C22}$$

and $M_1 = 2\gamma$ give

$$|\widehat{G}^{\mathsf{A}}_{R,Q} - G^{\mathsf{A}}_{R,Q}| \le \delta_G, \qquad \delta_G := \frac{s_D + \beta_p}{l} + \frac{2\gamma s_0}{l^2}. \tag{C23}$$

This decomposition holds on the common calibration and derivative event, even when those events are dependent. Its second term uses the true derivative.

Character inversion, Eq. (A10), of the fifteen estimated generator diagonals gives

$$\widehat{c}_a = \frac{1}{16}\sum_Q \chi_a(Q)\widehat{G}^{\mathsf{A}}_{Q,Q}, \qquad |\widehat{c}_a - c^{\mathsf{A}}_a| \le \frac{15}{16}\delta_G, \qquad c^+_a = \max\{0, \widehat{c}_a + \delta_G\}, \tag{C24}$$

where the identity diagonal is set to zero. Thus $c^{\mathsf{A}}_a \le c^+_a$ on the same event. The seven Kossakowski coordinates in Eq. (I9) are bounded by the square roots of their paired diagonal products, now bounded using c^+. At the true ratios, each empirical group scalar differs from its physical value by at most $e_G = (l + l^{-1})\delta_G/2$, each Kossakowski coordinate by at most $e_G/2$, and the canonical target by at most e_G.

One explicit outer interval retains all ratio pairs in $[l, l^{-1}]^2$ whose seven empirical Kossakowski coordinates lie within those bounds enlarged by $e_G/2$. Take the smallest interval containing their empirical targets and enlarge it by e_G at each endpoint. The true ratios are retained on the common event, so this interval contains the true canonical pair coefficient. Equation (C9) gives the same inclusion for the global pair coefficient. The interval-arithmetic procedure in Appendix M preserves this inclusion at any finite search budget, and enclosure accuracy determines the width.

For a positive tolerance τ, a lower endpoint above zero or an upper endpoint below zero certifies the corresponding sign. Containment in $[-\tau, \tau]$ certifies $|h| \le \tau$; lying wholly above τ or below $-\tau$ certifies $|h| > \tau$. An interval crossing a decision boundary leaves the decision unresolved. Physical ambiguity is established by constructing compatible models with distinct target values.

The mathematics also covers $\varepsilon = 0$. Both SPAM channels and all gains are then identity, so $r_A = r_B = 1$, and Eq. (I9) at unit ratios gives $h = \frac{1}{8}\sum_i \sigma_i (G^{\mathsf{A}}_{R_i,Q_i} - G^{\mathsf{A}}_{Q_i,R_i})$ with $\sigma = (1, -1, 1, -1)$. On the common event,

$$\widehat{h} = \frac{1}{8}\sum_{i=1}^{4} \sigma_i (\widehat{G}^{\mathsf{A}}_{R_i,Q_i} - \widehat{G}^{\mathsf{A}}_{Q_i,R_i}), \qquad |\widehat{h} - h| \le \frac{1}{8}\sum_{(R,Q)} |\widehat{G}^{\mathsf{A}}_{R,Q} - G^{\mathsf{A}}_{R,Q}| \le \delta_G, \tag{C25}$$

where the sum runs over the eight positions of Eq. (13). Thus $[\widehat{h} - \delta_G, \widehat{h} + \delta_G]$ supplies a direct interval. The numerical gain search assumes $0 < \varepsilon < 1$; Eq. (C25) covers the endpoint $\varepsilon = 0$.

6. Exact node constants and systematic errors

For the Chebyshev–Lobatto nodes

$$t_j = \frac{T}{2}[1 - \cos(j\pi/p)] = T\sin^2\left(\frac{j\pi}{2p}\right), \qquad j = 0, \dots, p, \tag{C26}$$

the two constants controlling the estimator are exactly

$$\prod_{j=1}^{p} t_j = \frac{pT^p}{4^{p-1}}, \qquad W = \frac{2p^2}{T}. \tag{C27}$$

For the product identity, put $\omega = e^{i\pi/p}$. Evaluating the polynomial $\sum_{k=0}^{2p-1} z^k = (z^{2p} - 1)/(z - 1) = \prod_{j=1}^{2p-1}(z - \omega^j)$ at $z = 1$, where it equals $2p$, and using $|1 - \omega^j| = 2\sin(j\pi/(2p))$ gives $\prod_{j=1}^{2p-1}\sin(j\pi/(2p)) = 2p/2^{2p-1}$. Reflection about $\pi/2$, whose sine is one, turns this into $\prod_{j=1}^{p}\sin^2(j\pi/(2p)) = p/4^{p-1}$. For the weight norm, Eq. (C15) gives $\mathrm{sgn}(w_j) = -(-1)^j$ for every j. Let T_p denote the Chebyshev polynomial, defined by $\mathsf{T}_p(\cos\phi) = \cos(p\phi)$. Then

$$\mathsf{T}'_p(1) = \lim_{\phi\to 0}\frac{\cos(p\phi) - 1}{\cos\phi - 1} = \lim_{\phi\to 0}\frac{\sin^2(p\phi/2)}{\sin^2(\phi/2)} = p^2. \tag{C28}$$

The degree-p polynomial $\mathsf{T}_p(1 - 2t/T)$ therefore has nodal values $\mathsf{T}_p(\cos(j\pi/p)) = (-1)^j$ and derivative $-2p^2/T$ at zero. Polynomial exactness gives

$$-W = \sum_{j=0}^{p} w_j(-1)^j = -\frac{2p^2}{T}, \tag{C29}$$

which proves the second identity, including $p = 1$.

At $T = 1/\gamma$, Eqs. (C16) and (C27) yield

$$\beta_p = \frac{4p(p+2)\gamma}{4^p}, \qquad W = 2\gamma p^2. \tag{C30}$$

The error radii include known systematic and numerical errors. Suppose each shot at node t_j uses a realized time $t' \geq 0$ with $|t' - t_j| \leq t_{\rm err}$ and has mean within b of $f(t')$. The mean value theorem and $|f'| \leq M_1$ bound the node mean μ_j by $|\mu_j - f(t_j)| \leq b + M_1 t_{\rm err}$, so $|W\mathbb{E}Z - d_f| \leq \sum_j |w_j||\mu_j - f(t_j)| \leq W(b + M_1 t_{\rm err})$. For fresh binary shots, Eq. (C19) holds about $W\mathbb{E}Z$, and the radius in Eq. (C23) gains $W(b + M_1 t_{\rm err})/l$. For the ideal pair schedule the two parts are $2\gamma p^2 b/l$ and $4\gamma^2 p^2 t_{\rm err}/l$; a calibration-mean bias b_0 replaces s_0 by $s_0 + b_0$. For rounded rational nodes, use their actual Lagrange weights, weight norm, and node product in the proof. At fixed nodes these systematic contributions persist as the number of shots increases.

The pair schedules in Appendices I and K have numbers of shots independent of register size for a fixed pair and fixed priors. Spectator preparation and randomization use $O(n)$ local operations per shot.

7. Estimating all entries of G in the unrestricted class

Let $n \geq 2$, $d = 2^n$, and let $\mathfrak{M}^U_{\varepsilon,\gamma_{\rm tot}}$ consist of physical n-qubit generators with $\|\mathcal{L}^\dagger\|_{\infty\to\infty,\rm cb} \leq \gamma_{\rm tot}$, for a known $\gamma_{\rm tot} > 0$, and CPTP SPAM channels obeying Eq. (2); $l = 1 - \varepsilon$. Logarithms are natural.

Theorem 4 (Estimation of all entries of G)**.** *For $0 < \alpha < 1$ and $N \geq K_n$, set*

$$\begin{aligned} J &= 4^n(4^n - 1), \qquad K_n = J + 4^n - 1 = 16^n - 1, \\ n_N &= \lfloor N/K_n \rfloor, \qquad \zeta_N = \min\{\alpha, N^{-1}\}, \\ p_N &= \max\{1, \lceil \log_2 N \rceil\}, \\ s_N &= \sqrt{2\log(2K_n/\zeta_N)/n_N}, \\ \beta_N &= \frac{4p_N\gamma_{\rm tot}}{(p_N+1)!\,4^{p_N}}, \\ \delta_N &= \frac{2\gamma_{\rm tot}p_N^2 s_N + \beta_N}{l} + \frac{\gamma_{\rm tot}s_N}{l^2}. \end{aligned} \tag{C31}$$

The estimator below uses $K_n n_N \leq N$ shots and obeys $\Pr_M\{\|\widehat{G} - G(M)\|_{\max} \leq \delta_N\} \geq 1 - \zeta_N$ for every $M \in \mathfrak{M}^U_{\varepsilon,\gamma_{\rm tot}}$. With $B_N = \log(2 \cdot 16^n \max\{N, \alpha^{-1}\})$,

$$\begin{aligned} \delta_N &\leq \frac{6\gamma_{\rm tot}4^n}{l^2}(1 + \log_2 N)^2\sqrt{\frac{B_N}{N}} + \frac{2\gamma_{\rm tot}}{lN^2} \\ &\leq C_* N^{-1/2}(\log N)^{5/2}, \\ C_* &= \frac{6\gamma_{\rm tot}4^n}{l^2}\Big(1 + \frac{1}{\log 2}\Big)^2\sqrt{1 + \log(2 \cdot 16^n/\alpha)} \\ &\quad + \frac{2\gamma_{\rm tot}}{l}. \end{aligned} \tag{C32}$$

Proof of Theorem 4. Fix $R \neq I$ and any Q. Apply the signed product-input construction preceding Eq. (C3) to these labels on the full register. Its sign average is P_Q/d, independently of the support of Q. The output parity for R, multiplied by the same input sign product, is binary. Independent boundary twirls thus give its mean

$$f_{R,Q}(t) = T(t)_{R,Q} = a_Q b_R d^{-1}\,\mathrm{Tr}[P_Q e^{t\mathcal{L}^\dagger}(P_R)].$$

The gains obey $q_Q = f_{Q,Q}(0) = a_Q b_Q \in [l, 1]$, so $f'_{R,Q}(0)/q_Q = (b_R/b_Q)L_{R,Q} = G_{R,Q}$. The trace-preserving twirls act as scalars on Pauli support sectors and fix I, so $q_I = 1$; trace preservation gives $G_{I,Q} = 0$. The unknown entries are the J entries with $R \neq I$.

The assumed norm bound gives $\|\mathcal{L}^\dagger\|_{\infty\to\infty} \leq \gamma_{\rm tot}$. The operator $X = (\mathcal{L}^\dagger)^p(P_R)$ is Hermitian with $\|X\|_\infty \leq \gamma_{\rm tot}^p$. The adjoint semigroup is positive and unital, so it maps $-\|X\|_\infty I \leq X \leq \|X\|_\infty I$ to the same bounds. Differentiation and Hölder's inequality give, for $u \geq 0$,

$$|f^{(p)}_{R,Q}(u)| \leq |a_Q b_R|\,d^{-1}\|P_Q\|_1\,\|e^{u\mathcal{L}^\dagger}(X)\|_\infty \leq \gamma_{\rm tot}^p.$$

Use the Chebyshev–Lobatto nodes with $p = p_N$ and $T = 1/\gamma_{\rm tot}$ in Eqs. (C14) and (C27) and in the first expression of Eq. (C16), whose proof holds with $M_{p+1} = \gamma_{\rm tot}^{p+1}$. They give $W = 2\gamma_{\rm tot}p^2$ and $\beta_p = 4p\gamma_{\rm tot}/((p+1)!\,4^p) \leq 2\gamma_{\rm tot}4^{-p}$, since $(p+1)!/p \geq 2$; hence $\beta_N \leq 2\gamma_{\rm tot}/N^2$.

Allocate n_N shots to each of the J randomized derivative means of Eq. (C18) and to each of the $4^n - 1$ zero-time calibrations q_Q, $Q \neq I$, redrawing nodes, signs, and twirls independently. Equation (C19) at threshold Ws_N and Hoeffding's inequality for the calibrations at threshold s_N each fail with probability at most $2e^{-n_N s_N^2/2} = \zeta_N/K_n$; the union bound over the K_n means gives a common event of probability at least $1 - \zeta_N$. Clip the calibrations to $[l, 1]$, set $\widetilde{q}_I = 1$ and $\widehat{G}_{R,Q} = \widehat{d}_{R,Q}/\widetilde{q}_Q$ for $R \neq I$, and $\widehat{G}_{I,Q} = 0$. The split before Eq. (C23), with $|f'_{R,Q}(0)| \leq \gamma_{\rm tot}$, bounds every error by δ_N on this event.

For $x \geq 1$, $\lfloor x \rfloor \geq x/2$, so $n_N \geq N/(2K_n)$ and $s_N \leq 2 \cdot 4^n\sqrt{B_N/N}$, because $2K_n/\zeta_N \leq 2 \cdot 16^n \max\{N, \alpha^{-1}\}$. With $p_N \leq 1 + \log_2 N$, $2p_N^2 + 1 \leq 3(1 + \log_2 N)^2$, and $l \leq 1$, this gives the first bound in Eq. (C32). Since $N \geq K_n \geq 15$, $\log N \geq 1$; hence $B_N \leq [1 + \log(2 \cdot 16^n/\alpha)]\log N$, $1 + \log_2 N \leq (1 + 1/\log 2)\log N$, and $N^{-2} \leq N^{-1/2}(\log N)^{5/2}$, which give the second bound. The entry count J enters the allocation through n_N, and $\log K_n = \log J + \log(1 + 4^{-n})$ enters through the union bound. □

Corollary 3 (Expected width)**.** *For $P \neq I$ and $N \geq K_n$, let I_N be the smallest closed interval containing*

$$\{h_P(M) : M \in \mathfrak{M}^U_{\varepsilon,\gamma_{\rm tot}},\ \|G(M) - \widehat{G}\|_{\max} \leq \delta_N\},$$

clipped to $[-\gamma_{\rm tot}, \gamma_{\rm tot}]$, and the whole interval when this set is empty or $N < K_n$. Then I_N is uniformly valid at confidence $1 - \alpha$ over $\mathfrak{M}^U_{\varepsilon,\gamma_{\rm tot}}$, and at every reference M_0 in this class,

$$\mathbb{E}_0|I_N| \leq 2\omega_P(2\delta_N) + 2\gamma_{\rm tot}\zeta_N, \tag{C33}$$

with ω_P the modulus of Theorem 1 for all entries of G at M_0. If M_0 satisfies the hypotheses of Theorem 1, that theorem supplies $C_P, \delta_P > 0$ with $\omega_P(t) \leq C_P t^\kappa$ for

$0 < t \le \delta_P$, *where* $\kappa = 1/2$ *on the square-root branch and* $\kappa = 1$ *on the linear branch; then for* $2\delta_N \le \delta_P$,

$$\mathbb{E}_0|I_N| \le 2C_P(2C_*)^\kappa N^{-\kappa/2}(\log N)^{5\kappa/2} + 2\gamma_{\rm tot}\zeta_N. \quad \text{(C34)}$$

If $\mathrm{wt}\, P = 1$, *Proposition 1 gives* $\mathbb{E}_0|I_N| \le 4\delta_N + 2\gamma_{\rm tot}\zeta_N$ *for every* $N \ge K_n$.

Proof of Corollary 3. Equation (A8) gives $|h_P| \le \|L\|_{\max}$. Hölder's inequality and the norm bound give $|L_{R,Q}| \le d^{-1}\|\mathcal{L}^\dagger(P_R)\|_\infty \|P_Q\|_1 \le \gamma_{\rm tot}$. The finite-valued estimator of Theorem 4 therefore meets Lemma 2 with $H = \gamma_{\rm tot}$ and the full maximum-entry metric. The modulus ω_P over the unrestricted class bounds the targets in the class with bounded strength, proving Eq. (C33).

Substitution of Eq. (C32) and the two branches of Theorem 1 gives Eq. (C34); for weight one, use $\omega_P(t) = t$ from Proposition 1. □

The square-root branch matches the lower-bound power under the width hypotheses of Corollary 1 at the same reference, with its physical path in $\mathfrak{M}^U_{\varepsilon,\gamma_{\rm tot}}$.

Appendix D: Proof of the local precision dichotomy

We prove Theorem 1, Corollary 1, and Proposition 1. After the setup, the reduction bounds the modulus by a positivity problem for the gauge-transformed reference, localization confines its nearly positive points to small $|x|$, and the Schur reduction rewrites near-positivity there as a matrix inequality on $\ker C_0$. First-order coercivity and the second-order margin give the upper bounds and isolation, the lower bound uses the direction of condition (i), and the modulus step combines the two. The remaining steps treat product SPAM channels, the lower bound on the expected length, single-qubit targets, and the two-qubit instances.

Setup. Let $d = 2^n$, $m = 4^n - 1$ and $M = \|L_0\|_{\max}$. For each nonempty support $s \subseteq \{1, \dots, n\}$ let W_s project onto the Pauli labels of support s, and for $x \in \mathbb{R}^{2^n-1}$ put $W(x) = \sum_s x_s W_s$, $S_x = e^{W(x)}$, $w_I = 0$ and $w_R = x_{\mathrm{supp}\, R}$ for $R \ne I$. As $W(x)$ is diagonal, $(S_x L_0 S_x^{-1})_{R,Q} = e^{w_R - w_Q}(L_0)_{R,Q}$ and $[W(x), L_0]_{R,Q} = (w_R - w_Q)(L_0)_{R,Q}$. Let $\mathcal{N} = \{x : [W(x), L_0] = 0\}$, fix a complement V, let π_V project onto V along $\mathcal{N}$, and use the norm $|x| = \max_s |x_s|$ on $\mathbb{R}^{2^n-1}$ and its subspaces; below $x, u, v, y, z \in V$.

For $n_0 \in \mathcal{N}$ every nonzero $(L_0)_{R,Q}$ has $w_R(n_0) = w_Q(n_0)$, so $S_{x+n_0} L_0 S_{x+n_0}^{-1} = S_x L_0 S_x^{-1}$; since $e^r = 1$ only for real $r = 0$, $S_x L_0 S_x^{-1} = L_0$ exactly when $x \in \mathcal{N}$. The maps $S_x^{\pm 1}$ are real, diagonal and fix I, so $S_x L_0 S_x^{-1}$ preserves Hermiticity and annihilates the trace. Its canonical Kossakowski matrix $\widetilde{C}(x)$ and target $\widetilde{h}_P(x)$ are therefore defined. It is physical exactly when $\widetilde{C}(x) \succeq 0$. By linearity of the canonical maps, $\widetilde{C}$ and $\widetilde{h}_P$ are finite exponential sums, hence continuous.

Put $C_1(x) = \mathrm{CanCov}([W(x), L_0])$, $C_2(x) = \frac{1}{2}\mathrm{CanCov}([W(x), [W(x), L_0]])$ and $\ell_P(x) = \mathrm{CanH}_P([W(x), L_0])$. Since $|w_R - w_Q| \le 2|x|$, the scalar bounds $|e^r - 1 - r - r^2/2| \le e^{|r|}|r|^3/6$, $|e^r - 1 - r| \le e^{|r|}r^2/2$ and $|e^r - 1| \le e^{|r|}|r|$, applied entrywise, together with Eqs. (A7) and (A8) and $2^n \le m$, give for $|x| \le 1$

$$\widetilde{C} = C_0 + C_1 + C_2 + R_3, \quad \|R_3(x)\| \le c_3|x|^3,$$
$$\widetilde{h}_P = h_{P,0} + \ell_P + R_h, \quad |R_h(x)| \le c_h|x|^2, \quad \text{(D1)}$$

where $c_3 = \frac{4}{3}e^2 mM$, $c_h = 2e^2 M$. We also have $\|C_1(x)\| \le 2mM|x|$, $\|C_2(x)\| \le 2mM|x|^2$, $\|\widetilde{C}(x) - C_0\| \le L_c|x|$ with $L_c = 2e^2 mM$, and $|\ell_P(x)| \le 2M|x|$. Matrix norms are operator norms.

Let $K = \ker C_0$, Π its projector, $\Pi^\perp = I - \Pi$, C_0^+ the inverse of C_0 on its range extended by zero, and, if $C_0 \ne 0$, a_* the smallest positive eigenvalue of C_0. Put $D = \Pi C_1 \Pi$, $\mathcal{B} = \Pi^\perp C_1 \Pi$ and $Q_2 = \Pi C_2 \Pi - \mathcal{B}^\dagger C_0^+ \mathcal{B}$. The diagonal matrices $W(v), W(w)$ commute, so $Q_2(x) = \mathsf{q}(x, x)$ for the symmetric bilinear $\mathsf{q}(v, w) = \frac{1}{4}\Pi\,\mathrm{CanCov}([W(v), [W(w), L_0]] + [W(w), [W(v), L_0]])\Pi - \frac{1}{2}[\mathcal{B}(v)^\dagger C_0^+ \mathcal{B}(w) + \mathcal{B}(w)^\dagger C_0^+ \mathcal{B}(v)]$, whose first part is the compression of the canonical Kossakowski matrix of a map with transfer entries $\frac{1}{2}(w_R(v) - w_Q(v))(w_R(w) - w_Q(w))(L_0)_{R,Q}$; hence $\|\mathsf{q}(v, w)\| \le c_Q|v||w|$ and, since $Q_2(z + y) - Q_2(z) = 2\mathsf{q}(z, y) + \mathsf{q}(y, y)$, $\|Q_2(z + y) - Q_2(z)\| \le c_Q(2|z||y| + |y|^2)$ with $c_Q = 2mM + 4m^2M^2/a_*$, or $c_Q = 2mM$ if $C_0 = 0$.

The geometric conditions are:

(i) If ℓ_P does not vanish on $\ker D$, there are $u \in \ker D$ with $|u| = 1$ and $\ell_P(u) \ne 0$, $\hat{u} \in u + \mathcal{N}$ and $\theta_{\rm adm} > 0$ such that $(S_{\theta\hat{u}} A_0, B_0 S_{\theta\hat{u}}^{-1})$ is completely positive, trace preserving and jointly within the budget for $0 \le \theta \le \theta_{\rm adm}$; we write $E_u = \{\theta u : 0 \le \theta \le \theta_{\rm adm}\}$.

(ii) With the gauge box $X_\varepsilon = \pi_V\{q : |q| \le \log(1/l)\}$, (G): $x \in X_\varepsilon$ and $\widetilde{C}(x) \succeq 0$ imply $x = 0$.

(iii) (H1) $D(x) \succeq 0$ only if $D(x) = 0$, and (H2) $f(u) = \sup_v \lambda_{\min}[D(v) + Q_2(u)] < 0$ for every unit $u \in \ker D$, eigenvalues being those of operators on K.

The box X_ε is compact, as a continuous image of a compact set, and contains $\{x \in V : |x| \le \log(1/l)\}$, which is a neighbourhood of 0 in V because $\varepsilon > 0$. Every gauge transformation with sector scalars in $[l, l^{-1}]$ is S_q with $|q| \le \log(1/l)$, and $S_q L_0 S_q^{-1} = S_x L_0 S_x^{-1}$ for its projection $x = \pi_V q \in X_\varepsilon$; so condition (ii) of Sec. III is (G). The range $[l, l^{-1}]$ contains every gain ratio b_Q/b'_Q of two admissible readouts, so (G) implies uniqueness among all gauge transformations relating admissible models. If $V \ne \{0\}$, then $K \ne \{0\}$: otherwise $\widetilde{C}(x) \succ 0$ near 0, contradicting (G).

Reduction. Here $\mathfrak{M}_\varepsilon$ denotes class (U); class (P) is treated below. Let $(L, A, B) \in \mathfrak{M}_\varepsilon$ have $\|G - G_0\|_{\max} \le \delta$. The twirled readouts $\bar{B}, \bar{B}_0$ are support scalars with gains $b_Q, b_{0,Q} \in [l, 1]$ and $b_I = b_{0,I} = 1$ (Appendix A), so $\bar{B}^{-1}\bar{B}_0 = S_q$ with $q_s = \log(b_{0,s}/b_s)$, $|q| \le \log(1/l)$, and $x = \pi_V q \in X_\varepsilon$. Since $L = \bar{B}^{-1} G \bar{B}$ and $G_0 = \bar{B}_0 L_0 \bar{B}_0^{-1}$, $L = S_x L_0 S_x^{-1} + \Delta'$ with $\Delta'_{R,Q} = (G - G_0)_{R,Q} b_Q/b_R$, so $\|\Delta'\|_{\max} \le \delta/l$; Δ' preserves Hermiticity and annihilates the trace, as a difference of two such maps. Positivity of $\mathrm{CanCov}(L) = \widetilde{C}(x) + \mathrm{CanCov}(\Delta')$ and Eqs. (A7) and (A8) give $\lambda_{\min}\widetilde{C}(x) \ge -2^n\delta/l$ and $|h_P - \widetilde{h}_P(x)| \le \delta/l$.

Conversely, let $x=\theta u\in E_u$, $t\ge 0$ and $\lambda_{\min}\widetilde{C}(x)\ge -t$, and put $\hat{q}=\theta\hat{u}$, so that $\hat{q}-x\in\mathcal{N}$. The generator $L_t = S_{\hat{q}}L_0S_{\hat{q}}^{-1}+4^nt(\mathcal{D}-\mathrm{id}) = S_xL_0S_x^{-1}+4^nt(\mathcal{D}-\mathrm{id})$ has Kossakowski matrix $\widetilde{C}(x)+tI_m\succeq 0$ and target $\widetilde{h}_P(x)$ by Eq. (A11), so $(L_t, S_{\hat{q}}A_0, B_0S_{\hat{q}}^{-1})\in\mathfrak{M}_\varepsilon$ by (i). The support scalar $S_{\hat{q}}$ commutes with local unitaries, so twirling gives the readout $\bar{B}_0S_{\hat{q}}^{-1}$, and $\mathcal{D}-\mathrm{id}$, $S_{\hat{q}}$ and $\bar{B}_0$ are Pauli diagonal. Hence $G=\bar{B}_0S_{\hat{q}}^{-1}L_tS_{\hat{q}}\bar{B}_0^{-1} = G_0+4^nt(\mathcal{D}-\mathrm{id})$, at entry distance 4^nt; with $t=\delta/4^n$ this model lies within δ of the reference.

Finally, $(L_0+l\delta A_P, A_0, B_0)$ changes only the Hamiltonian, so it is physical, with target $h_{P,0}+l\delta$ by Eq. (A8), and changes G by $l\delta\bar{B}_0A_P\bar{B}_0^{-1}$, whose entries $l\delta(A_P)_{R,Q}b_{0,R}/b_{0,Q}$ are at most δ. With $\omega_C(t;E)=\sup\{|\widetilde{h}_P(x)-h_{P,0}|: x\in E,\ \lambda_{\min}\widetilde{C}(x)\ge -t\}$, therefore, for every $\delta\ge 0$,

$$\max\{\omega_C(\delta/4^n;E_u), l\delta\}\le\omega_P(\delta)\le\omega_C(2^n\delta/l;X_\varepsilon)+\delta/l, \tag{D2}$$

where the first term is included when condition (i) supplies a direction.

Localization. Under (G), for every $\rho>0$ there is $t_0>0$ such that $x\in X_\varepsilon$ and $\lambda_{\min}\widetilde{C}(x)\ge -t_0$ imply $|x|<\rho$. If $F_\rho=\{x\in X_\varepsilon:|x|\ge\rho\}$ is empty, take $t_0=1$. Otherwise F_ρ is compact, (G) makes the continuous function $\lambda_{\min}\widetilde{C}$ negative on it, and $t_0=-\frac{1}{2}\max_{F_\rho}\lambda_{\min}\widetilde{C}>0$ works.

Schur reduction. Let $K\neq\{0\}$. If $C_0\neq 0$, put $A_c=2mM$, $R_c=2mM+c_3$,

$$c_E=c_3+\frac{4A_cR_c+2R_c^2}{a_*}+\frac{2A_c^2(L_c+1)}{a_*^2},$$
$$\rho_1=\min\Big\{1,\frac{a_*}{4L_c}\Big\},\qquad t_1=\min\Big\{1,\frac{a_*}{4}\Big\}; \tag{D3}$$

if $C_0=0$, put $c_E=c_3$ and $\rho_1=t_1=1$. Then, for $|x|\le\rho_1$ and $0\le t\le t_1$, $\lambda_{\min}\widetilde{C}(x)\ge -t$ is equivalent to

$$M_t(x):=D(x)+Q_2(x)+t\Pi+E(x,t)\succeq 0\quad\text{on } K, \tag{D4}$$

with $\|E(x,t)\|\le c_E(|x|^3+t|x|^2)$. If $C_0=0$, then $\Pi=I$, $\mathcal{B}=0$ and $\widetilde{C}+tI=D+Q_2+tI+R_3$, so $E=R_3$.

Otherwise $C_0\neq 0$ gives $M>0$, and on the range of C_0 the block $\mathsf{A}=\Pi^\perp(\widetilde{C}(x)+tI)\Pi^\perp$ satisfies $\mathsf{A}\succeq(a_*-L_c|x|+t)\Pi^\perp\succeq\frac{3}{4}a_*\Pi^\perp$, so $\|\mathsf{A}^{-1}\|\le 2/a_*$ and the resolvent identity $\mathsf{A}^{-1}-C_0^+=-\mathsf{A}^{-1}(\mathsf{A}-C_0)C_0^+$ gives $\|\mathsf{A}^{-1}-C_0^+\|\le 2a_*^{-2}(L_c|x|+t)$. Since $\Pi C_0=0$, $\Pi\widetilde{C}\Pi = D+\Pi C_2\Pi+\Pi R_3\Pi$ and $\Pi^\perp\widetilde{C}\Pi=\mathcal{B}+J$ with $J=\Pi^\perp(C_2+R_3)\Pi$, where $\|\mathcal{B}(x)\|\le A_c|x|$ and $\|J\|\le R_c|x|^2$.

As $\mathsf{A}\succ 0$, congruence with $\left(\begin{smallmatrix} I & -\mathsf{A}^{-1}(\mathcal{B}+J)\\ 0 & I\end{smallmatrix}\right)$ shows that $\widetilde{C}(x)+tI\succeq 0$ if and only if the Schur complement $\Pi(\widetilde{C}+tI)\Pi-(\mathcal{B}+J)^\dagger\mathsf{A}^{-1}(\mathcal{B}+J)$ is positive semidefinite on K. This complement is $M_t(x)$ with $E=\Pi R_3\Pi-\mathcal{B}^\dagger(\mathsf{A}^{-1}-C_0^+)\mathcal{B}-\mathcal{B}^\dagger\mathsf{A}^{-1}J-J^\dagger\mathsf{A}^{-1}\mathcal{B}-J^\dagger\mathsf{A}^{-1}J$, and the bounds above with $|x|\le 1$ give $\|E\|\le[c_3+(4A_cR_c+2R_c^2)/a_*+2A_c^2L_c/a_*^2]|x|^3+2A_c^2a_*^{-2}t|x|^2\le c_E(|x|^3+t|x|^2)$.

First-order coercivity. Write $V=\ker D\oplus V_\perp$ for a fixed complement $V_\perp$, $x=z+y$ accordingly, and let c_π be the norm of the projection $x\mapsto z$; then $D(x)=D(y)$, $|z|\le c_\pi|x|$ and $|x|\le|z|+|y|$. By (H1), $D(y)$ is not positive semidefinite for $y\in V_\perp\setminus\{0\}$; the continuous function $\lambda_{\min}D(y)$ is negative on the compact unit sphere of $V_\perp$, attains a maximum $-c_D<0$ there, and by homogeneity $\lambda_{\min}D(y)\le -c_D|y|$ on $V_\perp$ (take $c_D=1$ if $V_\perp=\{0\}$). By (H1), also $\lambda_{\min}D(v)\le 0$ for every v.

Second-order margin. Let $\ker D\neq\{0\}$. For fixed v, $\lambda_{\min}[D(v)+Q_2(u)]$ changes by at most $\|Q_2(u)-Q_2(u')\|\le c_Q(|u|+|u'|)|u-u'|$ when u is replaced by u', by Weyl's inequality; taking suprema, f obeys the same bound and is continuous, and $|f(u)|\le c_Q|u|^2$ by Weyl's inequality and the choice $v=0$. By (H2), f has a maximum $-\kappa<0$ on the compact unit sphere of $\ker D$. Since $D(v)+Q_2(sz)=s^2[D(v/s^2)+Q_2(z)]$ for $s>0$, $f(sz)=s^2f(z)$; hence $\lambda_{\min}[D(y)+Q_2(z)]\le f(z)\le -\kappa|z|^2$ for $z\in\ker D$ and every y. If $\ker D=\{0\}$, take $\kappa=1$ and $c_\pi=0$.

Upper bounds and isolation. With $a=1/c_D$, $c_4=c_Q+2c_E$ and $b=ac_4$, put $c_5=a+8b(a^2+1)$, $c_6=1+2c_Q(c_5+c_5^2)+c_E(33+32a^3)$, $\rho_2=\min\{\rho_1,1/(2+2b),1/(1+c_\pi),\kappa/(2c_6(1+c_\pi))\}$ and $t_2=t_1$. Let $r=|x|\le\rho_2$, $s=|z|$, $0\le t\le t_2$ and $\lambda_{\min}\widetilde{C}(x)\ge -t$, so that $M_t(x)\succeq 0$ and $\|E\|\le 2c_Er^2$. Weyl's inequality gives $0\le\lambda_{\min}M_t(x)\le -c_D|y|+t+c_4r^2$, so $|y|\le at+br^2$. As $br\le\frac{1}{2}$, $r\le s+at+r/2$, so $r\le 2s+2at$ and, by $(u+v)^2\le 2u^2+2v^2$ and $t\le 1$, $|y|\le at+8b(s^2+a^2t)\le c_5(t+s^2)$. Since $s\le c_\pi r\le 1$, $2s|y|\le 2c_5(t+s^3)$ and $|y|^2\le 2c_5^2(t+s^3)$, so $\|Q_2(x)-Q_2(z)\|\le 2c_Q(c_5+c_5^2)(t+s^3)$; and $(u+v)^3\le 4(u^3+v^3)$ gives $r^3\le 32(s^3+a^3t)$ and $tr^2\le t$. Combining Weyl's inequality, the second-order margin and the bound on E gives

$$\begin{aligned}0\le\lambda_{\min}M_t(x)&\le -\kappa s^2+\|Q_2(x)-Q_2(z)\|\\&\quad+t+\|E(x,t)\|\\&\le -\kappa s^2+c_6(t+s^3).\end{aligned} \tag{D5}$$

As $s\le c_\pi\rho_2\le\kappa/(2c_6)$, $s^2\le 2c_6t/\kappa$. Hence $|z|\le k_z\sqrt{t}$, $|y|\le k_yt$ and $|x|\le k_1\sqrt{t}$ with $k_z=(2c_6/\kappa)^{1/2}$, $k_y=c_5(1+k_z^2)$ and $k_1=k_z+k_y$. By Eq. (D1), $|\widetilde{h}_P(x)-h_{P,0}|\le 2M|x|+c_h|x|^2\le k_2\sqrt{t}$ with $k_2=1+2Mk_1+c_hk_1^2$, and, if ℓ_P vanishes on $\ker D$, $|\widetilde{h}_P(x)-h_{P,0}|=|\ell_P(y)+R_h(x)|\le(2Mk_y+c_hk_1^2)t\le k_2t$. At $t=0$ these bounds give $x=0$, so 0 is isolated in $\{x:\widetilde{C}(x)\succeq 0\}$. The constants depend only on L_0, the complements $V, V_\perp$ and the norm.

Lower bound. Let u and $\hat{u}$ be as in (i), $\Lambda=\|Q_2(u)\|+1$, and let $0<\theta_*\le\theta_{\mathrm{adm}}$ satisfy $\theta_*\le\rho_1$, $\Lambda\theta_*^2\le t_1$, $c_E(\theta_*+\Lambda\theta_*^2)\le 1$ and $c_h\theta_*\le|\ell_P(u)|/2$, for example

$$\theta_*=\min\Big\{\theta_{\mathrm{adm}},\rho_1,\sqrt{\frac{t_1}{\Lambda}},\frac{1}{2(1+c_E)},\frac{1}{\sqrt{2\Lambda(1+c_E)}},\frac{|\ell_P(u)|}{2(1+c_h)}\Big\}. \tag{D6}$$

For $0\le\theta\le\theta_*$, put $x=\theta u$ and $t=\Lambda\theta^2$. Then $D(x)=0$, $Q_2(x)=\theta^2Q_2(u)\succeq-\theta^2\|Q_2(u)\|\Pi$, and $M_t(x)\succeq\theta^2[1-c_E(\theta+\Lambda\theta^2)]\Pi\succeq 0$, so $\widetilde{C}(\theta u)+\Lambda\theta^2I\succeq 0$ by Eq. (D4);

and $|\widetilde{h}_P(\theta u) - h_{P,0}| \geq |\ell_P(u)|\theta - c_h\theta^2 \geq |\ell_P(u)|\theta/2$. For $0 < \delta \leq 4^n\Lambda\theta_*^2$, the choice $\theta = (\delta/(4^n\Lambda))^{1/2}$ and Eq. (D2) give Eq. (9).

Modulus. If $V = \{0\}$, then $\widetilde{C} \equiv C_0$, $\widetilde{h}_P \equiv h_{P,0}$, and Eq. (D2) gives $l\delta \leq \omega_P(\delta) \leq \delta/l$. Otherwise $K \neq \{0\}$; take $\rho = \rho_2$ in the localization and $\delta_0 = \min\{1, l\min\{t_0, t_2\}/2^n\}$. For $0 < \delta \leq \delta_0$, every point counted in $\omega_C(2^n\delta/l; X_\varepsilon)$ has $|x| < \rho_2$, so Eq. (D2) and the upper bounds give $\omega_P(\delta) \leq k_2(2^n\delta/l)^{1/2} + \delta/l \leq (k_2\sqrt{2^n/l} + 1/l)\sqrt{\delta}$, and $\omega_P(\delta) \leq (2^n k_2 + 1)\delta/l$ if ℓ_P vanishes on $\ker D$. If ℓ_P does not vanish on $\ker D$, Eq. (9) gives $\omega_P(\delta) \geq |\ell_P(u)|\sqrt{\delta}/(2^{n+1}\sqrt{\Lambda})$ for $0 < \delta \leq \min\{\delta_0, 4^n\Lambda\theta_*^2\}$; always $\omega_P(\delta) \geq l\delta$. Since C_1 and ℓ_P vanish on $\mathcal{N}$, a solution of Eq. (6) in $\mathbb{R}^{2^n-1}$ projects to an element of $\ker D$ on which ℓ_P does not vanish, and conversely. This proves Theorem 1 in class (U).

If $C_0 = 0$, the reference is linear: canonical uniqueness makes L_0 a Hamiltonian generator with antisymmetric transfer matrix, so $[W(x), L_0]$ is symmetric for the symmetric $W(x)$, its Frobenius pairing with the antisymmetric A_P vanishes, and $\ell_P \equiv 0$.

Product SPAM channels. In class (P), let $\mathsf{Ad} = \{Jy : y \in \mathbb{R}^n\}$ with $(Jy)_s = \sum_{j\in s} y_j$; since $(Jy)_{\{j\}} = y_j$, J is injective and $|Jy|$ is a norm on $\mathbb{R}^n$. Replace $\mathcal{N}$ by $\mathcal{N} \cap \mathsf{Ad}$, V by a complement V^{loc} of it in Ad, X_ε by $X_\varepsilon^{\mathrm{loc}} = \pi_{V^{\mathrm{loc}}}(\mathsf{Ad} \cap \{|q| \leq \log(1/l)\})$, and read (i)–(iii) on V^{loc} with $\hat{u} \in \mathsf{Ad}$. The class enters the proof only through the SPAM channels. In the reduction, product readouts have $b_s = \prod_{j\in s} b_{\{j\}}$ (Appendix A), so $q \in \mathsf{Ad}$ and $x \in X_\varepsilon^{\mathrm{loc}}$. For $\hat{q} = J\hat{y} \in \mathsf{Ad}$, $S_{\hat{q}} = \bigotimes_j F_j$ with $F_j = e^{\hat{y}_j}\mathrm{id} + (1 - e^{\hat{y}_j})\mathcal{D}_j$ and $\mathcal{D}_j$ the single-qubit depolarizer, as both sides scale each Pauli of support s by $e^{\hat{q}_s}$; so $S_{\hat{q}}A_0$ and $B_0S_{\hat{q}}^{-1}$ are tensor products of trace-preserving single-qubit maps, and each factor is completely positive because its normalized Choi matrix is a partial trace of the normalized Choi matrix of the completely positive product. The positive correction and the Hamiltonian perturbation change only the generator. Every other step, including the Taylor and Schur constants, uses the norm $|x|$ and remains valid on Ad.

Lower bound on the expected length. We now prove Corollary 1. Let $u, \hat{u}, \Lambda, \theta_*$ be as in the lower bound, and for $0 \leq \theta \leq \theta_*$ let $M_\theta = (L_t, S_{\theta\hat{u}}A_0, B_0S_{\theta\hat{u}}^{-1})$ with $t = \Lambda\theta^2$, an admissible model with target $\widetilde{h}_P(\theta u)$ by the reduction and lower bound.

Trace annihilation and unitality, $\mathrm{Tr}\, L_0(X) = 0$ and $L_0(I) = 0$, give $\mathcal{D}L_0 = L_0\mathcal{D} = 0$, and support scalars obey $S\mathcal{D} = \mathcal{D}S = \mathcal{D}$, so $S_{\theta\hat{u}}L_0S_{\theta\hat{u}}^{-1}$ commutes with $\mathcal{D} - \mathrm{id}$; $\mathcal{D} - \mathrm{id}$, $S_{\theta\hat{u}}$ and product unitaries also commute pairwise. The two summands of L_t therefore commute, and $e^{r4^n t(\mathcal{D}-\mathrm{id})} = \mathcal{D}_{e^{-4^n tr}}$, with $\mathcal{D}_c = c\,\mathrm{id} + (1-c)\mathcal{D}$, gives each segment of duration $r \geq 0$ the form $e^{rL_t} = S_{\theta\hat{u}}e^{rL_0}S_{\theta\hat{u}}^{-1}\mathcal{D}_{e^{-4^n tr}}$. Multiplying segments and product unitaries, cancelling the internal gauge transformations and using $\mathcal{D}_a\mathcal{D}_b = \mathcal{D}_{ab}$, each controlled evolution of M_θ is $S_{\theta\hat{u}}\mathcal{P}_0S_{\theta\hat{u}}^{-1}\mathcal{D}_c$, $c = e^{-4^n tT}$, where $\mathcal{P}_0$ is the same controlled reference evolution of total duration T, including controls immediately after preparation and before readout; as $S_{\theta\hat{u}}^{-1}\mathcal{D}_cS_{\theta\hat{u}} = \mathcal{D}_c$, the complete experiment is $B_0\mathcal{P}_0\mathcal{D}_cA_0$.

For an input state ρ, $\sigma = A_0(\rho)$ is a density operator, $Y = (\mathrm{id} - \mathcal{D})\sigma = \sigma - I/d$ is traceless with $\|Y\|_2^2 = \mathrm{Tr}\,\sigma^2 - 1/d \leq 1 - 2^{-n}$, and $\mathcal{D}_c\sigma - \sigma = -(1-c)Y$. The terminal states therefore differ by $\Delta\sigma = -(1-c)B_0\mathcal{P}_0(Y)$, and $1-c \leq 4^n tT$ and $Te^{-gT} \leq 1/(eg)$ give $\|\Delta\sigma\|_2 \leq \beta_n\theta^2$, uniformly in T and in the setting.

For orthonormal rank-one projectors E_j, $\|\Delta\sigma - \sum_j \mathrm{Tr}(E_j\Delta\sigma)E_j\|_2^2 = \|\Delta\sigma\|_2^2 - \sum_j \mathrm{Tr}(E_j\Delta\sigma)^2$, so the outcome probabilities $p_{\theta,j}$ of M_θ obey, for $\Delta p_j = p_{\theta,j} - p_{0,j} = \mathrm{Tr}(E_j\Delta\sigma)$, $\sum_j(\Delta p_j)^2 \leq \beta_n^2\theta^4$ and each $|\Delta p_j| \leq \beta_n\theta^2$. For $\theta^2 \leq \mu/(2\beta_n)$ every probability under M_θ is therefore at least $\mu/2$, and Lemma 1, with probability bound $\mu/2$ and $v = \beta_n\theta^2$, bounds the adaptive N-shot relative entropy by $2N\beta_n^2\theta^4/\mu$.

Since $\Lambda \geq 1$ and $\|B_0\|_{2\to 2} \geq 1$ (the adjoint of the trace-preserving B_0 fixes I), β_n and θ_N are positive. The three terms defining θ_N ensure admissibility, the probability bound, and total variation at most $\tau = (1 - 2\alpha)/2$, respectively. The target separation $|\widetilde{h}_P(\theta_N u) - h_{P,0}| \geq |\ell_P(u)|\theta_N/2$ and Eq. (B2) give $\mathbb{E}_0|I_N| \geq (1 - 2\alpha)|\ell_P(u)|\theta_N/4$. This proves Corollary 1; for fixed reference and α, $\theta_N = \Theta(N^{-1/4})$. In class (P), $\hat{u} \in \mathsf{Ad}$ keeps M_θ in the class.

Single-qubit targets. If P has weight one on qubit j, a nonzero $(A_P)_{R,Q}$ needs Q to anticommute with P, so $Q_j \notin \{I, P_j\}$, and $R \propto PQ$ then differs from Q only at qubit j, where it is the third nonidentity Pauli; hence $\mathrm{supp}\, R = \mathrm{supp}\, Q$. For every invertible support scalar S, Eq. (A5) gives $\mathrm{CanH}_P(SXS^{-1}) = \mathrm{CanH}_P(X)$. Applied to $G = \bar{B}L\bar{B}^{-1}$, this gives $h_P = \mathrm{CanH}_P(G)$, so Eq. (A8) gives $|h_P(M) - h_{P,0}| \leq \|G_M - G_0\|_{\max}$ for every model. The physical model $(L_0 + \delta A_P, A_0, B_0)$ has target $h_{P,0} + \delta$ and $G_M - G_0 = \delta\bar{B}_0A_P\bar{B}_0^{-1} = \delta A_P$, whose entries are 0 and $\pm\delta$. This proves Proposition 1 for every $\delta \geq 0$; the model keeps the reference SPAM channels, so the same holds in class (P).

Kossakowski kernels in the Pauli basis. Diagonal gauge transformations leave diagonal transfer entries unchanged, and by Eq. (A10) these entries determine the Kossakowski diagonal for every Hermitian Kossakowski matrix and Hamiltonian. Hence $\widetilde{C}_{aa}(x) = (C_0)_{aa}$ for all x, and C_1, C_2 have zero diagonal. If $K = \mathrm{span}\{e_a : a \in \mathcal{Z}\}$ for a set $\mathcal{Z}$ of Pauli labels, with e_a the coordinate unit vector of label a, then $D(x)$ and $\Pi C_2(x)\Pi$ are principal submatrices with zero diagonal; a positive semidefinite matrix with zero diagonal vanishes, so (H1) holds. If moreover $\mathcal{B}(u) \neq 0$ for every nonzero $u \in \ker D$, then for every unit $u \in \ker(D|_V)$ and every $v \in V$, $\mathrm{tr}[D(v) + Q_2(u)] = -\,\mathrm{tr}\,\mathcal{B}(u)^\dagger C_0^+\mathcal{B}(u) < 0$, because C_0^+ is positive definite on the range of C_0, which contains that of $\mathcal{B}(u)$. Hence $\lambda_{\min}[D(v) + Q_2(u)] \leq -|\mathcal{Z}|^{-1}\,\mathrm{tr}\,\mathcal{B}(u)^\dagger C_0^+\mathcal{B}(u)$ uniformly in v, and (H2) holds.

Two-qubit instances. In the remainder of this appendix, $n = 2$ and $\mathcal{D}_r$ is the two-qubit SPAM channel of Sec. IV B.

Target derivative. Proposition 2(iii), proved in Appendix E, specializes the general derivative to Eq. (12) for every complex Kossakowski matrix, with $\alpha_g = x_{12} - x_1$

and $\beta_g = x_{12} - x_2$. A local field term $-i[\frac{1}{2}h_a P_a, \cdot]$, with P_a of weight one, sends a Pauli Q to zero when they commute and otherwise to a multiple of P_aQ; then Q is nontrivial on the qubit of P_a, so P_aQ has the support of Q. Such terms are block diagonal in the support sectors, commute with every S_x and $W(x)$, and add neither Kossakowski coefficients nor h_{ZZ}; they leave $\widetilde{C}$, $\widetilde{h}$, C_1, C_2 and ℓ unchanged.

Structured references. Let L_0 be the reference of Eq. (14) with general $\lambda, m > 0$, $\lambda m > k^2$, $k \neq 0$ and $|h_0| > 2|k|$, with arbitrary local fields and SPAM channels $\mathcal{D}_r$, $r = 1 - \varepsilon/8$. Its Kossakowski matrix is supported on the six single-qubit labels and YZ, where it is positive definite because $\lambda > 0$ and $\lambda m > k^2$; the kernel has a Pauli coordinate basis, and (H1) holds. By the preceding derivative calculation, local fields leave $\widetilde{C}(x)$ and $\widetilde{h}(x)$ unchanged, so these are given by Eq. (G1) with $\alpha_g = x_{12} - x_1$ and $\beta_g = x_{12} - x_2$. Its only coordinates within the kernel block, $v_1 = -v_2 = -\frac{k}{2}\sinh\alpha_g$, give $D(x) = 0$ exactly when $x_{12} = x_1$. The common scaling $\mathbf{1} = (1,1,1)$ lies in $\mathcal{N}$ because $W(\mathbf{1}) = \mathrm{id} - \mathcal{D}$ commutes with the unital L_0, so $\ker D$ is spanned by the class of $e_2 = (0,1,0)$ modulo $\mathcal{N}$, that is, by its projection to V, with $W(e_2) = W_2$, $\ell(e_2) = -k \neq 0$ and $\mathcal{B}(e_2)_{YI,XZ} = h_0/4 \neq 0$. The kernel criterion gives (H2), and Eq. (6) holds.

The identification argument of Appendix G uses only these canonical coordinates and excludes every nonzero (α_g, β_g), so (G) holds for every ε. The SPAM channels $\mathcal{D}_r$ are interior: for $x \in \mathbb{R}^3$, $S_x\mathcal{D}_r$ and $\mathcal{D}_r S_x^{-1}$ are Pauli diagonal and trace preserving, with Pauli-mixture weights continuous in x and positive at $x = 0$, and with joint budget continuous in x and equal to $15\varepsilon/32 < \varepsilon$ at $x = 0$; and $\mathcal{D}_r(\sigma) \succeq (1-r)I/4$ gives outcome probabilities at least $\varepsilon/32$.

Finally, subtracting $c = (\lambda - k^2/m)/2$ from the six single-qubit diagonals leaves a real positive semidefinite Kossakowski matrix, since the (XI, YZ) block then has determinant $(\lambda m - k^2)/2 > 0$. As in Appendix H, the extracted local Pauli noise gives $\mathrm{Re}\langle X, L_0(X)\rangle \leq -4c\|X\|_2^2$ on traceless X, the Hermitian-jump remainder and the Hamiltonian contributing at most zero, and local unitaries preserve $\|X\|_2$. The reference therefore satisfies conditions (i)–(iii) and is unital with mixing gap $4c$, and Theorem 1 and Corollary 1 apply.

Appendix E: Target derivative from signed sums of real Kossakowski coefficients

We prove Proposition 2: after character sums and active pairs, the transfer-pair form gives the first equality in Eq. (11), the symmetric parts and a grouping by support give the second, and parts (i)–(iii) follow.

Let p be the label of P, let $a \oplus b$ denote the phase-free product label, and define $\chi_a(Q) \in \{\pm 1\}$ by $P_aP_QP_a = \chi_a(Q)P_Q$. Conjugation by P_aP_b equals conjugation by $P_{a\oplus b}$, so $\chi_{a\oplus b} = \chi_a\chi_b$; also $\chi_a(Q) = \chi_Q(a)$.

Character sums. For every label e, $\sum_Q \chi_e(Q) = d^2\mathbf{1}\{e = I\}$: the sum factorizes over qubits, and a qubit contributes 4 where e acts as I and $1 + 1 - 1 - 1 = 0$ elsewhere. Inserting the indicator $[1 - \chi_p(Q)]/2$ of $\mathcal{A}_p = \{Q : \chi_p(Q) = -1\}$ gives

$$\sum_{Q\in\mathcal{A}_p} \chi_e(Q) = \frac{d^2}{2}\big(\mathbf{1}\{e = I\} - \mathbf{1}\{e = p\}\big). \tag{E1}$$

For a support s, the same factorization over the qubits of s, where a qubit outside $\mathrm{supp}\, e$ contributes 3 and a qubit inside contributes $1-1-1 = -1$, gives $\sum_{\mathrm{supp}\, Q = s} \chi_e(Q) = 3^{|s\setminus \mathrm{supp}\, e|}(-1)^{|s\cap \mathrm{supp}\, e|}$. Since $w_I = 0$ and $w_Q = x_{\mathrm{supp}\, Q}$,

$$\sum_Q \chi_e(Q) w_Q = \widehat{w}(\mathrm{supp}\, e). \tag{E2}$$

Active pairs. By Eq. (E1) with $e = I$, $|\mathcal{A}_p| = d^2/2$. The map $Q \mapsto p \oplus Q$ preserves $\mathcal{A}_p$ and has no fixed point, so $\mathcal{A}_p$ splits into 4^{n-1} unordered pairs $\{Q, R\}$ with $R = p \oplus Q$. The map $-i[P/2, \cdot]$ annihilates P_Q for $Q \notin \mathcal{A}_p$ and sends P_Q, $Q \in \mathcal{A}_p$, to $-iPP_Q = \pm P_R$; thus $(A_P)_{R,Q} = \pm 1$, and $(A_P)_{Q,R} = -(A_P)_{R,Q}$ because $(-i[P/2, \cdot])^2 P_Q = -P_Q$. With the orientation $(A_P)_{R,Q} = +1$ we have $PP_Q = iP_R$, hence $P_RP_Q = -iP$, $P_QP_R = iP$, $d^{-1}\,\mathrm{Tr}(P_RP_QP) = -i$ and $d^{-1}\,\mathrm{Tr}(P_QP_RP) = i$.

Transfer-pair form. The map $X = [W(x), L_0]$ preserves Hermiticity because $W(x)$ is a real diagonal map, and it annihilates the trace because $\mathrm{Tr} \circ W(x) = 0$ and $\mathrm{Tr} \circ L_0 = 0$. Equation (A5) gives $\ell_P(x) = (2/d^2)\langle A_P, X\rangle$. Since $X_{R,Q} = (w_R - w_Q)(L_0)_{R,Q}$, an oriented pair contributes $X_{R,Q} - X_{Q,R} = (w_R - w_Q)[(L_0)_{R,Q} + (L_0)_{Q,R}]$, which proves the first equality in Eq. (11).

Symmetric parts. Fix an oriented active pair. Every dissipative anticommutator term vanishes at both entries, because $\mathrm{Tr}(P_R\{F, P_Q\}) = \mathrm{Tr}(\{P_Q, P_R\}F) = 0$. The Hamiltonian part has antisymmetric transfer matrix, since cyclicity gives $\mathrm{Tr}(P_Q[H, P_R]) = -\mathrm{Tr}(P_R[H, P_Q])$, and does not enter M_{RQ}. A jump term $C_{ab}P_a(\cdot)P_b$ contributes $C_{ab}d^{-1}\,\mathrm{Tr}(P_RP_aP_QP_b)$ to $(L_0)_{R,Q}$, which vanishes unless $a \oplus b = p$ because $P_RP_aP_QP_b$ has label $p \oplus a \oplus b$. Then $a \neq b$; write $P_aP_b = \omega P$ with $\omega \in \{\pm 1, \pm i\}$. Using $P_aP_Q = \chi_a(Q)P_QP_a$ and $\chi_b(Q) = \chi_a(Q)\chi_p(Q) = -\chi_a(Q)$, the terms (a, b) and (b, a), with $C_{ba} = \overline{C}_{ab}$, contribute

$$-i\chi_a(Q)(\omega C_{ab} - \overline{\omega C_{ab}}) = 2\chi_a(Q)\,\mathrm{Im}(\omega C_{ab}) \tag{E3}$$

to $(L_0)_{R,Q}$ and, by the same steps with $d^{-1}\,\mathrm{Tr}(P_QP_RP) = i$, $-2\chi_a(R)\,\mathrm{Im}(\omega C_{ab})$ to $(L_0)_{Q,R}$. Since $p = a \oplus b$, $\chi_a(R) = \chi_a(p)\chi_a(Q) = \chi_a(b)\chi_a(Q)$. If P_a, P_b anticommute, then $\omega = i\tau_{ab}$, $\chi_a(R) = -\chi_a(Q)$ and $\mathrm{Im}(\omega C_{ab}) = \tau_{ab}\,\mathrm{Re}\, C_{ab}$, so both entries receive $2\tau_{ab}\,\mathrm{Re}\, C_{ab}\chi_a(Q)$. If they commute, then $\omega = \pm 1$, $\chi_a(R) = \chi_a(Q)$, and the two contributions cancel in M_{RQ}. The anticommuting pairs with $a \oplus b = p$ are the $\{a, a \oplus p\}$ with $a \in \mathcal{A}_p$, since $\chi_a(a \oplus p) = \chi_a(p)$; neither endpoint is I or p, and the involution $a \mapsto a \oplus p$ shows that there are 4^{n-1} of them. These are the P-pairs. Index the oriented active

pairs by i and the P-pairs by j, and put $m_i = M_{R_iQ_i}$, $v_j = \tau_{a_jb_j} \operatorname{Re} C_{a_jb_j}$ and $Z_{ij} = \chi_{a_j}(Q_i)$. We have shown

$$\boldsymbol{m} = 2Z\boldsymbol{v}. \tag{E4}$$

For $e = a_j \oplus a_k$, $\chi_e(p) = \chi_{a_j}(p)\chi_{a_k}(p) = 1$, so $\chi_e(R_i) = \chi_e(Q_i)$, and Eq. (E1) gives $(Z^{\mathsf{T}}Z)_{jk} = \sum_i \chi_e(Q_i) = \frac{1}{2}\sum_{Q\in\mathcal{A}_p} \chi_e(Q) = 4^{n-1}(\mathbf{1}\{e = I\} - \mathbf{1}\{e = p\})$. Here $e = I$ exactly when $j = k$, and $e = p$ would give $a_k = b_j$, the same pair. Hence $Z^{\mathsf{T}}Z = 4^{n-1}I$. For two qubits and $P = ZZ$, with the active pairs ordered as in Eq. (13) and the P-pairs as in part (iii), $Z\operatorname{diag}(\tau)$ is the matrix of Eq. (I7).

Grouping real Kossakowski coefficients by support. For a P-pair, $\chi_a(R_i) = -\chi_a(Q_i)$ and $\chi_p\chi_a = \chi_b$, so Eq. (E2) gives

$$\begin{aligned}\sum_i \chi_a(Q_i)(w_{R_i} - w_{Q_i}) &= -\sum_{Q\in\mathcal{A}_p} \chi_a(Q) w_Q \\ &= -\frac{1}{2}\sum_Q [1 - \chi_p(Q)]\chi_a(Q) w_Q \\ &= \frac{1}{2}\big[\widehat{w}(\operatorname{supp} b) - \widehat{w}(\operatorname{supp} a)\big].\end{aligned} \tag{E5}$$

Inserting Eq. (E4) into the transfer-pair form yields

$$\ell_P(x) = \frac{4}{d^2}\sum_{P\text{-pairs}} \tau_{ab} \operatorname{Re} C_{ab}\big[\widehat{w}(\operatorname{supp} b) - \widehat{w}(\operatorname{supp} a)\big], \tag{E6}$$

and grouping the terms by endpoint support gives the second equality in Eq. (11). Only $\operatorname{Re} C$ on P-pairs enters.

Part (i). Each P-pair contributes once with each sign, so $\sum_S \Upsilon^P_S = 0$, and $\Upsilon^P_\varnothing = 0$. Put $F_{sS} = 3^{|s\setminus S|}(-1)^{|s\cap S|}$ for $s, S \subseteq [n]$. Ordering each membership bit as $(0, 1)$, $F = B^{\otimes n}$ with $B = \left(\begin{smallmatrix} 1 & 1 \\ 3 & -1 \end{smallmatrix}\right)$, and $B^2 = 4I_2$ gives $F^2 = 4^n I$. For $s \neq \varnothing$ the coefficient of x_s in Eq. (11) is $(4/d^2)(F\Upsilon^P)_s$, while $(F\Upsilon^P)_\varnothing = \sum_S \Upsilon^P_S = 0$. Hence $\ell_P \equiv 0$ exactly when $F\Upsilon^P = 0$, that is, when $\Upsilon^P = 0$.

Part (ii). Let $x_s = \sum_{j\in s} y_j$, and put $g_k = -1$ for $k \in S$ and $g_k = 3$ for $k \notin S$. Writing $s = \{j\} \cup t$ with $t \subseteq [n] \setminus \{j\}$,

$$\widehat{w}(S) = \sum_s \sum_{j\in s} y_j \prod_{k\in s} g_k = \sum_j y_j g_j \prod_{k\neq j}(1 + g_k). \tag{E7}$$

The factor $1 + g_k$ vanishes for $k \in S \setminus \{j\}$, so $\widehat{w}(S) = 0$ for $|S| \geq 2$ and $\widehat{w}(\{j\}) = -4^{n-1}y_j$. With $\Upsilon^P_\varnothing = 0$, Eq. (11) gives $\ell_P = -\sum_j y_j \Upsilon^P_{\{j\}}$. If a P-pair has an endpoint a acting on qubit j alone, then a anticommutes with P, so $j \in \operatorname{supp} P$ and a differs from p at j; its partner $a \oplus p$ carries the third Pauli at j and agrees with p elsewhere, so it has support $\operatorname{supp} P$. For $\operatorname{wt} P \geq 2$ this partner acts on more than one qubit, so each P-pair has at most one such endpoint; orienting it first, the pair contributes $-\tau_{ab} \operatorname{Re} C_{ab}$ to $\Upsilon^P_{\{j\}}$, and no other pair contributes. For $\operatorname{wt} P = 1$ the two labels of every P-pair agree off $\operatorname{supp} P$ and are nonidentity on it, so they have equal supports and $\Upsilon^P = 0$.

Part (iii). For $P = ZZ$, $XY = iZ$ and $YX = -iZ$ give $\tau = (1, -1, 1, -1)$ on the four listed pairs, which exhaust the $4^{n-1} = 4$ P-pairs. Direct evaluation gives $\widehat{w}(\{1\}) = -x_1 + 3x_2 - 3x_{12}$, $\widehat{w}(\{2\}) = 3x_1 - x_2 - 3x_{12}$ and $\widehat{w}(\{1, 2\}) = -x_1 - x_2 + x_{12}$, so $\widehat{w}(\{1, 2\}) - \widehat{w}(\{1\}) = 4\beta_g$ and $\widehat{w}(\{1, 2\}) - \widehat{w}(\{2\}) = 4\alpha_g$ with $\alpha_g = x_{12} - x_1$ and $\beta_g = x_{12} - x_2$. With $4/d^2 = 1/4$, Eq. (E6) becomes $\ell = (U_1 - U_2)\beta_g + (U_3 - U_4)\alpha_g$, and $\Upsilon^{ZZ}_{\{1\}} = U_2 - U_1$, $\Upsilon^{ZZ}_{\{2\}} = U_4 - U_3$.

Contributing correlations. Equation (E6) shows that a pair can contribute only if its real Kossakowski coefficient is nonzero and its supports differ. Distinct pair contributions may cancel in the signed Kossakowski sums for each support.

Appendix F: Many-body references

We prove Proposition 3 by verifying the hypotheses of Theorem 1 for the many-body reference, using the criterion proved in Appendix D: if $\ker C_0$ is spanned by Pauli coordinate vectors, then (H1) holds; if additionally $\mathcal{B}$ is injective on $\ker(D|_V)$, then (H2) holds. With c and Λ defined below, the bound is

$$\omega_P(\delta) \geq \frac{|k|\sqrt{\delta}}{2^{n+1}c\sqrt{\Lambda}}, \qquad \Lambda = 1 + \frac{\max\{h^2, 4k^2\}}{16\lambda c^2}. \tag{F1}$$

Proof of Proposition 3. Write $T = Z_2 \cdots Z_w$, $y = Y_1$, $f = X_1T$ and $z = Z_1$, so $P = zT$ and $b = yT$. The occupied labels are the $3n$ single-qubit labels and b; C_0 is positive definite on their span, since its only coupled block $\left(\begin{smallmatrix} \lambda & k \\ k & m_0 \end{smallmatrix}\right)$ is, and it vanishes elsewhere, so K has this form. As P_a and P_b anticommute with $P_aP_b = iP$, the anticommutator terms of the (a, b) correlation cancel, and

$$\begin{aligned} L_0 &= L_{\mathrm{diag}} + h\mathcal{A}_P + kJ_1, \qquad \mathcal{A}_P = -i[P/2, \cdot], \\ J_1(X) &= P_aXP_b + P_bXP_a, \end{aligned} \tag{F2}$$

with L_{diag} the dissipator of the Kossakowski diagonal. Each diagonal Pauli dissipator annihilates I, and $J_1(I) = \{P_a, P_b\} = 0$, so $L_0(I) = 0$. By Eq. (A10), $\widetilde{C}(x)$ has the diagonal of C_0, and $C_1(x)$, $C_2(x)$ have zero diagonal. The canonical coefficients of L_0 lie in the identity sector and the sector p, so sector preservation (Appendix A) gives $\widetilde{C}_{\alpha\beta}(x) = 0$ for $\alpha \neq \beta$ with $\alpha \oplus \beta \neq p$ and $\widetilde{h}_Q(x) = 0$ for $Q \neq I, P$; the same holds for the canonical coefficients of $[W(x), L_0]$.

(G). Let $\widetilde{C}(x) \succeq 0$. Unoccupied labels have zero diagonal, so their rows vanish. Two single-qubit labels have product of weight at most $2 < w$, and the only single-qubit label α with $\alpha \oplus b = p$ is a, so $\{a, b\}$ is the only pair of distinct occupied labels in the sector p. Hence the only off-diagonal entries are $\widetilde{C}_{ab} = \zeta$ and $\widetilde{C}_{ba} = \bar{\zeta}$. Put $\widetilde{L}(x) = S_xL_0S_x^{-1}$. As S_x fixes I, $\widetilde{L}(x)(I) = S_xL_0(I) = 0$; the (a, b) correlation contributes $\zeta[P_a, P_b] + \bar{\zeta}[P_b, P_a] = -4\operatorname{Im}(\zeta)P$, and the other terms annihilate I, so $\zeta = \tilde{k}$ is real and $\widetilde{L}(x) = L_{\mathrm{diag}} + \tilde{h}\mathcal{A}_P + \tilde{k}J_1$

by canonical uniqueness. Pauli multiplication gives $\mathcal{A}_P(P_a) = P_b$, $\mathcal{A}_P(P_b) = -P_a$, $\mathcal{A}_P(P_y) = -P_f$, $\mathcal{A}_P(P_f) = P_y$, $J_1(P_a) = 2P_b$, $J_1(P_b) = 2P_a$, $J_1(P_y) = 2P_f$ and $J_1(P_f) = 2P_y$. The labels a, y have support $\{1\}$ and b, f have support $[w]$, so with $\varrho = e^{x_{[w]} - x_{\{1\}}}$ the four entries at (b,a), (y,f), (a,b), (f,y) give

$$\begin{aligned} \tilde{h} + 2\tilde{k} &= \varrho(h + 2k) = \varrho^{-1}(h + 2k), \\ -\tilde{h} + 2\tilde{k} &= \varrho^{-1}(2k - h) = \varrho(2k - h). \end{aligned} \tag{F3}$$

Thus $(\varrho - \varrho^{-1})(h + 2k) = (\varrho - \varrho^{-1})(h - 2k) = 0$; subtracting gives $4k(\varrho - \varrho^{-1}) = 0$, so $\varrho = 1$ since $k \neq 0$, and then $\tilde{h} = h$, $\tilde{k} = k$. Hence $S_x L_0 S_x^{-1} = L_0$, every nonzero entry has $e^{w_R - w_Q} = 1$, and $x \in \mathcal{N}$. This conclusion holds for arbitrary h.

Injectivity. Let $D(x) = \mathcal{B}(x) = 0$ and $J = [W(x), L_0]$, which preserves Hermiticity, annihilates the trace and satisfies $J(I) = 0$. As $C_1(x)$ is Hermitian, it is supported on occupied labels; with zero diagonal and the sector restriction, its only entries are at (a,b) and (b,a), and $J(I) = 0$ makes them real, as above. Thus $J = \dot{h}\mathcal{A}_P + \dot{k}J_1$. With $\Delta = x_{[w]} - x_{\{1\}}$, $J_{R,Q} = (w_R - w_Q)(L_0)_{R,Q}$ gives at the same four entries $\dot{h} + 2\dot{k} = \Delta(h + 2k) = -\Delta(h + 2k)$ and $-\dot{h} + 2\dot{k} = -\Delta(2k - h) = \Delta(2k - h)$, so $\Delta(h + 2k) = \Delta(h - 2k) = 0$, $\Delta = 0$ and $\dot{h} = \dot{k} = 0$. Hence $J = 0$ and $x \in \mathcal{N}$. Conversely, $x \in \mathcal{N}$ gives $C_1(x) = 0$. So $\ker D \cap \ker \mathcal{B} = \mathcal{N}$, $\mathcal{B}$ is injective on $\ker(D|_V)$, and the kernel criterion gives (H1) and (H2).

A direction satisfying the criterion. Let E_1 project onto Pauli strings that act as I on qubit 1. Then $W(q) = \mathrm{id} - E_1$ and $S_{sq} = E_1 + e^s(\mathrm{id} - E_1)$, which commutes with L_{diag}. Put $J_2(X) = P_y X P_f + P_f X P_y$ and $J_3(X) = i(P_z X P_T - P_T X P_z)$; these are the dissipative maps of $C_{yf} = C_{fy} = 1$ and of $C_{zT} = i$, $C_{Tz} = -i$, whose anticommutator terms cancel because P_y, P_f anticommute and P_z, P_T commute. For an operator $\mathcal{R}$ on qubits $2, \ldots, n$, set $K_{\mathcal{R}} = -i[P_T, \mathcal{R}]$ and $N_{\mathcal{R}} = \{P_T, \mathcal{R}\}$. Pauli multiplication on qubit 1 gives

	$\mathcal{A}_P$	J_1	J_2	J_3
$I \otimes \mathcal{R}$	$\frac{1}{2} Z \otimes K_{\mathcal{R}}$	$Z \otimes K_{\mathcal{R}}$	$-Z \otimes K_{\mathcal{R}}$	$Z \otimes K_{\mathcal{R}}$
$Z \otimes \mathcal{R}$	$\frac{1}{2} I \otimes K_{\mathcal{R}}$	$-I \otimes K_{\mathcal{R}}$	$I \otimes K_{\mathcal{R}}$	$I \otimes K_{\mathcal{R}}$
$X \otimes \mathcal{R}$	$\frac{1}{2} Y \otimes N_{\mathcal{R}}$	$Y \otimes N_{\mathcal{R}}$	$Y \otimes N_{\mathcal{R}}$	$-Y \otimes N_{\mathcal{R}}$
$Y \otimes \mathcal{R}$	$-\frac{1}{2} X \otimes N_{\mathcal{R}}$	$X \otimes N_{\mathcal{R}}$	$X \otimes N_{\mathcal{R}}$	$X \otimes N_{\mathcal{R}}$

(F4)

Conjugation by S_{sq} multiplies the image of the first row by e^s and of the second by e^{-s} and leaves the last two rows unchanged. Matching rows shows $S_{sq} L_0 S_{sq}^{-1} = L_{\mathrm{diag}} + g\mathcal{A}_P + \alpha J_1 + \beta J_2 + \gamma J_3$ with

$$\begin{aligned} g &= \tfrac{h}{2}(1 + \cosh s) + k \sinh s, \\ \alpha &= \tfrac{k}{2}(1 + \cosh s) + \tfrac{h}{4} \sinh s, \\ \beta &= \tfrac{k}{2}(1 - \cosh s) - \tfrac{h}{4} \sinh s, \\ \gamma &= \tfrac{h}{4}(\cosh s - 1) + \tfrac{k}{2} \sinh s, \end{aligned} \tag{F5}$$

since the four rows require $g/2 + \alpha - \beta + \gamma = e^s(h/2 + k)$, $g/2 - \alpha + \beta + \gamma = e^{-s}(h/2 - k)$, $g/2 + \alpha + \beta - \gamma = h/2 + k$ and $-g/2 + \alpha + \beta + \gamma = k - h/2$. By canonical uniqueness, $\widetilde{h}_P(sq) = g$, $\widetilde{C}_{ab} = \alpha$, $\widetilde{C}_{yf} = \beta$, $\widetilde{C}_{zT} = i\gamma$, with their conjugates, and the diagonal is unchanged. Differentiating at $s = 0$ gives $\ell_P(q) = k$ and the only possibly nonzero entries $C_1(q)_{ab} = h/4$, $C_1(q)_{yf} = -h/4$ and $C_1(q)_{zT} = ik/2$, with conjugates. The labels f and T, of weights w and $w - 1 \geq 2$ and different from b, are unoccupied, while a, b, y, z are occupied. Hence $D(q) = 0$ and $\mathcal{B}(q) = -\frac{h}{4}|y\rangle\langle f| + \frac{ik}{2}|z\rangle\langle T| \neq 0$. The second derivatives give $C_2(q)_{ab} = k/4$, $C_2(q)_{yf} = -k/4$ and $C_2(q)_{zT} = ih/8$, each with an occupied endpoint, so $\Pi C_2(q)\Pi = 0$; with $C_0^+|y\rangle = \lambda^{-1}|y\rangle$ and $C_0^+|z\rangle = \lambda^{-1}|z\rangle$, $Q_2(q) = -\frac{h^2}{16\lambda}|f\rangle\langle f| - \frac{k^2}{4\lambda}|T\rangle\langle T|$. For $n_0 \in \mathcal{N}$, $W(n_0)$ commutes with $W(x)$ and L_0, so $S_{x+n_0} L_0 S_{x+n_0}^{-1} = S_x L_0 S_x^{-1}$, and C_1, C_2, ℓ_P and Q_2 are constant along $\mathcal{N}$. As $\ell_P(q) = k \neq 0$, $q \notin \mathcal{N}$ and $c = \|\pi_V q\|_\infty > 0$. The vectors $u = \pi_V q/c$ and $\hat{u} = q/c$ satisfy $u \in \ker(D|_V)$, $\|u\|_\infty = 1$, $\hat{u} - u \in \mathcal{N}$, $\ell_P(u) = k/c$ and $Q_2(u) = Q_2(q)/c^2$, so $\Lambda = 1 + \max\{h^2, 4k^2\}/(16\lambda c^2)$.

SPAM channels. For $0 \leq p \leq 1$, $\mathcal{D}_p^{(1)} = \frac{1+3p}{4}\mathrm{id} + \frac{1-p}{4}\sum_{\sigma \in \{X,Y,Z\}} \mathrm{Ad}_{\sigma_1}$ is a Pauli channel. So is $\mathcal{D}_p^{(1)} \otimes \mathrm{id}$, with identity coefficient $p_I = (1+3p)/4$, and the Pauli-channel diamond distance $2(1 - p_I)$ derived before Eq. (H9) in Appendix H gives $\|\mathcal{D}_p^{(1)} \otimes \mathrm{id} - \mathrm{id}\|_\diamond = \frac{3}{2}(1-p)$. Now $S_{sq} A_0 = \mathcal{D}_{re^s}^{(1)} \otimes \mathrm{id}$ and $B_0 S_{sq}^{-1} = \mathcal{D}_{re^{-s}}^{(1)} \otimes \mathrm{id}$. For $0 \leq s \leq \log(1/r)$, both parameters lie in $[r^2, 1]$, so both maps are CPTP, with summed diamond distances $\frac{3}{2}(1 - re^s) + \frac{3}{2}(1 - re^{-s}) = 3(1 - r\cosh s) \leq 3(1 - r) = \varepsilon$. As $S_{\theta\hat{u}} = S_{(\theta/c)q}$, condition (i) holds with $\theta_{\mathrm{adm}} = c\log(1/r) > 0$, positive because $\varepsilon > 0$. The reference satisfies conditions (i)–(iii) with $\ell_P(u) \neq 0$. Theorem 1, with its lower bound Eq. (9) for sufficiently small δ, gives $\omega_P(\delta) = \Theta(\sqrt{\delta})$ and Eq. (F1).

Appendix G: Full physical construction and exact identification

We derive the canonical coefficients of every gauge transformation of the reference in Eq. (14), prove that the exact data identify its target, and construct the physical path used in Theorem 2. The last subsection treats Remark 1 and a positive noise background.

1. Canonical decomposition of the gauge-transformed reference

For the structured reference, let $h = h_0$, and define $\alpha_g = \log(s_{12}/s_1)$, $\beta_g = \log(s_{12}/s_2)$. The only off-diagonal transfer entries of L_0 are the four reciprocal pairs in Eq. (13). Their antisymmetric parts are $h(1, -1, 1, -1)$ and their symmetric parts are $2k(1, 1, 1, -1)$. Apply the hyperbolic transformation in Eq. (A12) to the first two pairs with α_g and to the last two with β_g.

Write the real Kossakowski coordinates as $u_1 = C^{\mathrm{Re}}_{XI,YZ}$, $u_2 = C^{\mathrm{Re}}_{YI,XZ}$, $u_3 = C^{\mathrm{Re}}_{IX,ZY}$, $u_4 = C^{\mathrm{Re}}_{IY,ZX}$, and the imaginary coordinates as $v_0 = C^{\mathrm{Im}}_{ZI,IZ}$, $v_1 = C^{\mathrm{Im}}_{XX,YY}$, $v_2 = C^{\mathrm{Im}}_{XY,YX}$. The complete canonical inverse is

$$\begin{aligned}
\widetilde{h} &= \tfrac{h}{2}(\cosh\alpha_g + \cosh\beta_g) + k\sinh\beta_g,\\
u_1 &= \tfrac{k}{2}(\cosh\alpha_g + \cosh\beta_g) + \tfrac{h}{4}\sinh\beta_g,\\
u_2 &= \tfrac{k}{2}(\cosh\alpha_g - \cosh\beta_g) - \tfrac{h}{4}\sinh\beta_g,\\
u_3 &= \tfrac{h}{4}\sinh\alpha_g, \qquad u_4 = -\tfrac{h}{4}\sinh\alpha_g,\\
v_0 &= \tfrac{h}{4}(\cosh\beta_g - \cosh\alpha_g) + \tfrac{k}{2}\sinh\beta_g,\\
v_1 &= -\tfrac{k}{2}\sinh\alpha_g, \qquad v_2 = \tfrac{k}{2}\sinh\alpha_g.
\end{aligned} \tag{G1}$$

The Kossakowski diagonal is unchanged; all other off-diagonal Kossakowski and Hamiltonian coefficients are zero. Every displayed real pair has anticommuting jump labels, every imaginary pair has commuting jump labels, and all their phase-free products equal ZZ. These dissipators and the Hamiltonian term $\widetilde{h}ZZ/2$ vanish on inputs commuting with ZZ and contribute only to the eight active entries. With the pairs ordered as in Eq. (13), they give

$$\begin{aligned}
K &= \widetilde{h}(1,-1,1,-1) - 2v_0(1,-1,-1,1)\\
&\quad - 2v_1(1,1,1,1) + 2v_2(1,1,-1,-1),\\
M &= 2u_1(1,1,1,-1) + 2u_2(1,1,-1,1)\\
&\quad + 2u_3(1,-1,1,1) + 2u_4(-1,1,1,1).
\end{aligned}$$

Both coefficient matrices have orthogonal columns, so these relations invert uniquely, and the hyperbolic transforms of $K = h(1,-1,1,-1)$ and $M = 2k(1,1,1,-1)$ yield Eq. (G1). Together with the unchanged diagonal dissipator, this reconstructs all 256 transfer entries. Canonical uniqueness, which extends to indefinite Hermitian Kossakowski matrices (Appendix A), therefore fixes the remaining Kossakowski and Hamiltonian coefficients at zero.

A real Kossakowski matrix C_0 can be factored as $\sum_j z_j z_j^T$, with Hermitian jumps $V_j = \sum_a (z_j)_a P_a$. Its dissipator is $-\frac{1}{2}\sum_j [V_j,[V_j,\cdot]]$. Equivalently, average unitary evolution with Stratonovich Hamiltonian increments $H_0 dt + \sum_a P_a \circ dW_a$ and real Wiener covariance $\mathbb{E}[dW_a dW_b] = (C_0)_{ab}dt$. The Itô form $d\rho = -i[H_0,\rho]dt - \frac{1}{2}\sum_{a,b}(C_0)_{ab}[P_a,[P_b,\rho]]dt - i\sum_a [P_a,\rho]dW_a$ contains exactly that double commutator; the Itô integral of the bounded integrand has zero mean, so $\mathbb{E}\rho$ obeys the reference GKSL equation. This realizes the reference as correlated local and two-qubit Hamiltonian fluctuations. The class of Kossakowski matrices for alternatives is specified independently of this realization.

2. Global identification at the reference

The kernel of the Kossakowski matrix is spanned by $XX, XY, XZ, YX, YY, ZX, ZY, ZZ$. Exact-record equivalence preserves all diagonal rates. In a positive semidefinite matrix, $C_{aa} = 0$ implies $|C_{ab}|^2 \le C_{aa}C_{bb} = 0$ for every b. Thus $v_1 = v_2 = u_2 = 0$ in every physical equivalent model. For $k \neq 0$, Eq. (G1) first forces $\alpha_g = 0$. The remaining constraint factors as

$$\begin{aligned}
0 &= \tfrac{k}{2}(1-\cosh\beta_g) - \tfrac{h}{4}\sinh\beta_g\\
&= -\tfrac{1}{2}\sinh(\beta_g/2)\,(2k\sinh(\beta_g/2) + h\cosh(\beta_g/2))\,.
\end{aligned} \tag{G2}$$

For $|h| \ge 2|k|$, the nonzero root would require $\tanh(\beta_g/2) = -h/(2k)$, which is impossible for finite real β_g. Therefore $\alpha_g = \beta_g = 0$ and the canonical generator is unchanged. A common scaling of all nonidentity sectors commutes with this unital generator and also changes no coefficient. This proves identification over the full physical class, with the support of the Kossakowski matrix determined by the exact observed record.

The sufficient identification condition is $|h| \ge 2|k|$. For $k = 0$, the zero rows also force $u_3 = u_2 = 0$, that is, $h\sinh\alpha_g = h\sinh\beta_g = 0$, so again $\widetilde{h} = h$. For $0 < |h| < 2|k|$, the nonzero root gives $\widetilde{h} = 0$, $u_1 = k$, and $v_0 = -h/2$, with the other off-diagonal coordinates zero. This Kossakowski matrix can be positive when $|h| \le 2\lambda$, and sufficiently small roots can be absorbed by interior SPAM channels: if A, B have positive-definite Choi matrices and satisfy Eq. (2) strictly, then with $s_1 = s_{12} = 1$ and $s_2 = e^{-\beta_g}$, SA and BS^{-1} remain completely positive, trace preserving, and within budget for small $|\beta_g|$ by continuity, and Eq. (A2) gives the same exact data.

3. Restoring positivity with a quadratic correction

For the gauge transformation that scales only the sector supported on the second qubit, $(\alpha_g,\beta_g) = (0,-\theta)$. Set $c = \cosh\theta$, $s = \sinh\theta$. Only

$$\begin{aligned}
u_1 &= \tfrac{k}{2}(1+c) - \tfrac{h}{4}s, \quad u_2 = \tfrac{k}{2}(1-c) + \tfrac{h}{4}s,\\
v_0 &= \tfrac{h}{4}(c-1) - \tfrac{k}{2}s.
\end{aligned} \tag{G3}$$

remain off diagonal. Apart from nonnegative singletons, the Kossakowski matrix before correction consists of three disjoint blocks:

$$\begin{array}{l|l}
(XI,YZ) & \begin{pmatrix} \lambda & u_1 \\ u_1 & m \end{pmatrix}\\
(YI,XZ) & \begin{pmatrix} \lambda & u_2 \\ u_2 & 0 \end{pmatrix}\\
(ZI,IZ) & \begin{pmatrix} \lambda & iv_0 \\ -iv_0 & \lambda \end{pmatrix}.
\end{array} \tag{G4}$$

Its block on the kernel of the reference Kossakowski matrix is zero. Locally, adding u_2^2/λ at XZ, or that amount on the entire diagonal, makes the middle block positive semidefinite. Its sole negative eigenvalue before correction is

$$\frac{\lambda - \sqrt{\lambda^2 + 4u_2^2}}{2} = -\frac{h^2}{16\lambda}\theta^2 + O(\theta^3). \tag{G5}$$

The other two blocks remain positive by continuity and $\lambda m > k^2$.

For explicit constants at Eq. (14), throughout $|\theta| \le 0.01$ use $|\sinh\theta| \le 1.001|\theta|$ and $0 \le \cosh\theta - 1 \le 0.501\theta^2$. They imply

$$|u_1| < 0.0103, \quad |u_2| \le 0.0251|\theta|, \quad |v_0| < 0.000052. \tag{G6}$$

The first and third blocks of Eq. (G4) are positive definite. Adding $q_\theta = 0.01\theta^2$ to all diagonal entries makes the middle determinant at least

$$(0.1 + q_\theta)q_\theta - u_2^2 \ge 0.00036999\theta^2 + q_\theta^2 \ge 0. \tag{G7}$$

Every remaining diagonal is nonnegative. The corrected matrix is positive semidefinite at zero and positive definite away from zero. The added depolarizing noise is the diagonal map $16q_\theta(\mathcal{D} - \mathrm{id})$ of Eq. (A11) at $n = 2$ and changes no canonical Hamiltonian coefficient. Moreover,

$$|h_\theta - h_0| \ge 0.01|\theta| - 0.02505\theta^2 \ge 0.0097|\theta|. \tag{G8}$$

Scaling only the sector supported on the first qubit gives $(\alpha_g, \beta_g) = (-\theta, 0)$, zero target derivative, and kernel-block eigenvalues $\pm|k\sinh\theta|/2$. This first-order defect persists under a quadratic positive correction. This direction fails both conditions in Eq. (6).

For two qubits all canonical jump labels have weight at most two. The constructed path has a uniform finite norm bound. Factor $C_\theta = \sum_j z_j z_j^\dagger$ and set $V_j = \sum_a (z_j)_a P_a$. Then $\|V_j\|_{\mathrm{op}}^2 \le \|V_j\|_{\mathrm{HS}}^2 = 4\|z_j\|_2^2$. For every ancilla, each adjoint jump term $V_j^\dagger X V_j - \frac{1}{2}\{V_j^\dagger V_j, X\}$ has $\infty \to \infty$ norm at most $2\|V_j\|_{\mathrm{op}}^2$, and the Hamiltonian term at most $2\|H_\theta\|_{\mathrm{op}} = |h_\theta|$. Treating the register as one term gives strength at most

$$|h_\theta| + 8\,\mathrm{Tr}\, C_\theta, \tag{G9}$$

uniformly finite on the displayed interval. The pair upper bounds use a prescribed common bound on the summed norms of the physical single- and two-qubit terms acting on each qubit throughout the inference class (Appendix C).

4. Zero coupling and a positive noise background

For Remark 1, keep λ, m, k and the SPAM channels of Eq. (14) but set $h_0 = 0$. The zero Kossakowski rows in Eq. (G1) force $v_1 = 0$, hence $\alpha_g = 0$, and then $u_2 = k(1 - \cosh\beta_g)/2 = 0$, hence $\beta_g = 0$. Thus the exact data still identify the generator. On $\ker D = \{\alpha_g = 0\}$ modulo the common scaling, however, $\mathcal{B} = 0$ and $\Pi C_2 \Pi = 0$: the first derivative of u_2 vanishes, and v_0 connects two occupied directions. Consequently $Q_2 = 0$ and the supremum in Eq. (8) is zero, attained at $v = 0$.

Along $(\alpha_g, \beta_g) = (0, -\theta)$, the three blocks in Eq. (G4) have

$$u_1 = \tfrac{k}{2}(1 + \cosh\theta), \qquad u_2 = \tfrac{k}{2}(1 - \cosh\theta),$$
$$v_0 = -\tfrac{k}{2}\sinh\theta, \qquad \widetilde{h} = -k\sinh\theta. \tag{G10}$$

The first and third blocks stay positive definite near zero. The middle block has negative eigenvalue $-k^2\theta^4/(16\lambda) + O(\theta^6)$. Adding $t_\theta I_{15}$ with $t_\theta = u_2^2/\lambda$ makes its determinant $(\lambda + t_\theta)t_\theta - u_2^2 = t_\theta^2 \ge 0$. This gives a physical generator $L_\theta = S_\theta L_0 S_\theta^{-1} + 16 t_\theta(\mathcal{D} - \mathrm{id})$. The boundary proof in Appendix H is independent of h_0, so the same A_θ, B_θ are admissible for sufficiently small $|\theta| \le \varepsilon/100$. Their compensation leaves entry distance $16t_\theta$. Choosing this distance to equal δ gives, for sufficiently small $\delta > 0$,

$$\omega_{ZZ}(\delta) \ge \left(|k|\sqrt{\lambda\delta} + \lambda\delta/4\right)^{1/2} \ge (k^2\lambda\delta)^{1/4}. \tag{G11}$$

Removing the reference Hamiltonian leaves the mixing proof of Eq. (H13) unchanged, with rate 1/5. Equations (H15)–(H16) apply with q_θ replaced by $t_\theta = O(\theta^4)$, giving outcome differences $O(\theta^4)$ uniformly over all allowed controls and durations. The boundary probability floor $\varepsilon/64$ also remains valid. Lemma 1 therefore bounds the adaptive relative entropy by $O_\varepsilon(N\theta^8)$. For fixed $0 < \alpha < 1/2$, choosing $\theta = cN^{-1/8}$ with sufficiently small $c > 0$ and using $|\widetilde{h}| \ge |k|\theta$ in Eq. (B2) proves $\mathbb{E}_0|I_N| = \Omega(N^{-1/8})$ for intervals uniformly valid over a class containing this path.

For the positive-background claim, return to $h_0 = 0.1$ and set $C_{0,\xi} = C_0 + \xi I_{15}$, $\xi > 0$, so $L_{0,\xi} = L_0 + 16\xi(\mathcal{D} - \mathrm{id})$. Since the depolarizer commutes with S_θ, the gauge-transformed generator has Kossakowski matrix $\widetilde{C}(\theta) + \xi I_{15}$. The quadratic repair above shows that this is at least $\xi I_{15}/2$ at

$$\theta_\xi = \min\{\varepsilon/200, \sqrt{\xi/(2K)}\}, \qquad K = 0.01. \tag{G12}$$

Pairing $S_{\theta_\xi} L_{0,\xi} S_{\theta_\xi}^{-1}$ with the admissible SPAM channels $A_{\theta_\xi}, B_{\theta_\xi}$ gives the same exact data as $(L_{0,\xi}, \mathcal{D}_r, \mathcal{D}_r)$ by Eq. (A2). The target separation is at least $0.0097\theta_\xi$. Thus, for fixed ε and sufficiently small ξ, the exact ambiguity is at least of order $\sqrt{\xi}$; Eq. (B2) with $\tau = 0$ gives an expected-width lower bound $(1 - 2\alpha)0.0097\theta_\xi$ for every N whenever both models belong to the coverage class.

Appendix H: Expected confidence-interval length at the reference model

We prove the lower bound Eq. (16) of Theorem 2 along the physical path of Appendix G: we establish the admissibility of its SPAM channels, bound every outcome change uniformly in duration, and convert this bound into a bound on the expected length with Lemma 1. Throughout this appendix the reference acts on two qubits, and $\mathcal{D}$ and $\mathcal{D}_r$ denote its two-qubit depolarizers. We use the observation model of Sec. II and Table I. Here shot durations and control-sequence lengths are finite but have no common upper bound. Let $\mathfrak{M}_\varepsilon$ denote the surrounding physical class, and a possibly randomized interval is uniformly valid if it obeys Eq. (5) over this class. The lower bound below requires $\mathfrak{M}_\varepsilon$ to contain the explicit path of Appendix G. The upper bound additionally imposes a common norm bound that admits this path (Appendix C).

1. The physical path and its SPAM channels

The reference is Eq. (14). Let S_θ multiply the transfer coordinates IX, IY, IZ by e^θ and leave all other coordinates unchanged. Put $\mathcal{D}(X) = \mathrm{Tr}(X)I/4$, $\mathcal{D}_a = a\mathrm{id} + (1-a)\mathcal{D}$, and $K = 1/100$. The physical construction in Appendix G gives

$$q_\theta = K\theta^2,$$
$$\mathcal{L}_\theta = S_\theta \mathcal{L}_0 S_\theta^{-1} + 16 q_\theta(\mathcal{D} - \mathrm{id}), \tag{H1}$$
$$h_\theta = \frac{1+\cosh\theta}{20} - \frac{\sinh\theta}{100}. \tag{H2}$$

These formulas hold for $|\theta| \le 10^{-2}$. By Eq. (A11) at $n = 2$, an identity Kossakowski matrix on the fifteen traceless two-qubit Paulis represents $16(\mathcal{D} - \mathrm{id})$. The added Kossakowski term $q_\theta I_{15}$ makes the generator physical and leaves its canonical Hamiltonian unchanged. For the positive alternatives used below,

$$|h_\theta - h_0| \ge \frac{\theta}{200}, \qquad 0 < \theta \le 10^{-2}. \tag{H3}$$

Indeed, Eq. (G8) gives $|h_\theta - h_0| \ge 0.0097\theta \ge \theta/200$ on this interval.

Set

$$r = 1 - \varepsilon/8, \qquad \theta_{\max} = \varepsilon/100,$$
$$A_\theta = S_\theta \mathcal{D}_r, \qquad B_\theta = \mathcal{D}_r S_\theta^{-1}. \tag{H4}$$

Both SPAM channels are fixed across settings. To verify complete positivity, write $\chi_a(p) \in \{-1, 1\}$ for the commutation character of Pauli labels a, p. A Pauli-diagonal trace-preserving map with eigenvalues λ_p has Pauli-mixture coefficients

$$p_a = \frac{1}{16}\sum_p \chi_a(p)\lambda_p. \tag{H5}$$

For $\mathcal{D}_r$, each nonidentity coefficient is $(1-r)/16 = \varepsilon/128$. Only three eigenvalues change in each map in Eq. (H4). Since $|e^{\pm\theta} - 1| \le 2|\theta|$ for the allowed θ,

$$|p_a(\theta) - p_a(0)| \le \frac{3r}{16}|e^{\pm\theta} - 1| \le \frac{3\varepsilon}{800}. \tag{H6}$$

Thus every coefficient, including the larger identity coefficient, is at least

$$\frac{\varepsilon}{128} - \frac{3\varepsilon}{800} = \frac{13\varepsilon}{3200} > \frac{\varepsilon}{256}. \tag{H7}$$

The coefficients sum to one, proving that both maps are unital CPTP channels for either sign of θ.

For a Pauli channel, the unhalved diamond distance to identity is $2(1 - p_I)$. The upper bound follows by the triangle inequality for its Pauli mixture; a maximally entangled input gives the matching trace distance between the orthogonal Pauli Choi states. Here

$$p_I^\pm = \frac{1 + 12r + 3re^{\pm\theta}}{16}, \tag{H8}$$

and consequently

$$\|A_\theta - \mathrm{id}\|_\diamond + \|B_\theta - \mathrm{id}\|_\diamond = 4 - 2(p_I^+ + p_I^-)$$
$$= \frac{15\varepsilon}{32} - \frac{3r}{4}(\cosh\theta - 1) \le \varepsilon. \tag{H9}$$

The zero-time calibration is constant along the path:

$$B_\theta A_\theta = \mathcal{D}_r^2. \tag{H10}$$

2. Uniform comparison over arbitrary finite durations

Subtracting $1/20$ from all six single-qubit diagonals of C_0 leaves a real positive semidefinite Kossakowski matrix. Its only coupled block has diagonal $(1/20, 1/50)$, off-diagonal $1/100$, and determinant

$$\frac{1}{20}\frac{1}{50} - \left(\frac{1}{100}\right)^2 = \frac{9}{10000} > 0. \tag{H11}$$

The residual Kossakowski matrix therefore factors into Hermitian jump operators. For a Hermitian jump V and any operator X,

$$\mathrm{Re}\,\mathrm{Tr}\left[X^\dagger\left(VXV - \tfrac{1}{2}\{V^2, X\}\right)\right]$$
$$= -\tfrac{1}{2}\|[V, X]\|_2^2 \le 0. \tag{H12}$$

The Hamiltonian commutator contributes zero to this real quadratic form. The extracted local Pauli noise has eigenvalue $-w/5$ on a Pauli of weight w. Thus, on traceless operators, $\mathrm{Re}\langle X, \mathcal{L}_0(X)\rangle \le -\|X\|_2^2/5$. Differentiating the squared norm and integrating gives contraction by $e^{-t/5}$ for each reference evolution segment. Local-unitary conjugations preserve the Hilbert–Schmidt norm, so any controlled reference evolution $\mathcal{P}_0$ of total duration T obeys

$$\|\mathcal{P}_0(X)\|_2 \le e^{-T/5}\|X\|_2, \qquad \mathrm{Tr}\,X = 0. \tag{H13}$$

The Kossakowski matrix is real, so $\mathcal{L}_0$ is unital. Its trace preservation and the gauge transformation S_θ satisfy the commutation hypotheses of the width proof in Appendix D. Applying its segment factorization with $n = 2$ and depolarizing coefficient q_θ gives

$$e^{t\mathcal{L}_\theta} = S_\theta e^{t\mathcal{L}_0} S_\theta^{-1} \mathcal{D}_{e^{-16q_\theta t}}. \tag{H14}$$

The same cancellation against the SPAM channels in Eq. (H4) yields, for total duration T,

$$\mathcal{R}_\theta := B_\theta \mathcal{P}_\theta A_\theta = \mathcal{D}_r \mathcal{P}_0 \mathcal{D}_{e^{-16q_\theta T}} \mathcal{D}_r. \tag{H15}$$

For a density operator ρ, $\|\rho - I/4\|_2^2 = \mathrm{Tr}\,\rho^2 - 1/4 \le 3/4$. Using Eq. (H13), the two factors $r \le 1$, and $1 - e^{-x} \le x$, we obtain

$$\|\mathcal{R}_\theta(\rho) - \mathcal{R}_0(\rho)\|_2 \le (1 - e^{-16q_\theta T})e^{-T/5}\frac{\sqrt{3}}{2}$$
$$\le 16K\theta^2 T e^{-T/5}\frac{\sqrt{3}}{2}$$
$$\le \frac{40\sqrt{3}}{e}K\theta^2 \le 32K\theta^2. \tag{H16}$$

The last step uses $\sup_{T\ge 0} Te^{-T/5} = 5/e$. This bound is uniform in the input, total duration, number of intervals, and all local controls. A terminal rank-one product projector has Hilbert–Schmidt norm one. Each of its outcome probabilities therefore changes by at most $D\theta^2$, where $D = 32K$.

3. Conditional information and the interval lower bound

Equation (H7) gives a uniform lower bound on the outcome probabilities. For every density operator σ,

$$B_\theta(\sigma) \succeq \frac{\varepsilon}{256}\sum_a P_a \sigma P_a = \frac{\varepsilon}{64} I. \tag{H17}$$

The input to B_θ is a density operator because both the preparation and the intervening evolution are physical. All four terminal probabilities are therefore at least $\mu = \varepsilon/64$ under both hypotheses, for every allowed setting. For their probability vectors, the bound $|p_{0,j} - p_{\theta,j}| \le D\theta^2$ gives $\sum_{j=1}^4 (p_{0,j} - p_{\theta,j})^2 \le 4D^2\theta^4$. Lemma 1 therefore gives

$$K_{\mathrm{stat}} := 4D^2/\mu = 262144K^2/\varepsilon = 26.2144/\varepsilon, \tag{H18}$$

$$D_{\mathrm{KL}}(P_0^{(N)} \| P_\theta^{(N)}) \le N K_{\mathrm{stat}} \theta^4. \tag{H19}$$

This applies uniformly to every allowed adaptive setting policy.

The following theorem is Eq. (16) of Theorem 2; the two forms agree because $8K_{\mathrm{stat}} = 209.7152/\varepsilon$ by Eq. (H18).

Theorem 5 (Expected interval length at the reference)**.** *For $0 < \alpha < 3/8$, every protocol described above and every interval satisfying Eq. (5) obey*

$$\mathbb{E}_0|I_N| \ge \frac{3/4 - 2\alpha}{200} \times \min\left\{\frac{\varepsilon}{100}, \left(\frac{\varepsilon}{209.7152N}\right)^{1/4}\right\}. \tag{H20}$$

Proof of Theorem 5. Choose

$$\theta_N = \min\{\theta_{\max}, (8K_{\mathrm{stat}}N)^{-1/4}\}. \tag{H21}$$

Equation (H19) bounds the relative entropy by 1/8, so Lemma 1 gives total variation at most 1/4 and expected length at least $(3/4 - 2\alpha)|h_{\theta_N} - h_0|$. Substituting the separation $|h_{\theta_N} - h_0| \ge \theta_N/200$ from Eq. (H3) proves Eq. (H20). □

For each fixed positive ε, the asymptotic lower rate is $N^{-1/4}$. Its constants and the onset of this regime depend on the SPAM budget: $\theta_{\max}$ tends to zero as ε does.

Appendix I: Identification and the sharp local modulus

We prove the exact identification in Theorem 2, the square-root modulus of Eq. (23), and the upper bound Eq. (17).

1. The 23 observable entries and canonical inversion

For each candidate model, twirling its own SPAM channels gives the generator in the readout gauge of Eq. (4),

$$G = \overline{B}\mathcal{L}\overline{B}^{-1}, \tag{I1}$$

so the preparation cancels and $G_{Q,Q} = L_{Q,Q}$, even for complex Kossakowski matrices and nonunital alternatives. By Appendix A, the readout gains b_Q lie in $[l, 1]$, so the support ratios obey

$$\begin{aligned} r_A &= \frac{b_{\{1,2\}}}{b_{\{1\}}}, \\ r_B &= \frac{b_{\{1,2\}}}{b_{\{2\}}}, \\ r_A, r_B &\in [l, l^{-1}]. \end{aligned} \tag{I2}$$

The upper bounds use this box as an outer bound on the admissible gain ratios.

The measured index set $\mathcal{J}$ consists of all fifteen (Q, Q) with $Q \ne I$, together with both orientations of the four pairs (R_i, Q_i) of Eq. (13). Measure the error on these entries by

$$\|G - G_0\|_{\mathcal{J}} := \max_{(R,Q)\in\mathcal{J}} |G_{R,Q} - (G_0)_{R,Q}|. \tag{I3}$$

The identity diagonal $G_{I,I} = 0$ is known from trace preservation.

By Eq. (A10), the fifteen measured diagonals determine all canonical diagonal rates $c_a = C_{aa}$. If Eq. (I3) is at most δ, each rate changes by at most $15\delta/16 \le \delta$.

Write $x_i = G_{R_i,Q_i}$ and $y_i = G_{Q_i,R_i}$. For the consecutive groups $A = (1, 2)$ and $B = (3, 4)$ define, with (i, j) the group's indices,

$$\begin{aligned} a_g &= (x_i - x_j)/2, \\ b_g &= (y_j - y_i)/2, \\ u_g &= (x_i + x_j)/2, \\ v_g &= (y_i + y_j)/2. \end{aligned} \tag{I4}$$

Since $x_i = r_g L_{R_i,Q_i}$ and $y_i = L_{Q_i,R_i}/r_g$, the physical signed and unsigned group coordinates are

$$\begin{aligned} k_g &= \tfrac{1}{2}(a_g/r_g + b_g r_g), \\ m_g &= \tfrac{1}{2}(a_g/r_g - b_g r_g), \\ k_g^+ &= \tfrac{1}{2}(u_g/r_g - v_g r_g), \\ m_g^+ &= \tfrac{1}{2}(u_g/r_g + v_g r_g). \end{aligned} \tag{I5}$$

The superscript + denotes an unsigned combination, not a derivative.

To obtain the Kossakowski coordinates entering this inverse, define

$$\begin{aligned} U_1 &= \mathrm{Re}\, C_{XI,YZ}, \\ U_2 &= \mathrm{Re}\, C_{YI,XZ}, \\ U_3 &= \mathrm{Re}\, C_{IX,ZY}, \\ U_4 &= \mathrm{Re}\, C_{IY,ZX}, \\ V_0 &= \mathrm{Im}\, C_{ZI,IZ}, \\ V_1 &= \mathrm{Im}\, C_{XX,YY}, \\ V_2 &= \mathrm{Im}\, C_{XY,YX}. \end{aligned} \tag{I6}$$

At the physical generator let $K_i = (L_{R_i,Q_i} - L_{Q_i,R_i})/2$ and $M_i = (L_{R_i,Q_i} + L_{Q_i,R_i})/2$. Collect these as column vectors $\boldsymbol{K}, \boldsymbol{M}$, and similarly collect $U_1, \ldots, U_4$ and V_0, V_1, V_2 as $\boldsymbol{U}, \boldsymbol{V}$. With $\boldsymbol{\sigma} = (1, -1, 1, -1)^{\mathsf{T}}$, the matrices relating these coordinates in the target sector are

$$\boldsymbol{M} = 2 \begin{pmatrix} 1 & 1 & 1 & -1 \\ 1 & 1 & -1 & 1 \\ 1 & -1 & 1 & 1 \\ -1 & 1 & 1 & 1 \end{pmatrix} \boldsymbol{U}, \tag{I7}$$

$$\boldsymbol{K} = h\boldsymbol{\sigma} + 2 \begin{pmatrix} -1 & -1 & 1 \\ 1 & -1 & 1 \\ 1 & -1 & -1 \\ -1 & -1 & -1 \end{pmatrix} \boldsymbol{V}. \tag{I8}$$

Here and below $h = h_{ZZ}$. To check that these matrices contain every term, recall from the symmetric-part computation leading to Eq. (E4) in Appendix E that the dissipative anticommutator contributes nothing at these positions and that a jump-pair trace can be nonzero only if the two labels have phase-free product ZZ. The seven unordered nonidentity pairs with this product are exactly the four U pairs and three V pairs above. For the ordered labels (a, b) set $z_i(a, b) = \mathrm{Tr}(R_i P_a Q_i P_b)/4$. Combining the two conjugate jump terms gives $2\,\mathrm{Re}\, C_{ab}\,\mathrm{Re}\, z_i$ in M_i and $-2\,\mathrm{Im}\, C_{ab}\,\mathrm{Im}\, z_i$ in K_i. Using $XY = iZ$, $YZ = iX$, and $ZX = iY$, the U traces are the real matrix in Eq. (I7); the V traces are $-i$ times the real matrix in Eq. (I8). For example, $z_1(XI, YZ) = 1$ and $z_1(ZI, IZ) = i$. The only Hamiltonian label contributing is ZZ, with signs $(1, -1, 1, -1)$. These matrices hold for arbitrary remaining complex Kossakowski coefficients and Hamiltonian terms.

Taking group sums and differences and inverting gives

$$\begin{aligned} U_1 &= (m_A^+ + m_B)/4, \\ U_2 &= (m_A^+ - m_B)/4, \\ U_3 &= (m_B^+ + m_A)/4, \\ U_4 &= (m_B^+ - m_A)/4, \\ V_0 &= (k_B - k_A)/4, \\ V_1 &= -(k_A^+ + k_B^+)/4, \\ V_2 &= (k_A^+ - k_B^+)/4, \\ h &= (k_A + k_B)/2. \end{aligned} \tag{I9}$$

2. Exact identification from observable zero rows

At the reference the detector is $\mathcal{D}_r$, and $\mathcal{L}_0$ is unital, so $G_0 = L_0$. The group data and the corresponding functions of a candidate ratio are

$$\begin{aligned} (a, b, u, v)_A^0 &= (0.1, 0.1, 0.02, 0.02), \\ (a, b, u, v)_B^0 &= (0.12, 0.08, 0, 0), \end{aligned} \tag{I10}$$

$$\begin{aligned} k_A^0(r) &= 0.05(r^{-1} + r), \\ m_A^0(r) &= 0.05(r^{-1} - r), \\ (m_A^+)^0(r) &= 0.01(r^{-1} + r), \\ k_B^0(r) &= 0.06/r + 0.04r, \\ m_B^0(r) &= 0.06/r - 0.04r, \\ (m_B^+)^0(r) &= 0. \end{aligned} \tag{I11}$$

Any model with the same exact data has these same 23 entries. Equation (A10) fixes its entire Kossakowski diagonal. For a positive semidefinite Kossakowski matrix,

$$|C_{ab}|^2 \le C_{aa} C_{bb}. \tag{I12}$$

The zero reference diagonals at XZ, ZX, ZY thus force their entire complex rows and columns to vanish in every compatible model. In particular $U_2 = U_3 = U_4 = 0$. The last two equations imply $m_A = 0$, so $r_A^{-1} - r_A = 0$ and positivity gives $r_A = 1$. Then $U_2 = 0$ implies $m_B = (m_A^+)^0(1) = 0.02$, or

$$\frac{0.06}{r_B} - 0.04 r_B - 0.02 = -\frac{(r_B - 1)(2r_B + 3)}{50 r_B} = 0. \tag{I13}$$

Its only positive root is $r_B = 1$. Equation (I9) now gives $h = 0.1$ for every compatible physical model, with unknown SPAM channels and complex Kossakowski matrices allowed. The zero rows follow from the exact observable profile.

3. A quantitative square-root modulus

Suppose a physical candidate satisfies $\|G - G_0\|_{\mathcal{J}} \le \delta$. Define

$$\begin{aligned} u_\varepsilon &= \tfrac{1}{2}(l + l^{-1}), \\ e_\delta &= u_\varepsilon \delta, \\ s_\delta &= \sqrt{(0.1 + \delta)\delta}, \\ d_A(\delta) &= 20(4 s_\delta + 2 e_\delta), \\ d_B(\delta) &= 25\big\{0.01(1 + l^{-2}) d_A(\delta) \\ &\qquad + 4 s_\delta + 2 e_\delta\big\}. \end{aligned} \tag{I14}$$

Rate inversion and Eq. (I12) bound $|U_2|, |U_3|, |U_4|$ by s_δ: the relevant local diagonals are at most $0.1 + \delta$, and the diagonals at XZ, ZX, ZY are at most δ. Each coordinate

in Eq. (I4) changes by at most δ. At any fixed ratio in $[l, l^{-1}]$, each coordinate in Eq. (I5) therefore changes by at most $(r + r^{-1})\delta/2 \le e_\delta$.

Next, subtracting $4U_3 = m_B^+ + m_A$ and $4U_4 = m_B^+ - m_A$ gives $|m_A| \le 4s_\delta$. Hence $|m_A^0(r_A)| \le 4s_\delta + e_\delta \le 4s_\delta + 2e_\delta$. Because $m_A^0(1) = 0$ and

$$\left|\frac{d}{dr} m_A^0(r)\right| = 0.05(1 + r^{-2}) \ge 0.05, \tag{I15}$$

the mean value theorem yields $|r_A - 1| \le d_A(\delta)$. The remaining Kossakowski bound gives

$$|m_B^0(r_B) - (m_A^+)^0(r_A)| \le 4s_\delta + 2e_\delta. \tag{I16}$$

Since $(m_A^+)^0(1) = m_B^0(1) = 0.02$ and

$$\begin{aligned} \left|\frac{d}{dr}(m_A^+)^0(r)\right| &\le 0.01(1 + l^{-2}), \\ \left|\frac{d}{dr} m_B^0(r)\right| &= 0.04 + 0.06r^{-2} \ge 0.04, \end{aligned} \tag{I17}$$

another application of the mean value theorem proves $|r_B - 1| \le d_B(\delta)$. Finally, $|(k_A^0)'| \le 0.05(1 + l^{-2})$ and $|(k_B^0)'| \le 0.04 + 0.06l^{-2}$ on the ratio box. Including the entry perturbation in $h = (k_A + k_B)/2$ gives the explicit bound

$$\begin{aligned} &|h - h_0| \le F_\varepsilon(\delta), \\ &F_\varepsilon(\delta) := \tfrac{1}{2}\big\{0.05(1 + l^{-2}) d_A(\delta) \\ &\qquad + (0.04 + 0.06l^{-2}) d_B(\delta)\big\} + e_\delta. \end{aligned} \tag{I18}$$

In particular $F_\varepsilon(\delta) = O_\varepsilon(\sqrt{\delta})$. These inequalities hold for every physical candidate, so they bound the target range over the physical class.

It remains to show that the physical path attains the same local exponent in this metric. Let Π_0 be the transfer-space projector onto the fifteen nonidentity Paulis. Using the SPAM channels in Eq. (H4) in the normalization Eq. (I1) gives exactly

$$\begin{aligned} G_\theta &= G_0 - 16K\theta^2 \Pi_0, \\ \|G_\theta - G_0\|_{\mathcal{J}} &= 16K\theta^2. \end{aligned} \tag{I19}$$

Indeed the gauge transformation cancels, and $\mathcal{D}_r$ commutes with the unital reference generator and with Π_0. For $0 < \delta \le 16K(\varepsilon/100)^2$, take $\theta = \sqrt{\delta/(16K)}$. Then

$$|h_\theta - h_0| \ge \frac{\sqrt{\delta}}{80}. \tag{I20}$$

Thus the supremum of $|h - h_0|$ over physical candidates in the δ-neighborhood is bounded below by $\sqrt{\delta}/80$ and above by $F_\varepsilon(\delta)$. Its local Hölder exponent is exactly $1/2$ at each fixed positive SPAM budget.

4. A uniformly valid interval from estimated entries of G

For physical terms acting on at most two sites, impose the bound of Appendix C on the summed norms of the terms acting on each qubit throughout the inference class. Denote the known bound by γ and the resulting class by $\mathfrak{M}_{\varepsilon,\gamma}$. Every relevant physical transfer entry has magnitude at most 2γ. Equation (A8) then gives $|h| \le H_* := 2\gamma$. Estimate $\widehat{G}_N$ on $\mathcal{J}$ with simultaneous error bound δ_N and failure probability $\zeta_N \le \min\{\alpha, N^{-1}\}$ uniformly over this class. Apply Lemma 2 with $g = G|_{\mathcal{J}}$, the maximum-entry metric, and $H = H_*$. The finite shot outcomes and randomized node choices give finitely many possible estimates. Using Eq. (I18) as the modulus bound yields an interval uniformly valid at level $1 - \alpha$ with

$$\mathbb{E}_0|I_N| \le 2F_\varepsilon(2\delta_N) + 2H_*\zeta_N. \tag{I21}$$

The following allocation gives explicit numbers of shots and logarithmic factors. For $N \ge 46$ choose

$$\begin{aligned} &p_N = \max\{6, \lceil \log_2 N \rceil\}, \quad B_N = \log(76/\zeta_N), \\ &N_D = \lfloor N/46 \rfloor, \qquad N_0 = \lfloor N/30 \rfloor, \\ &W_N = 2\gamma p_N^2, \qquad \beta_N = \frac{4p_N(p_N + 2)\gamma}{4^{p_N}}. \end{aligned} \tag{I22}$$

Use the Chebyshev–Lobatto estimation procedure of Appendix C on $[0, 1/\gamma]$. The total number of preparations is $23N_D + 15N_0 \le N$, including calibration. Its simultaneous radius is

$$\begin{aligned} \delta_N = &\frac{W_N\sqrt{2B_N/N_D} + \beta_N}{l} \\ &+ \frac{2\gamma}{l^2}\sqrt{2B_N/N_0}. \end{aligned} \tag{I23}$$

Taking $\zeta_N = \min\{\alpha, N^{-1}\}$ gives, for fixed $\varepsilon, \gamma, \alpha$,

$$\begin{aligned} \delta_N &= O_{\varepsilon,\gamma,\alpha}\big(N^{-1/2}(\log N)^{5/2}\big), \\ \mathbb{E}_0|I_N| &= O_{\varepsilon,\gamma,\alpha}\big(N^{-1/4}(\log N)^{5/4}\big) + O_\gamma(N^{-1}). \end{aligned} \tag{I24}$$

For smaller N the whole bounded interval is a uniformly valid procedure. An outer numerical enclosure can replace the physical set if it preserves inclusion and its excess width tends to zero at the required rate in Eq. (I24).

If the invertible SPAM channels are known, their inverse removes the gauge transformation in Eq. (I1); h is then a fixed linear functional of the acquired entries. With the same norm bound, the interval construction has expected length $O_{\varepsilon,\gamma,\alpha}(N^{-1/2}(\log N)^{5/2}) + O_\gamma(N^{-1})$, with constants also depending on the known inverse gains.

Appendix J: Linear stability under a Kossakowski constraint

Under one Kossakowski constraint, the square-root modulus bound of Appendix I improves to a linear bound.

Impose $\operatorname{Im} C_{ZI,IZ} = 0$ on every admissible alternative, keeping the reference, SPAM budget, and observations. Wholly real Kossakowski matrices satisfy this condition and admit the classical white Hamiltonian-noise realization of Appendix G. Equation (I9) gives $k_A = h - 2V_0$ with $V_0 = \operatorname{Im} C_{ZI,IZ}$, so $h = k_A$. At its ratio r_A the physical k_A differs from $k_A^0(r_A)$ by at most e_δ. The identity

$$k_A^0(r_A) - 0.1 = 0.05\,(r_A - 1)^2/r_A \tag{J1}$$

together with $r_A \geq l$ and $|r_A - 1| \leq d_A(\delta)$ from Appendix I gives, using $s_\delta^2 = 0.1\delta + \delta^2$ and $e_\delta = u_\varepsilon \delta$ in Eq. (I14),

$$\begin{aligned} |h - h_0| \leq R_\varepsilon(\delta) &:= e_\delta + \frac{0.05}{l} d_A(\delta)^2 \\ &= \Big(u_\varepsilon + \frac{32}{l}\Big)\delta + O_\varepsilon(\delta^{3/2}). \end{aligned} \tag{J2}$$

Restricting the confidence set to this class preserves uniform validity over it, and the $2\delta_N$ argument with R_ε in place of F_ε gives $\mathbb{E}_0|I_N| \leq 2R_\varepsilon(2\delta_N) + 2H_*\zeta_N = O_{\varepsilon,\gamma,\alpha}(N^{-1/2}(\log N)^{5/2}) + O_\gamma(N^{-1})$.

Conversely, $(L_0 + \delta A_{ZZ}, \mathcal{D}_r, \mathcal{D}_r)$ keeps the Kossakowski matrix real, moves the target by δ, and changes G by $\mathcal{D}_r \delta A_{ZZ} \mathcal{D}_r^{-1} = \delta A_{ZZ}$, since $\mathcal{D}_r$ is the scalar r on the traceless operators that A_{ZZ} preserves; its nonzero entries are $\pm\delta$ on the target pairs; so the linear entry modulus is exact in this class.

Appendix K: A correlation-dependent crossover and four additional responses

We prove Theorem 3 and the corresponding confidence bounds. A second real noise correlation leaves the original 23 entries of G unchanged, but four additional entries with exchanged indices reveal a positivity constraint. The inference class stays fixed while η indexes the references.

1. Model, reference family, and record metric

We use the conventions of Sec. II, with

$$\begin{gathered} \lambda = 0.1, \quad m = 0.02, \quad k = 0.01, \quad h_0 = 0.1, \\ |\eta| \leq \eta_0 = 0.01. \end{gathered} \tag{K1}$$

The reference generator $\mathcal{L}_\eta$ adds $(C_\eta)_{IX,YZ} = (C_\eta)_{YZ,IX} = \eta$ to Eq. (14). Its occupied block on (XI, IX, YZ) is

$$\begin{pmatrix} \lambda & 0 & k \\ 0 & \lambda & \eta \\ k & \eta & m \end{pmatrix} \succ 0, \qquad \lambda m > k^2 + \eta^2. \tag{K2}$$

Since $\lambda > 0$, this block is positive definite exactly when $m - (k^2 + \eta^2)/\lambda > 0$; here that Schur complement is at least 0.018. The labels YI, ZI, IY, IZ contribute λI_4, and the remaining eight labels have zero rows. Thus C_η has rank seven and the same kernel throughout the closed interval in Eq. (K1):

$$\begin{aligned} \mathcal{K} = \operatorname{span}\{&XX, XY, XZ, YX, \\ &YY, ZX, ZY, ZZ\}. \end{aligned} \tag{K3}$$

Since C_η is real symmetric and $[P_a, P_b]$ is antisymmetric in (a, b), $\mathcal{L}_\eta(I) = \sum_{a,b}(C_\eta)_{ab}[P_a, P_b] = 0$: the reference is unital.

The reference SPAM channels are $A_0 = B_0 = \mathcal{D}_r$ with $r = 1 - \varepsilon/8$, as in Appendix H. Candidate models range over the common class $\mathfrak{M}_\varepsilon$ of Appendix H (Table I): arbitrary complex physical Kossakowski matrices, other Hamiltonian coefficients, possibly nonunital generators, and fixed CPTP SPAM channels within the budget. Twirling gives the generator G of Eq. (4) with gains in $[l, 1]$ (Appendix A). At the reference, $\mathcal{D}_r$ acts as a scalar on each Pauli support sector, so twirling leaves it unchanged. Trace preservation and unitality give $\mathcal{D}\mathcal{L}_\eta = \mathcal{L}_\eta \mathcal{D} = 0$. Hence $\mathcal{D}_r \mathcal{L}_\eta = \mathcal{L}_\eta \mathcal{D}_r = r\mathcal{L}_\eta$ and $G_\eta = L_\eta$.

Let $\mathcal{E}_{23}$ contain the fifteen nonidentity diagonal positions and both orientations of Eq. (13), and let $\mathcal{E}_{27}$ add the four entries of Eq. (27). For a matrix X, $\|X\|_{\max,\mathcal{E}}$ is the maximum absolute entry on $\mathcal{E}$. The local target modulus is

$$\begin{aligned} \omega_\eta(\delta) = \sup\{&|h_{ZZ}(M) - h_0| : M \in \mathfrak{M}_\varepsilon, \\ &\|G(M) - G_\eta\|_{\max,\mathcal{E}_{27}} \leq \delta\}. \end{aligned} \tag{K4}$$

Theorem 6 (Uniform local crossover)**.** *For each fixed $0 < \varepsilon < 1$, there are positive $c_\varepsilon, C_\varepsilon, \delta_0$, independent of $|\eta| \leq 0.01$, such that, for $0 < \delta \leq \delta_0$,*

$$\begin{aligned} \omega_\eta(\delta) &\geq c_\varepsilon \min\{\sqrt{\delta}, \delta/|\eta|\}, \\ \omega_\eta(\delta) &\leq C_\varepsilon \min\{\sqrt{\delta}, \delta/|\eta|\}. \end{aligned} \tag{K5}$$

Here and below $x/|\eta| = +\infty$ at $\eta = 0$ for $x > 0$. Every reference exactly identifies $h_{ZZ} = 0.1$ from $\mathcal{E}_{23}$, and hence from the exact data. The orders in Eq. (K5) also hold for the maximum over all transfer entries. For the $\mathcal{E}_{23}$ record, the modulus remains $\Theta_\varepsilon(\sqrt{\delta})$ for every reference in this family, in the same surrounding class.

2. Canonical coefficients under gauge transformations

Let S fix II and multiply the three nonidentity support sectors by positive scalars s_1, s_2, s_{12}. To distinguish gauge coordinates from the confidence level used below, write

$$\begin{gathered} a = \log(s_{12}/s_1), \qquad b = \log(s_{12}/s_2), \\ \widetilde{L}_{\eta,a,b} = S L_\eta S^{-1}. \end{gathered} \tag{K6}$$

At $\eta = 0$, the full canonical inverse is Eq. (G1), with $(\alpha_g, \beta_g) = (a, b)$ and $h = h_0$. In particular,

$$\widetilde{h}_{ZZ} = \tfrac{h_0}{2}(\cosh a + \cosh b) + k \sinh b. \tag{K7}$$

The diagonal Kossakowski coefficients are unchanged. The additional coefficients produced by η are as follows.

The additional correlation contributes $\eta\mathcal{V}$, where

$$\mathcal{V}(O) = IX\,O\,YZ + YZ\,O\,IX. \tag{K8}$$

Its anticommutators cancel because IX and YZ anticommute. More generally, write $PQ = \chi_P(Q)QP$ for Pauli labels. A Kossakowski pair $C_{AB} = \overline{C_{BA}}$ that is real with $\{A, B\} = 0$, or imaginary with $[A, B] = 0$, has cancelling anticommutator terms and contributes

$$Q \mapsto C_{AB}\,[\chi_A(Q) - \chi_B(Q)]\,QAB. \tag{K9}$$

For $\mathcal{V}$, $IX\,YZ = -iYY$ and $\chi_{IX}\chi_{YZ} = \chi_{YY}$, so $\mathcal{V}(Q)$ vanishes unless Q anticommutes with YY, and then it is proportional to QYY. At $Q = XI, ZI, IX, IZ$ it gives $\mathcal{V}(Q) = 2ZY, -2XY, 2YZ, 2YX$. The other four inputs give the reverse entries, which are equal because $\mathcal{V}$ is Hilbert–Schmidt self-adjoint. The nonzero transfer pairs are therefore

(R, Q)	$V_{R,Q} = V_{Q,R}$
(ZY, XI)	2
(XY, ZI)	-2
(YZ, IX)	2
(YX, IZ)	2

(K10)

Under $S(\cdot)S^{-1}$ an entry (R, Q) is multiplied by s_R/s_Q, so the first two pairs acquire factors $e^{\pm a}$ and the last two acquire $e^{\pm b}$. Their complete additional canonical coefficients are

$$\begin{aligned}
\Delta\widetilde{h}_{YY} &= -\eta\sinh a,\\
\Delta\widetilde{C}_{IX,YZ} &= \tfrac{\eta}{2}(\cosh a + \cosh b),\\
\Delta\widetilde{C}_{IZ,YX} &= \tfrac{\eta}{2}(\cosh b - \cosh a),\\
\Delta\widetilde{C}_{IY,YI} &= -\tfrac{i\eta}{2}\sinh a,\\
\Delta\widetilde{C}_{XX,ZZ} &= \tfrac{i\eta}{2}\sinh b,\\
\Delta\widetilde{C}_{XZ,ZX} &= \tfrac{i\eta}{2}\sinh b.
\end{aligned} \tag{K11}$$

Include the conjugate Kossakowski coefficients; all other added coefficients vanish. Each listed Kossakowski pair has $AB \propto YY$ and is real anticommuting or imaginary commuting. By Eq. (K9), these pairs and the YY Hamiltonian term act only on inputs anticommuting with YY, mapping each to its partner in Eq. (K10). Let Λ be the transfer matrix of these added terms, and for the jth listed pair (R_j, Q_j) put $\Lambda_j^{\pm} = (\Lambda_{R_j,Q_j} \pm \Lambda_{Q_j,R_j})/2$. Write $\kappa_0, \kappa_1, \kappa_2$ for the added YY, (IX, YZ), and (IZ, YX) coefficients and $i\kappa_3, i\kappa_4, i\kappa_5$ for the three imaginary Kossakowski coefficients, in the order displayed. Evaluating Eq. (K9) and the commutator gives

$$\begin{aligned}
\Lambda^+ &= 2(\kappa_1 - \kappa_2,\ \kappa_2 - \kappa_1,\ \kappa_1 + \kappa_2,\ \kappa_1 + \kappa_2),\\
\Lambda^- &= (-\kappa_0 - 2\kappa_3 + 2\kappa_4 - 2\kappa_5,\\
&\qquad \kappa_0 + 2\kappa_3 + 2\kappa_4 - 2\kappa_5,\\
&\qquad -\kappa_0 + 2\kappa_3 + 2\kappa_4 + 2\kappa_5,\\
&\qquad \kappa_0 - 2\kappa_3 + 2\kappa_4 + 2\kappa_5).
\end{aligned} \tag{K12}$$

Equation (K11) gives $\Lambda^+ = 2\eta(\cosh a, -\cosh a, \cosh b, \cosh b)$ and $\Lambda^- = 2\eta(\sinh a, -\sinh a, \sinh b, \sinh b)$, precisely the scaled entries of $\eta S\mathcal{V}S^{-1}$. The canonical decomposition is linear and unique, so these are the complete additional coefficients; with Eq. (G1) they give the whole gauge transformation.

In particular, $\widetilde{h}_{ZZ}$ in Eq. (K7) is independent of η. The entire block of $\widetilde{C}$ inside $\mathcal{K}$ has zero diagonal and only

$$\begin{aligned}
\widetilde{C}_{XX,YY} &= -\tfrac{ik}{2}\sinh a,\\
\widetilde{C}_{XY,YX} &= \tfrac{ik}{2}\sinh a,\\
\widetilde{C}_{XX,ZZ} &= \tfrac{i\eta}{2}\sinh b,\\
\widetilde{C}_{XZ,ZX} &= \tfrac{i\eta}{2}\sinh b,
\end{aligned} \tag{K13}$$

and their conjugates. The extra response sector is YY, while the reference entries on $\mathcal{E}_{23}$ are independent of η.

3. A universal four-entry physical constraint

Lemma 4 (Four-entry canonical functional)**.** *For any complex, possibly nonunital two-qubit generator in the canonical convention of Eq.* (1)*,*

$$\begin{aligned}
\Phi(L) &:= \operatorname{Im} C_{XX,ZZ} + \operatorname{Im} C_{XZ,ZX}\\
&= \tfrac{1}{8}\big(L_{YZ,IX} + L_{YX,IZ}\\
&\qquad - L_{IX,YZ} - L_{IZ,YX}\big).
\end{aligned} \tag{K14}$$

For the transformed reference, $\Phi(\widetilde{L}_{\eta,a,b}) = \eta\sinh b$.

Proof. Specializing Eq. (A6) to $d = 4$ gives

$$\operatorname{Im} C_{ab} = \tfrac{1}{64}\sum_{R,Q\in\mathcal{P}} \operatorname{Im}\operatorname{Tr}(P_a R P_b Q)\,L_{R,Q}, \tag{K15}$$

where $\mathcal{P} = \{I, X, Y, Z\}^{\otimes 2}$ includes II. Transfer entries are real for a Hermiticity-preserving map. With $PR = \chi_P(R)RP$, the products $XX\,ZZ = -YY$ and $XZ\,ZX = YY$ give

$$\begin{aligned}
&\operatorname{Tr}(XX\,R\,ZZ\,Q) + \operatorname{Tr}(XZ\,R\,ZX\,Q)\\
&\quad = [\chi_{ZX}(R) - \chi_{ZZ}(R)]\operatorname{Tr}(YY\,RQ).
\end{aligned} \tag{K16}$$

This vanishes unless $R \oplus Q = YY$, is real when R commutes with YY, and has zero prefactor when R commutes with $ZX\,ZZ \propto IY$. Imaginary contributions therefore occur only at $(R, Q) = (YZ, IX), (YX, IZ), (IX, YZ), (IZ, YX)$, where the sum equals $8i, 8i, -8i, -8i$. Their coefficients are respectively $1/8, 1/8, -1/8, -1/8$. This proves Eq. (K14) over all 256 transfer positions, including the identity input column, and covers nonunital generators. Equation (K11) gives the final assertion. □

Next, for any candidate in Eq. (K4), undo its own detector gauge transformation with $S = \bar{B}^{-1}$. Put $r_A = b_{12}/b_1$, $r_B = b_{12}/b_2$. Then

$$\begin{aligned} r_A, r_B &\in [l, l^{-1}], \\ a = -\log r_A, &\qquad b = -\log r_B. \end{aligned} \tag{K17}$$

The candidate physical transfer matrix and $\widetilde{L}_{\eta,a,b}$ differ on each of the required off-diagonal entries by at most δ/l. Diagonal entries are unchanged by the gauge transformation, and Walsh inversion, Eq. (A10), also holds for nonunital generators because trace preservation fixes $L_{II,II} = 0$. Thus the error in each diagonal Kossakowski coefficient is at most $15\delta/16 \le \delta$.

The four diagonal Kossakowski coefficients XX, ZZ, XZ, ZX vanish at the reference. They therefore lie between zero and δ in a physical candidate. Positivity of its two-by-two minors gives

$$\begin{aligned} |\Phi(L)| &\le \sqrt{C_{XX,XX}C_{ZZ,ZZ}} + \sqrt{C_{XZ,XZ}C_{ZX,ZX}} \\ &\le 2\delta. \end{aligned} \tag{K18}$$

The four coefficients in Eq. (K14) contribute at most $\delta/(2l)$ error. Hence, with $A_\varepsilon = 2 + 1/(2l)$ and $|\sinh b| \ge |b|$,

$$\begin{aligned} |\eta \sinh b| &\le A_\varepsilon \delta, \\ |b| &\le A_\varepsilon \delta/|\eta| \qquad (\eta \neq 0). \end{aligned} \tag{K19}$$

This necessary inequality holds for every compatible complex physical model. The construction below supplies the matching lower bound.

4. Exact identification and an upper bound on the modulus

The reference $\mathcal{E}_{23}$ entries and all recovered diagonal rates are independent of η. The exact identification proof in Appendix I therefore applies unchanged to every reference: its three zero-row constraints force $r_A = 1$, followed by $.06/r_B - .04 r_B = .02$, whose only positive solution is $r_B = 1$. Hence $h_{ZZ} = .1$ for every exactly compatible physical model in the common inference class.

The finite-error inequalities in Eqs. (I14) and (I18) likewise apply to every complex, possibly nonunital candidate:

$$\begin{aligned} |r_A - 1| &\le d_A(\delta) = O_\varepsilon(\sqrt{\delta}), \\ |h_{ZZ}(M) - h_0| &\le F_\varepsilon(\delta) = O_\varepsilon(\sqrt{\delta}). \end{aligned} \tag{K20}$$

The constants are those of Eq. (I14); they do not depend on η, since the reference entries coincide.

We now turn to the augmented record. The mean value theorem for log on $[l, l^{-1}]$ and Eq. (K20) give $|a| \le |r_A - 1|/l \le d_A/l$. We take $\delta_0 \le 1$; for $0 < \delta \le 1$, Eq. (I14) gives $d_A \le K_\varepsilon\sqrt{\delta}$ with $K_\varepsilon = 20(4\sqrt{1.1} + l + l^{-1})$. On the box $|a|, |b| \le B := \log(l^{-1})$, Taylor's theorem gives $0 \le \cosh a - 1 \le (\cosh B)a^2/2 \le (\cosh B)K_\varepsilon^2\delta/(2l^2)$. The target formula in Eq. (K7) and the eight-entry projection in Eq. (I9) give

$$\begin{aligned} &|h_{ZZ}(M) - h_0| \\ &\quad \le \delta/l + \tfrac{h_0}{2}|\cosh a - 1| \\ &\quad + \left|\tfrac{h_0}{2}(\cosh b - 1) + k \sinh b\right|. \end{aligned} \tag{K21}$$

The function $\varphi(t) = \frac{h_0}{2}(\cosh t - 1) + k \sinh t$ has $\varphi(0) = 0$ and $|\varphi'| \le \frac{h_0}{2}\sinh B + k \cosh B =: L_\varepsilon$ on $[-B, B]$, so the last term is at most $L_\varepsilon|b|$. Equation (K19) therefore bounds Eq. (K21) by $C_\varepsilon(\delta + \delta/|\eta|) \le C'_\varepsilon\delta/|\eta|$ for $0 < |\eta| \le .01$. Taking the smaller of this bound and Eq. (K20) proves the upper inequality in Theorem 6. At $\eta = 0$, only the square-root bound is needed.

5. Adding depolarizing noise with explicit Schur bounds

Set $a = 0$, $b = -\theta$, where $|\theta| \le .01$, and let S_θ scale only IX, IY, IZ by e^θ. Thus $\widetilde{L}_{\eta,0,-\theta} = S_\theta L_\eta S_\theta^{-1}$. Write $c = \cosh\theta$, $s = \sinh\theta$. Equations (G1) and (K11) reduce to

$$\begin{aligned} u_1 &= \tfrac{k}{2}(1 + c) - \tfrac{h_0}{4}s, \\ u_2 &= \tfrac{k}{2}(1 - c) + \tfrac{h_0}{4}s, \\ v_0 &= \tfrac{h_0}{4}(c - 1) - \tfrac{k}{2}s, \\ w &= \tfrac{\eta}{2}(1 + c), \\ z &= \tfrac{\eta}{2}(c - 1). \end{aligned} \tag{K22}$$

Decompose the Kossakowski matrix relative to the range and kernel of C_η:

$$\widetilde{C}_{\eta,0,-\theta} = \begin{pmatrix} \mathsf{A} & \mathsf{B} \\ \mathsf{B}^\dagger & \mathsf{D} \end{pmatrix}. \tag{K23}$$

Here A consists of

$$\begin{aligned} &\begin{pmatrix} \lambda & 0 & u_1 \\ 0 & \lambda & w \\ u_1 & w & m \end{pmatrix} \quad \text{on } (XI, IX, YZ), \\ &\begin{pmatrix} \lambda & iv_0 \\ -iv_0 & \lambda \end{pmatrix} \quad \text{on } (ZI, IZ), \end{aligned} \tag{K24}$$

and the unchanged YI, IY singletons. The only entries of B are u_2 on (YI, XZ) and z on (IZ, YX). The kernel block D has two disjoint Hermitian phase blocks, with entries $-i\eta s/2$ on (XX, ZZ) and (XZ, ZX), their conjugates, and zero elsewhere.

Lemma 5 (Uniform depolarizing correction)**.** *For every $|\eta| \le .01$ and $|\theta| \le .01$, set*

$$K_\times = 0.6, \qquad q_{\eta,\theta} = K_\times(\theta^2 + |\eta\theta|). \tag{K25}$$

Then $\widetilde{C}_{\eta,0,-\theta} + q_{\eta,\theta} I_{15} \succeq 0$. The corresponding physical generator is

$$\mathcal{L}_{\eta,\theta} = S_\theta \mathcal{L}_\eta S_\theta^{-1} + 16 q_{\eta,\theta}(\mathcal{D} - \mathrm{id}), \tag{K26}$$

and its canonical target satisfies

$$\begin{aligned} h_\theta &= .05(1+\cosh\theta) - .01\sinh\theta, \\ |h_\theta - h_0| &\geq .0097|\theta|. \end{aligned} \tag{K27}$$

All statements and constants are uniform on the specified rectangle.

Proof. The formulas for u_1, u_2, v_0 coincide with those of Appendix G on the same interval, so Eq. (G6) applies; the cosh estimate used there also bounds w:

$$\begin{aligned} |u_1| &< .0103, & |u_2| &\leq .0251|\theta|, \\ |v_0| &< .000052, & |w| &< .010001. \end{aligned} \tag{K28}$$

To bound the occupied block below by $a_* = .01$, subtract $a_* I$ from its diagonal. The Schur complement of the first two diagonals in the three-by-three block is strictly positive because

$$.01 - \frac{.0103^2 + .010001^2}{.09} = \frac{693889999}{90000000000} > 0. \tag{K29}$$

The other blocks have remaining diagonal .09 and, at most, off-diagonal magnitude .000052. Hence $\mathsf{A} \succeq .01 I$. The only possibly nonzero entries of B, u_2 and z, lie in distinct rows and columns. Since

$$|z| \leq .2505|\eta|\theta^2 \leq .00002505|\theta|, \tag{K30}$$

we obtain the operator-norm estimates

$$\begin{aligned} \|\mathsf{B}\| &= \max\{|u_2|, |z|\} \leq .0251|\theta|, \\ \|\mathsf{D}\| &= \tfrac{1}{2}|\eta\sinh\theta| \leq .5005|\eta\theta|. \end{aligned} \tag{K31}$$

For $q = q_{\eta,\theta}$, the inverse occupied block is at most $a_*^{-1} I$. The Schur complement after adding this noise therefore satisfies

$$\begin{aligned} &qI + \mathsf{D} - \mathsf{B}^\dagger(\mathsf{A} + qI)^{-1}\mathsf{B} \\ &\quad\succeq \left[q - .5005|\eta\theta| - \frac{.0251^2}{.01}\theta^2\right] I \\ &\quad= \left[.536999\theta^2 + .0995|\eta\theta|\right] I \succeq 0. \end{aligned} \tag{K32}$$

This proves physicality, including the rank-deficient point $\theta = 0$. By Eq. (A11) at $n = 2$, adding qI_{15} to the Kossakowski matrix gives $16q(\mathcal{D} - \mathrm{id})$. It changes no Hamiltonian coefficient. Finally, h_θ coincides with the target of the path in Appendix G, so Eq. (G8) gives

$$|h_\theta - h_0| \geq .01|\theta| - .02505\theta^2 \geq .0097|\theta|. \tag{K33}$$

□

6. Physical SPAM channels and the matching lower bound

The compensating SPAM channels $A_\theta = S_\theta \mathcal{D}_r$ and $B_\theta = \mathcal{D}_r S_\theta^{-1}$ of Eq. (H4) do not depend on the generator. For $|\theta| \leq \theta_{\max} := \varepsilon/100$ they are CPTP with Pauli-mixture coefficients above $\varepsilon/256$, obey the budget, and keep the zero-time calibration $B_\theta A_\theta = \mathcal{D}_r^2$ [Eqs. (H7), (H9), and (H10)].

Write $\Pi_0 = \mathrm{id} - \mathcal{D}$ for the traceless transfer projector. Twirling leaves B_θ unchanged. The maps S_θ and $\mathcal{D}_r$ commute with Π_0, and $\mathcal{D}_r$ commutes with $\mathcal{L}_\eta$. Boundary compensation therefore gives exactly $G_{\eta,\theta} = \mathcal{D}_r S_\theta^{-1}(S_\theta L_\eta S_\theta^{-1} - 16 q_{\eta,\theta}\Pi_0) S_\theta \mathcal{D}_r^{-1}$, that is,

$$\begin{aligned} G_{\eta,\theta} &= G_\eta - 16 q_{\eta,\theta}\Pi_0, \\ \|G_{\eta,\theta} - G_\eta\|_{\max} &= 16 q_{\eta,\theta}. \end{aligned} \tag{K34}$$

The maximum is the same for $\mathcal{E}_{27}$ and the full transfer matrix, since Π_0 has unit entries exactly on the fifteen nonidentity diagonal positions. For a desired $\delta > 0$, put

$$\begin{aligned} x &= \frac{\delta}{16 K_\times}, \\ \theta(x,\eta) &= \frac{\sqrt{\eta^2 + 4x} - |\eta|}{2}. \end{aligned} \tag{K35}$$

This is the nonnegative root of $t^2 + |\eta| t = x$. If $R_x = \min\{\sqrt{x}, x/|\eta|\}$, then

$$\tfrac{1}{2} R_x \leq \theta(x,\eta) \leq R_x. \tag{K36}$$

To check both constants, the increasing function $f(t) = t^2 + |\eta| t$ has $f(R_x/2) \leq 3x/4$ and $f(R_x) \geq x$. Also $\theta(x,\eta) \leq \sqrt{x}$. Consequently

$$0 < \delta \leq 16 K_\times \theta_{\max}^2 \tag{K37}$$

places every such alternative inside the physical boundary interval, uniformly in η. These alternatives satisfy $16 q_{\eta,\theta} = 16 K_\times x = \delta$, so Eqs. (K27), (K34), and (K36) give

$$\omega_\eta(\delta) \geq .0097\,\theta \geq .00485 R_x \geq \frac{.00485}{9.6}\min\{\sqrt{\delta}, \delta/|\eta|\}, \tag{K38}$$

the lower inequality in Theorem 6. These alternatives also satisfy the constraints on all entries of G, which imply the $\mathcal{E}_{27}$ constraints. The upper bound therefore establishes the theorem for both metrics, after decreasing δ_0 if needed.

For the last assertion of the theorem, the centers $G_\eta|_{\mathcal{E}_{23}}$ coincide for all η, and the admissible class is the same. Their entire compatible target sets for this metric are therefore equal. The upper bound (K20) and the construction just given at $\eta = 0$ show that their common modulus is $\Theta_\varepsilon(\sqrt{\delta})$.

Remark 2. The argument constructs finite physical alternatives directly, and the statistical comparison below uses $\theta \geq 0$. For $\eta \neq 0$, the correction $q_{\eta,\theta}$ is not C^2 in θ at zero.

7. Comparison for all durations and adaptive confidence lower bound

Proposition 4 (Adaptive shot lower bound)**.** *Let $0 < \alpha < 1/2$. For any allowed adaptive N-shot protocol and any interval I_N uniformly valid at confidence $1-\alpha$ over a physical class containing all the reference models and alternatives above,*

$$\begin{aligned}&\mathbb{E}_{\eta,0}|I_N| \\ &\geq c_{\varepsilon,\alpha}\min\{\theta_{\max}, N^{-1/4}, N^{-1/2}/|\eta|\}.\end{aligned} \tag{K39}$$

The positive constant is independent of $|\eta| \leq .01$ and of the protocol, its finite durations, and its sequence lengths.

Proof. The complete-record argument of Appendix H applies with q_θ replaced by $q_{\eta,\theta}$. Its only new input is a mixing constant uniform in η. Subtracting .05 from the six single-qubit diagonals of C_η leaves a real positive semidefinite residual, since

$$.05 \cdot .02 > k^2 + \eta^2 \qquad (|\eta| \leq .01). \tag{K40}$$

The proof of Eq. (H13) therefore gives, uniformly in η,

$$\|\mathcal{P}_\eta(O)\|_2 \leq e^{-T/5}\|O\|_2, \qquad \operatorname{Tr} O = 0, \tag{K41}$$

for every allowed local-unitary sequence of total duration T. The complete-experiment identity Eq. (H15) holds with $\mathcal{P}_\eta$ and $16q_{\eta,\theta}$, so the estimate of Eq. (H16) bounds each outcome-probability change by $32q_{\eta,\theta}$ for all finite durations and control sequences. The four outcomes give a squared probability difference at most $4(32q_{\eta,\theta})^2$. Each outcome probability is at least $\mu = \varepsilon/64$ by Eq. (H17). Lemma 1 therefore yields

$$\begin{aligned}&D_{\mathrm{KL}}(P^{(N)}_{\eta,0}\|P^{(N)}_{\eta,\theta}) \\ &\quad\leq NM_\varepsilon(\theta^2 + |\eta\theta|)^2, \\ &M_\varepsilon = \frac{262144K_\times^2}{\varepsilon}.\end{aligned} \tag{K42}$$

For $0 < \alpha < 1/2$, set $v = (1-2\alpha)/2$, $x_N = \sqrt{2v^2/(M_\varepsilon N)}$, and $\theta_N = \min\{\theta_{\max}, \theta(x_N, \eta)\}$. Equation (K42) bounds the relative entropy by $2v^2$. Lemma 1 and the weaker gap $\theta_N/200$ from Eq. (K27) give $\mathbb{E}_{\eta,0}|I_N| \geq (1-2\alpha-v)\theta_N/200$. The root comparison in Eq. (K36), including clipping at $\theta_{\max}$, proves Eq. (K39) with constants uniform in η. □

8. Estimating the 27 entries and bounding the expected length

For the upper result, assume the known bound $\gamma > 0$ in Eq. (C1) on the summed norms of the physical two-local terms acting on each qubit. Fix this local norm bound independently of N, η, with a strict margin for the displayed family. A finite bound suffices: the strength estimate of Eq. (G9), applied to the Kossakowski matrix after adding depolarizing noise, whose trace is $6\lambda + m + 15q_{\eta,\theta}$, gives at most

$$|h_\theta| + 8(6\lambda + m + 15q_{\eta,\theta}), \tag{K43}$$

uniformly on the parameter rectangle. The estimator applies uniformly over unknown η and complex Kossakowski matrices subject to this norm bound.

Apply the estimator of Appendix C to the 27 derivative responses and the same fifteen calibration means. All added responses have Pauli support at most two, so its derivative, interpolation, and normalization bounds apply unchanged to every candidate, with the Chebyshev–Lobatto constants of Eq. (C30) at degree $p \geq 1$ on $[0, 1/\gamma]$. The number of means is $27 + 15 = 42$: for failure probability $0 < \zeta < 1$, the factor $\log(76/\alpha)$ in Eq. (C20) becomes $\log(84/\zeta)$. With fresh time, input-sign, and boundary randomizations on every shot, Eq. (C23) becomes

$$\begin{aligned}&\|\widehat{G} - G\|_{\max,\mathcal{E}_{27}} \leq \delta_G, \\ &\delta_G = \frac{s_D + \beta_p}{l} + \frac{2\gamma s_0}{l^2},\end{aligned} \tag{K44}$$

with probability at least $1 - \zeta$.

Proposition 5 (Upper bound on the expected length without an η prior)**.** *For fixed $0 < \alpha < 1/2$ and the common local norm bound above, a single procedure, independent of η, is uniformly valid at confidence $1-\alpha$ over the bounded-strength class and satisfies, for all sufficiently large N,*

$$\begin{aligned}&\mathbb{E}_{\eta,0}|I_N| \\ &\quad\leq C_\varepsilon \min\{\sqrt{\delta_N}, \delta_N/|\eta|\} + 2H_*\zeta_N, \\ &\delta_N = O_{\varepsilon,\gamma,\alpha}\big(N^{-1/2}(\log N)^{5/2}\big),\end{aligned} \tag{K45}$$

uniformly for $|\eta| \leq .01$, with $H_* = 2\gamma$ and $\zeta_N = \min\{\alpha, N^{-1}\}$.

Proof. Set $n_N = \lfloor N/42 \rfloor$ and allocate n_N shots to each of the 42 means. Leave the remaining shots unused and take

$$\begin{aligned}&p = \max\{1, \lceil \log_2(N+1) \rceil\}, \\ &s_0 = \sqrt{2\log(84/\zeta_N)/n_N}, \qquad s_D = Ws_0.\end{aligned} \tag{K46}$$

For $N \geq 42$, the concentration bounds apply directly. Since $W = O_\gamma((\log N)^2)$ and $\beta_p = O_\gamma((\log N)^2 N^{-2})$, Eq. (K44) gives the displayed δ_N. Small budgets can return $[-H_*, H_*]$.

Apply Lemma 2 to the class with this local norm bound, using the finite-valued estimate on $\mathcal{E}_{27}$ and target bound $H_* = 2\gamma$ from Eq. (A8). The modulus ω_η over the larger class bounds the retained targets, giving

$$\mathbb{E}_{\eta,0}|I_N| \leq 2\omega_\eta(2\delta_N) + 2H_*\zeta_N. \tag{K47}$$

Since $\delta_N \to 0$ independently of η, sufficiently large N satisfy $2\delta_N \leq \delta_0$, and Theorem 6 gives $2\omega_\eta(2\delta_N) \leq 2C_\varepsilon \min\{\sqrt{2\delta_N}, 2\delta_N/|\eta|\} \leq 4C_\varepsilon \min\{\sqrt{\delta_N}, \delta_N/|\eta|\}$. This proves Eq. (K45), with its constant equal to four times that of Theorem 6. □

Appendix L: Lift to n-qubit physical two-local models

We prove Corollary 2 and Theorem 3 by reducing every n-qubit physical two-local model to its pair block (Lemmas 6 and 7) and then applying the two-qubit arguments of Appendices H, I, and K.

1. Class, pair reduction, and lifted references

Let $n \geq 2$, $\mathsf{A} = \{1, 2\}$, $\mathsf{E} = \{3, \dots, n\}$, $d_{\mathsf{E}} = 2^{n-2}$, and $\iota(Q) = Q \otimes I_{\mathsf{E}}$ for two-qubit Pauli labels Q. The physical two-local class $\mathfrak{M}_{\varepsilon}^{\mathrm{L2}}$ consists of n-qubit boundary channels obeying Eq. (2) and generators

$$\mathcal{L} = \sum_{Z \subseteq \{1,\dots,n\},\ 1 \leq |Z| \leq 2} \mathcal{L}_Z \otimes \mathrm{id}_{Z^c}, \tag{L1}$$

where each $\mathcal{L}_Z$ is a GKSL generator on the qubits of Z. Its subclass $\mathfrak{M}_{\varepsilon,\gamma}^{\mathrm{L2}}$ also obeys Eq. (C1) with $k_{\mathrm{loc}} = 2$, which bounds the summed norms of the terms acting on each qubit. Put $l = 1 - \varepsilon$, take the pair-reduction maps $\mathcal{E}_{\mathsf{A}}$, $\mathcal{R}_{\mathsf{A}}$, and $\mathcal{L}_{\mathsf{A}}$ of Eq. (C5), and write $G^{\mathsf{A}}_{R,Q} = G_{\iota(R),\iota(Q)}$ for the pair block of G; d_{23} and d_{27} are evaluated on G^{A}. The target is $h = h_{ZZ \otimes I_{\mathsf{E}}}$.

Fix an allowance $0 < \varepsilon_{\mathsf{A}} \leq \varepsilon$ for the active SPAM channels, and put $r = 1 - \varepsilon_{\mathsf{A}}/8$ and $\theta_{\max} = \varepsilon_{\mathsf{A}}/100$. The maps $\mathcal{D}$, $\mathcal{D}_r$, $\Pi_0 = \mathrm{id} - \mathcal{D}$, and S_θ of Appendix H act on A. Spectator data consist of a generator $\mathcal{L}_{\mathsf{E}}$ that is a sum of single- and two-qubit GKSL terms on E, and CPTP maps $A_{\mathsf{E}}, B_{\mathsf{E}}$ on E with

$$\varepsilon_{\mathsf{E}} := \|A_{\mathsf{E}} - \mathrm{id}\|_\diamond + \|B_{\mathsf{E}} - \mathrm{id}\|_\diamond \leq \varepsilon - \varepsilon_{\mathsf{A}}.$$

Let $\mathcal{L}_\eta^{\mathsf{A}}$ be the two-qubit generator with Hamiltonian $h_0 ZZ/2$ and Kossakowski matrix C_η of Sec. VI, $|\eta| \leq .01$; $\eta = 0$ gives Eq. (14). The lifted reference is

$$\begin{aligned} \mathcal{L}_0 &= \mathcal{L}_\eta^{\mathsf{A}} \otimes \mathrm{id}_{\mathsf{E}} + \mathrm{id}_{\mathsf{A}} \otimes \mathcal{L}_{\mathsf{E}}, \\ A_0 &= \mathcal{D}_r \otimes A_{\mathsf{E}}, \qquad B_0 = \mathcal{D}_r \otimes B_{\mathsf{E}}. \end{aligned} \tag{L2}$$

For $n = 2$, E is empty, $\varepsilon_{\mathsf{E}} = 0$, and $\varepsilon_{\mathsf{A}} = \varepsilon$ is allowed.

Lemma 6 (Factorized lift)**.** *Let $(\mathcal{L}^{\mathsf{A}}, A^{\mathsf{A}}, B^{\mathsf{A}})$ be a physical two-qubit model and $(\mathcal{L}_{\mathsf{E}}, A_{\mathsf{E}}, B_{\mathsf{E}})$ spectator data as above, and set*

$$\mathcal{L} = \mathcal{L}^{\mathsf{A}} \otimes \mathrm{id}_{\mathsf{E}} + \mathrm{id}_{\mathsf{A}} \otimes \mathcal{L}_{\mathsf{E}}, \quad A = A^{\mathsf{A}} \otimes A_{\mathsf{E}}, \quad B = B^{\mathsf{A}} \otimes B_{\mathsf{E}}.$$

(i) $\|A - \mathrm{id}\|_\diamond + \|B - \mathrm{id}\|_\diamond \leq \|A^{\mathsf{A}} - \mathrm{id}\|_\diamond + \|B^{\mathsf{A}} - \mathrm{id}\|_\diamond + \varepsilon_{\mathsf{E}}$. (ii) *For every allowed n-qubit setting s, the outcome law is $p(o_{\mathsf{A}}, o_{\mathsf{E}} \mid s) = p^{\mathsf{A}}(o_{\mathsf{A}} \mid s_{\mathsf{A}})\, p^{\mathsf{E}}(o_{\mathsf{E}} \mid s_{\mathsf{E}})$, where s_{A} is an allowed two-qubit setting, p^{A} is its law under $(\mathcal{L}^{\mathsf{A}}, A^{\mathsf{A}}, B^{\mathsf{A}})$, and p^{E} depends only on the spectator data and s_{E}.* (iii) *Two such lifts with the same spectator data have, at every setting, the relative entropy of their active factors; if their two-qubit models have identical exact data, so do the lifts.* (iv) *Twirling gives $\bar{B} = \bar{B}^{\mathsf{A}} \otimes \bar{B}_{\mathsf{E}}$. If $\|A - \mathrm{id}\|_\diamond + \|B - \mathrm{id}\|_\diamond < 1$, both factors are invertible, the pair block of G is $G^{\mathsf{A}} = \bar{B}^{\mathsf{A}} \mathcal{L}^{\mathsf{A}} (\bar{B}^{\mathsf{A}})^{-1}$, and*

$$G = G^{\mathsf{A}} \otimes \mathrm{id}_{\mathsf{E}} + \mathrm{id}_{\mathsf{A}} \otimes \bar{B}_{\mathsf{E}} \mathcal{L}_{\mathsf{E}} \bar{B}_{\mathsf{E}}^{-1}.$$

Two such lifts with the same spectator data obey $G - G' = (G^{\mathsf{A}} - G'^{\mathsf{A}}) \otimes \mathrm{id}_{\mathsf{E}}$ and $\|G - G'\|_{\max} = \|G^{\mathsf{A}} - G'^{\mathsf{A}}\|_{\max}$. (v) *If $\|(\mathcal{L}^{\mathsf{A}})^\dagger \otimes \mathrm{id}_F\|_{\infty\to\infty} \leq g_{\mathsf{A}}$ for every register F and the terms of $\mathcal{L}_{\mathsf{E}}$ obey the local norm bound γ_{E}, the lifted generator has the decomposition of Eq. (L1) with local norm bound $\max\{g_{\mathsf{A}}, \gamma_{\mathsf{E}}\}$.*

Proof. (i) The diamond norm is submultiplicative under composition, unchanged by tensoring with an identity map, and equal to one on channels. Since $\Phi \otimes \Psi = (\Phi \otimes \mathrm{id})(\mathrm{id} \otimes \Psi)$, the decomposition

$$A - \mathrm{id} = (A^{\mathsf{A}} - \mathrm{id}) \otimes A_{\mathsf{E}} + \mathrm{id}_{\mathsf{A}} \otimes (A_{\mathsf{E}} - \mathrm{id})$$

gives $\|A - \mathrm{id}\|_\diamond \leq \|A^{\mathsf{A}} - \mathrm{id}\|_\diamond + \|A_{\mathsf{E}} - \mathrm{id}\|_\diamond$, and likewise for B.

(ii) A setting consists of a product input $\bigotimes_j \rho_j$, durations $t_1, \dots, t_{\mathsf{k}} \geq 0$, products $\mathcal{U}^{(0)}, \dots, \mathcal{U}^{(\mathsf{k})}$ of single-qubit unitary channels applied before, between, and after the evolution intervals (the first immediately after A and the last immediately before B), and a rank-one product projective measurement. Its experiment map is $B\mathcal{U}^{(\mathsf{k})} e^{t_{\mathsf{k}}\mathcal{L}} \cdots \mathcal{U}^{(1)} e^{t_1 \mathcal{L}} \mathcal{U}^{(0)} A$. Let s_{A} and s_{E} keep the input, unitary, and measurement factors on A and on E. The two summands of $\mathcal{L}$ commute, so $e^{t\mathcal{L}} = e^{t\mathcal{L}^{\mathsf{A}}} \otimes e^{t\mathcal{L}_{\mathsf{E}}}$; every other factor of the experiment map is a tensor product over $\mathsf{A}|\mathsf{E}$. The output state is therefore $\sigma_{\mathsf{A}} \otimes \sigma_{\mathsf{E}}$, with σ_{A} the output of s_{A} under the active model, and a projector $\Pi_{\mathsf{A}} \otimes \Pi_{\mathsf{E}}$ has probability $\mathrm{Tr}(\Pi_{\mathsf{A}}\sigma_{\mathsf{A}})\,\mathrm{Tr}(\Pi_{\mathsf{E}}\sigma_{\mathsf{E}})$.

(iii) For probability vectors p, p', q, $D_{\mathrm{KL}}(p \otimes q \| p' \otimes q) = \sum_{j: q_j > 0} q_j D_{\mathrm{KL}}(p \| p') = D_{\mathrm{KL}}(p \| p')$. The exact data are the collection of the laws in (ii) over all settings.

(iv) Independent uniformly random local Cliffords $V = V_{\mathsf{A}} \otimes V_{\mathsf{E}}$ give $\bar{B} = \mathbb{E}\, V^{-1} B V = \mathbb{E}\, V_{\mathsf{A}}^{-1} B^{\mathsf{A}} V_{\mathsf{A}} \otimes \mathbb{E}\, V_{\mathsf{E}}^{-1} B_{\mathsf{E}} V_{\mathsf{E}}$. In the label order (a, s), the transfer matrix of a tensor product of maps is the Kronecker product of their transfer matrices. The gains of $\bar{B}$ are the products $b_a^{\mathsf{A}} b_s^{\mathsf{E}}$; under the stated budget they are positive by Appendix A, so every factor gain is nonzero. Inserting $\bar{B}^{-1} = (\bar{B}^{\mathsf{A}})^{-1} \otimes \bar{B}_{\mathsf{E}}^{-1}$ in $G = \bar{B}\mathcal{L}\bar{B}^{-1}$ gives the tensor sum. The map $\widetilde{\mathcal{L}}_{\mathsf{E}} = \bar{B}_{\mathsf{E}} \mathcal{L}_{\mathsf{E}} \bar{B}_{\mathsf{E}}^{-1}$ annihilates the trace, because $\bar{B}_{\mathsf{E}}^{\pm 1}$ preserve it and $\mathcal{L}_{\mathsf{E}}$ annihilates it. Hence the pair-block entries $(\mathrm{id}_{\mathsf{A}} \otimes \widetilde{\mathcal{L}}_{\mathsf{E}})_{\iota(R),\iota(Q)} = \delta_{RQ} (\widetilde{\mathcal{L}}_{\mathsf{E}})_{I,I}$ vanish. For common spectator data the second summands cancel, and $[(G^{\mathsf{A}} - G'^{\mathsf{A}}) \otimes \mathrm{id}_{\mathsf{E}}]_{(R,s),(Q,t)} = (G^{\mathsf{A}} - G'^{\mathsf{A}})_{R,Q} \delta_{st}$ attains every active entry at $s = t$.

(v) Assign $\mathcal{L}^{\mathsf{A}}$ to the single term $Z = \mathsf{A}$; all other terms have supports in E. A site of A meets only $Z = \mathsf{A}$, and a site of E meets only spectator terms. □

Lemma 7 (Pair reduction under physical locality)**.** *Let $(\mathcal{L}, A, B) \in \mathfrak{M}_{\varepsilon}^{\mathrm{L2}}$ have canonical data (H, C), and extend C by a zero row and column for the global identity.* (i) *If $C_{ab} \neq 0$, then $\mathrm{supp}\, a \cup \mathrm{supp}\, b \subseteq Z$ for some $|Z| \leq 2$; in*

particular every nonzero canonical jump label has weight at most two. (ii) $\mathcal{L}_{\mathsf{A}}$ *is a physical two-qubit generator with canonical Kossakowski matrix* $(J_{ab})_{a,b\neq 0}$*, where* $J_{ab} = \sum_s C_{(a,s),(b,s)}$*, and its ZZ coefficient is* h*. If* $\operatorname{supp} a \cup \operatorname{supp} b = \mathsf{A}$*, then* $J_{ab} = C_{(a,0),(b,0)}$*.* (iii) $G^{\mathsf{A}} = \bar{B}_{\mathsf{A}}\mathcal{L}_{\mathsf{A}}\bar{B}_{\mathsf{A}}^{-1}$*, where* $\bar{B}_{\mathsf{A}}(Q) = b_{\iota(Q)}Q$ *and* $b_{\iota(Q)} \in [l, 1]$*.* (iv) *At the lifted reference of Eq.* (L2)*,* $\mathcal{L}_{\mathsf{A}} = \mathcal{L}_{\eta}^{\mathsf{A}}$*,* $b_{\iota(Q)} = r$ *for* $Q \neq I$*, and* $G_0^{\mathsf{A}} = \mathcal{L}_{\eta}^{\mathsf{A}}$*.*

Proof. (i) Tensoring the traceless Hamiltonian and the nonidentity jump labels of the canonical form of $\mathcal{L}_Z$ with identities on Z^c represents $\mathcal{L}_Z \otimes \mathrm{id}_{Z^c}$ in the form of Eq. (1), with labels supported in Z. The sum of these representations represents $\mathcal{L}$ in the same form, so uniqueness of canonical coefficients makes C the sum of the embedded Kossakowski matrices. A nonzero C_{ab} therefore occurs in a term whose support contains both labels.

(ii) The reduction in Appendix C, Eq. (C8) and the steps before it, applies to every global generator and gives a physical $\mathcal{L}_{\mathsf{A}}$ with the stated Kossakowski matrix. In Eq. (C9), each correction with $s \neq 0$ contains the label (ZZ, s) of weight $2 + \operatorname{wt} s \geq 3$, and vanishes by (i). For $s \neq 0$ and $\operatorname{supp} a \cup \operatorname{supp} b = \mathsf{A}$, the labels $(a, s), (b, s)$ have union support $\mathsf{A} \cup \operatorname{supp} s$ of size at least three, so $C_{(a,s),(b,s)} = 0$ by (i).

(iii) Since $d = 4d_{\mathsf{E}}$, $d^{-1}\operatorname{Tr}[\iota(R)\mathcal{L}(\iota(Q))] = 4^{-1}\operatorname{Tr}[R\,\mathcal{L}_{\mathsf{A}}(Q)]$, that is, $\mathcal{L}_{\iota(R),\iota(Q)} = (\mathcal{L}_{\mathsf{A}})_{R,Q}$. The gauge transformation $G = \bar{B}\mathcal{L}\bar{B}^{-1}$ multiplies this entry by $b_{\iota(R)}/b_{\iota(Q)}$; the gains lie in $[l, 1]$ by Appendix A.

(iv) $\mathcal{R}_{\mathsf{A}}(\mathcal{L}_{\eta}^{\mathsf{A}} \otimes \mathrm{id}_{\mathsf{E}})\mathcal{E}_{\mathsf{A}} = \mathcal{L}_{\eta}^{\mathsf{A}}$, and $\mathcal{R}_{\mathsf{A}}(\mathrm{id}_{\mathsf{A}} \otimes \mathcal{L}_{\mathsf{E}})\mathcal{E}_{\mathsf{A}}(X) = X\operatorname{Tr}[\mathcal{L}_{\mathsf{E}}(I_{\mathsf{E}})]/d_{\mathsf{E}} = 0$ by trace preservation. The map $\mathcal{D}_r$ acts as a scalar on each Pauli support sector and is unchanged by twirling, so Lemma 6(iv) gives $\bar{B}_0 = \mathcal{D}_r \otimes \bar{B}_{\mathsf{E}}$; since $\bar{B}_{\mathsf{E}}$ has unit gain on the empty sector, $b_{\iota(Q)} = r$ for $Q \neq I$. The Kossakowski matrix C_η is real symmetric, so $\mathcal{L}_{\eta}^{\mathsf{A}}(I) = \sum_{a,b}(C_\eta)_{ab}[P_a, P_b] = 0$; together with trace preservation, the identity row and column of $\mathcal{L}_{\eta}^{\mathsf{A}}$ vanish. The equal gains r on the remaining entries cancel in (iii). □

2. The identifiable reference on n qubits

Proof of Corollary 2. We first show that the lifted path is admissible. Take $\eta = 0$ and, for $|\theta| \leq \theta_{\max}$, the lifted path

$$\begin{aligned} \mathcal{L}_\theta &= \mathcal{L}_\theta^{\mathsf{A}} \otimes \mathrm{id}_{\mathsf{E}} + \mathrm{id}_{\mathsf{A}} \otimes \mathcal{L}_{\mathsf{E}}, \\ A_\theta = S_\theta\mathcal{D}_r \otimes A_{\mathsf{E}}, &\qquad B_\theta = \mathcal{D}_r S_\theta^{-1} \otimes B_{\mathsf{E}}, \end{aligned} \tag{L3}$$

with $\mathcal{L}_\theta^{\mathsf{A}}$ the active generator of Eq. (H1). Since $\theta_{\max} < .01$, it is physical by Appendix G. By Lemma 7(i), its canonical coefficients are the embedded data of its summands, giving target h_θ of Eq. (H2). Equations (H7) and (H9), with ε replaced by ε_{A}, make the active SPAM channels CPTP with budget at most $15\varepsilon_{\mathsf{A}}/32$, so Lemma 6(i) bounds the lifted budget by $15\varepsilon_{\mathsf{A}}/32 + \varepsilon_{\mathsf{E}} < \varepsilon$. The path lies in $\mathfrak{M}_\varepsilon^{\mathrm{L2}}$. Its active Kossakowski matrix has trace $.62 + .15\theta^2$, and the strength estimate at the end of Appendix G gives $g_{\mathsf{A}} \leq |h_\theta| + 8\operatorname{Tr} C_\theta < 5.07$; by Lemma 6(v), the path obeys every $\gamma \geq 6$ that also bounds the local strength of the spectator generator.

We next prove the lower bound. For each setting, Lemma 6(ii)–(iii) reduces the relative entropy to that of the active setting s_{A}, an allowed two-qubit experiment for the active reference, path, and SPAM channels. Equations (H13)–(H18) therefore hold with ε replaced by ε_{A}: outcome changes are at most $32K\theta^2$, active outcome probabilities are at least $\varepsilon_{\mathsf{A}}/64$, and the per-shot relative entropy is at most $K_{\mathrm{stat}}\theta^4$ with $K_{\mathrm{stat}} = 26.2144/\varepsilon_{\mathsf{A}}$. Let the history H_{i-1} contain all earlier settings and active and spectator outcomes. The policy kernel is common to both models given H_{i-1}, so Eq. (H19) bounds the N-shot relative entropy by $NK_{\mathrm{stat}}\theta^4$. The proof of Eq. (H20), with $\theta_{\max} = \varepsilon_{\mathsf{A}}/100$ and this K_{stat}, gives Eq. (16) with ε replaced by ε_{A}.

Next, for every candidate in $\mathfrak{M}_\varepsilon^{\mathrm{L2}}$, Lemma 7 supplies a physical reduced generator, the target h as its ZZ coefficient, readout gain ratios in $[l, l^{-1}]$, and the reference pair block $\mathcal{L}_0^{\mathsf{A}}$. These are the hypotheses of Eqs. (I14)–(I18), so $|h - h_0| \leq F_\varepsilon(\delta)$ whenever $d_{23}(G^{\mathsf{A}}, G_0^{\mathsf{A}}) \leq \delta$, with $l = 1 - \varepsilon$; $F_\varepsilon(0) = 0$ proves identification from the 23 pair entries. Conversely, Eq. (I19) and Lemma 6(iv) give $G_\theta - G_0 = -16K\theta^2\,\Pi_0 \otimes \mathrm{id}_{\mathsf{E}}$, so both d_{23} and the full maximum-entry distance equal $16K\theta^2$. For $0 < \delta \leq 16K\theta_{\max}^2$, the choice $\theta = \sqrt{\delta/(16K)}$ and Eq. (H3) give a candidate with $|h - h_0| \geq \sqrt{\delta}/80$.

For the upper rate, consider the class $\mathfrak{M}_{\varepsilon,\gamma}^{\mathrm{L2}}$, with γ admitting the lifted reference. The estimator in Appendix C applies to n-qubit physical two-local generators. The 23 pair responses and 15 calibrations, the derivative bound Eq. (C10), and the target protection of Lemma 7(ii) are independent of the number of spectators. The interval construction and Eqs. (I21)–(I24) of Appendix I then hold verbatim with the n-independent δ_N of Eq. (I23), giving Eq. (17). For $n = 2$ and $\varepsilon_{\mathsf{A}} = \varepsilon$, all statements and constants are those of Theorem 2. □

3. The crossover with four additional matrix elements in the two-local class

a. Upper bound on the modulus. For every candidate in $\mathfrak{M}_\varepsilon^{\mathrm{L2}}$, Lemma 7 gives a physical two-qubit generator $\mathcal{L}_{\mathsf{A}}$ with Kossakowski matrix $J \succeq 0$ and the same target h. Its generator in the readout gauge is $G^{\mathsf{A}} = \bar{B}_{\mathsf{A}}\mathcal{L}_{\mathsf{A}}\bar{B}_{\mathsf{A}}^{-1}$ with gain ratios in $[l, l^{-1}]$. At the lifted reference, $G_\eta^{\mathsf{A}} = \mathcal{L}_\eta^{\mathsf{A}}$. The upper-bound proof of Theorem 6 uses these properties through Walsh inversion of the fifteen diagonals, positive minors of the Kossakowski matrix, inversion of the entries with exchanged indices, and Lemma 4. Applying those inequalities with $l = 1 - \varepsilon$ gives

$$|h - h_0| \leq C_\varepsilon \min\{\sqrt{\delta}, \delta/|\eta|\}$$

for $d_{27}(G^{\mathsf{A}}, G^{\mathsf{A}}_\eta) \le \delta$ in the theorem's uniform local domain. Constraining all entries of G implies the pair constraint, so the same bound applies.

b. Physical alternatives and their strength. Lift the active path $S_\theta \mathcal{L}^{\mathsf{A}}_\eta S_\theta^{-1} + 16 q_{\eta,\theta}(\mathcal{D} - \mathrm{id})$, where $q_{\eta,\theta} = .6(\theta^2 + |\eta\theta|)$, with the SPAM channels of Eq. (L3). Lemma 5 proves positivity for $|\eta|, |\theta| \le .01$; the boundary argument above applies for $|\theta| \le \theta_{\max} = \varepsilon_{\mathsf{A}}/100$. The Kossakowski diagonal is the reference diagonal plus $q_{\eta,\theta}$, so $\operatorname{Tr} C = .62 + 15 q_{\eta,\theta} \le .6218$. The Hamiltonian is $h_\theta ZZ/2$ with $|h_\theta| < .101$ by Eq. (19). The strength estimate of Eq. (G9), applied to this Kossakowski matrix and Hamiltonian, bounds the completely bounded norm of the Heisenberg-picture generator by $|h_\theta| + 8 \operatorname{Tr} C < 5.076 < 6$, and the conclusion drawn from Lemma 6(v) for $\eta = 0$ holds for this path as well.

For the matching lower bound, Eq. (K34) and Lemma 6(iv) give

$$G_\theta - G_\eta = -16 q_{\eta,\theta} \Pi_0 \otimes \mathrm{id}_{\mathsf{E}}.$$

Both pair and full entry distances equal $16 q_{\eta,\theta}$, and the canonical target is unchanged by the spectator lift. The root construction and bounds in Eqs. (K35)–(K37), with $\theta_{\max} = \varepsilon_{\mathsf{A}}/100$, therefore give the lower constant $.00485/9.6$ on $0 < \delta \le 9.6(\varepsilon_{\mathsf{A}}/100)^2$. The 23 observed reference entries are identical for all η and the candidate class is fixed. Their compatible target sets therefore coincide with those at $\eta = 0$, whose modulus is $\Theta(\sqrt{\delta})$ by Corollary 2. This proves Theorem 3.

c. Confidence widths. At each adaptive setting, Lemma 6(ii)–(iii) cancels the spectator law. The active mixing rate $1/5$ of Eq. (K41) and the lower bound $\varepsilon_{\mathsf{A}}/64$ on each active outcome probability give Proposition 4 with ε replaced by ε_{A}.

For the upper width bound, the 27 pair responses have output support at most two. The derivative and error bounds for the entries of G of Appendix K therefore apply under the local norm bound. Lemma 7(ii)–(iii) preserves the global target. Its eight-entry projection and Eq. (M7) give $|h| \le \gamma$, so the clipping bound $H_* = 2\gamma$ in Proposition 5 is valid. The same inclusion and failure-probability argument gives the lifted upper bound with $\delta_N = O_{\varepsilon,\gamma,\alpha}(N^{-1/2}(\log N)^{5/2})$. Every constant is independent of n.

Appendix M: Constraint from four additional matrix elements and construction checks

This appendix derives the Kossakowski constraint used to compute the intervals, bounds the target under the common local norm bound, and checks the physical constructions. The references have Kossakowski matrix C_η, target $h_0 = 0.1$, and SPAM channels $A_0 = B_0 = \mathcal{D}_{79/80}$.

1. Kossakowski constraint from four additional matrix elements

Let s_D and s_0 be the simultaneous derivative and calibration error allowances. The interpolation bias β_p and the gain lower bound $l = 1 - \varepsilon$ give the entrywise error bound in Eq. (C23),

$$\delta = \frac{s_D + \beta_p}{l} + \frac{2\gamma s_0}{l^2}. \tag{M1}$$

Character inversion of the fifteen observed generator diagonals gives upper bounds $d_P = \max\{0, \widehat{C}_{PP} + \delta\}$ on the diagonal Kossakowski coefficients of every compatible candidate, by Eq. (C24).

For the four additional entries, define

$$\begin{aligned} U &= \widehat{G}_{YZ,IX} + \widehat{G}_{YX,IZ}, \\ V &= \widehat{G}_{IX,YZ} + \widehat{G}_{IZ,YX}. \end{aligned} \tag{M2}$$

A candidate readout has the gain ratio $r_B = b_{12}/b_2 \in [l, l^{-1}]$. Undoing its gauge transformation gives the empirical canonical functional

$$\widehat{\Phi}(r_B) = \frac{U/r_B - V r_B}{8}. \tag{M3}$$

Each of the four entries has error at most δ. Their contribution to the functional error is at most $\delta(r_B + r_B^{-1})/4 \le \delta(l + l^{-1})/4$. Meanwhile, Eq. (28) and Kossakowski matrix positivity imply

$$\begin{aligned} |\Phi(L)| &\le |C_{XX,ZZ}| + |C_{XZ,ZX}| \\ &\le \sqrt{d_{XX} d_{ZZ}} + \sqrt{d_{XZ} d_{ZX}}. \end{aligned} \tag{M4}$$

Every compatible candidate must therefore satisfy

$$\left|\widehat{\Phi}(r_B)\right| \le \sqrt{d_{XX} d_{ZZ}} + \sqrt{d_{XZ} d_{ZX}} + \frac{\delta(l + l^{-1})}{4}. \tag{M5}$$

This inequality holds for arbitrary complex Kossakowski matrices and uses the measured entries, their errors, and the candidate gain ratio. The reference parameter η enters the precision bound through Eq. (30).

The zero-time data supply a further necessary condition. Put

$$q_{\min} = \max\{l, \min_Q(\widehat{q}_Q - s_0)\}. \tag{M6}$$

Complete positivity and the SPAM budget give $l \le a_Q, b_Q \le 1$ and $a_Q b_Q \ge l$ (Appendix A). Compatibility with the calibration data also requires $|a_Q b_Q - \widehat{q}_Q| \le s_0$, hence $a_Q b_Q \ge \max\{l, \widehat{q}_Q - s_0\} \ge q_{\min}$. Since $a_Q, b_Q \le 1$, both gains are at least $q_{\min}$ and each readout support ratio lies in $[q_{\min}, q_{\min}^{-1}]$.

The numerical procedure evaluates this condition and the original seven Kossakowski constraints over boxes in that ratio square. It replaces $l + l^{-1}$ in the bounds on canonical coefficients and on Φ by $q_{\min} + q_{\min}^{-1}$ and intersects the result with the enclosure over $[l, l^{-1}]^2$. Both

enclosures contain the target on the common error event. Rational interval arithmetic gives outward bounds for every target, Kossakowski coefficient, and square-root calculation. A box is discarded only when its entire enclosure violates a necessary physical constraint. Each bisection covers its parent, and every remaining box contributes to the target hull at the computation limit. Thus the true calibration ratios remain in the search and the returned interval contains the target on that event. The remaining boxes form an outer relaxation of the physically feasible set, and the smallest interval containing their target enclosures gives the reported width.

2. Target bound under the common local norm bound

The local norm bound γ of Eq. (C1) also bounds the two-qubit canonical target. Its eight-entry projection is linear in the generator, and its absolute weights sum to one. Each position pairs Paulis that differ on both sites. By Pauli orthogonality, a term of Eq. (C1) acting on one site therefore has zero entry there. Duality and Hölder's inequality bound every other term by $|(\mathcal{L}_Z)_{R,Q}| \le d^{-1}\|Q\|_1\|\mathcal{L}_Z^\dagger(R)\|_\infty \le g_Z$, giving

$$|h_{ZZ}| \le \sum_{Z \supseteq \{1,2\}} g_Z \le \gamma. \tag{M7}$$

3. Checks of the physical constructions

a. Physical paths and assumptions on the Kossakowski matrix. Figure 1(b) checks ten signed path values with magnitudes from 10^{-5} to 10^{-3} at $\varepsilon = 0.1$. Forty product-input, measurement, and local-control configurations per value give 400 checks, including zero duration and total durations from 0.01 to 100 in the reference time unit. Calculations with the full superoperator verify physicality of the Kossakowski matrix and SPAM channels, canonical reconstruction, and Eq. (21). The fitted logarithmic slopes for the target change are 0.9995 on the positive-θ branch and 1.0005 on the negative branch, and the generator-change slope is 2 on both.

Figure 1(c) fixes the record and varies only the assumption of a real Kossakowski matrix for every candidate. Nine entrywise tolerances from 10^{-8} to 10^{-4} give 18 deterministic outer intervals, all containing $h_0 = 0.1$. Each search starts from $[l, l^{-1}]^2$ with $l = 0.9$, bisects a widest surviving box along its longest side, and stops at target half-width δ or a budget of 255 evaluated boxes. All 18 runs reach that budget. Arithmetic is rational, with square roots bounded upward on a 2^{-80} grid and reported floating-point endpoints rounded outward. The half-width slopes of these fixed-budget outer enclosures are 0.501 for complex Kossakowski matrices and 0.993 under the assumption of a real Kossakowski matrix.

b. Correlation-dependent precision. Figure 2 uses 91 logarithmically spaced distances from 10^{-11} to 9.6×10^{-6} for each $\eta \in \{0, 10^{-5}, 10^{-4}, 10^{-3}, 10^{-2}\}$. The roots of Eq. (K35) obey $0 < \theta \le \sqrt{\delta/9.6} \le 10^{-3} = \varepsilon/100$, within the domains for the positive correction and physical SPAM channels. The 455 constructed physical models exhibit the square-root branch at $\eta = 0$ and a transition toward linear dependence at nonzero η. Theorem 3 supplies the matching upper bound over all compatible physical models.

Further calculations with both signs of the correlation and of the gauge parameter, including zero and long durations, confirm positivity, the SPAM channels, canonical reconstruction, and all 27 entries. Calculations with random generators, including nonunital ones, confirm the functional Φ of Eq. (28).

Appendix N: Quantum-processor measurements and analysis

The native data comprise three devices with three selected pairs per device. Table II collects the acquisition and resampling settings. Runs of idle evolution disable dynamical decoupling. The injected-rotation measurements were acquired separately, with their own background noise.

For idle-evolution data in the computational basis, bit strings are ordered as control then target. The count of target outcomes equal to 1 sums both control outcomes. For each pair, time, and neighbor preparation c, we divide by the number of shots per configuration to obtain $\hat{p}_1^{(c)}$ without postselection or readout error mitigation. Figure 3(c) shows the observed contrasts $|\hat{p}_1^{(0)} - \hat{p}_1^{(1)}|$ for all 90 pair–time combinations. The largest is 6.0×10^{-4}, from counts of 61 and 37 target outcomes equal to 1 on the second Pittsburgh pair at zero idle time.

a. Frequency estimator for idle evolution. For prepared control state c, retain shots whose final control outcome equals c. Let m be the measured fraction of target outcomes equal to 0 among the M retained shots. A column-stochastic 2×2 readout assignment matrix R for the target, estimated by pooling the computational-basis calibration counts over the control preparations, gives $v = R^{-1}(m, 1-m)^T$. Set $v_s^+ = \max\{v_s, 0\}$ and $p_0 = v_0^+/(v_0^+ + v_1^+)$. The estimator uses the effective count $k = \mathrm{round}(Mp_0)$ and probability $\widetilde{p}_0 = k/M$. This selection fixes the final control state.

For basis $b \in \{X, Y\}$, define

$$z_c(t) = 2\widetilde{p}_{0,cX}(t) - 1 + i[2\widetilde{p}_{0,cY}(t) - 1],$$
$$r(t) = z_1(t)z_0(t)^*, \qquad P(f) = \left|\sum_t r(t)e^{-2\pi i f t}\right|. \tag{N1}$$

Times are in seconds. We maximize $P(f)$ over 40,001 equally spaced frequencies from -260 to 260 kHz, with

TABLE II. Sampling settings for the processor measurements. Native configurations are indexed by pair, prepared control state, and idle time, with the probe basis specified separately. Numbers of shots are before postselection. Matched totals are per configuration for $n = 3$ and $n = 4$, respectively, and apply to the visibility comparison; angle recovery uses the original injection counts. The idle-time grid is $0, 1, 2, 4, 7, 11, 17, 25, 35, 47\,\mu$s; the prediction check excludes $2, 7, 25\,\mu$s from fitting.

Analysis	Scope	Counts used	Resampling
Idle evolution, populations	9 pairs, 10 times	40,000 shots per configuration	None
Idle evolution, Ramsey	9 pairs, X, Y bases	8000 shots per basis/configuration	50,000 bootstrap resamples
Injected visibility	$n = 3, 4$; 18 cases	Matched 25,000 / 50,000 shots	1000 random subsamples
Recovery of injected angles	66 estimates	250,000 shots per estimate	4000 shot resamples
Joint-model check	9 pairs	Probe and calibration counts	199 refits per pair

spacing $\Delta f = 13$ Hz. For an interior maximum at f_k, the refined estimate is

$$\widehat{f} = f_k + \frac{\Delta f[P(f_{k-1}) - P(f_{k+1})]}{2[P(f_{k-1}) - 2P(f_k) + P(f_{k+1})]}. \tag{N2}$$

The grid value is retained at an endpoint or when the absolute denominator is at most 10^{-18}. The phasors are neither normalized nor weighted. Each of 50,000 resamples independently redraws the retained raw counts from Binomial(M, m) and repeats the readout inversion, clipping, rounding, and fit, holding the fitted calibration and retained shot totals fixed. The root-mean-square deviation of the fitted frequencies from their resampling mean gives the plotted standard error. The random seed is 20260814, with devices ordered Boston, Kingston, and Pittsburgh.

The injected comparison pairs equal rotation magnitudes and draws random subsamples without replacement of the counts in the additional basis within each preparation to match the number of shots in the computational basis. Figure 4 reports the median TV in the additional basis over the subsamples in Table II and its ratio to the observed TV in the computational basis. This ratio quantifies the increase in visibility relative to the nonzero TV in the computational basis.

b. Angle recovery. Table III identifies the six acquisition groups. Each is repeated on all three devices, and the two signs at each angle provide one estimate. Within each sign, counts are pooled over the computational preparations u with their original shot allocations. Normalization uses the nominal preparation polarizations of Table III. Because the shot allocations are integers, the realized pooled polarizations differ from these values by at most 0.12%. Normalizing by the realized values instead gives a pooled slope of 0.9823 and a median absolute angle error of 0.0182 rad, so the values reported in Sec. VII are unchanged at their stated precision. A recorded bit string $u_0 \cdots u_{n-1}$ labels logical qubits from left to right, so the Y_j marginal weights outcomes by $(-1)^{u_j}$. The difference of these marginals gives $\Delta\langle Y_j\rangle$ in Eq. (32).

The estimates use $\widehat{\psi} = \arcsin[-\Delta\langle Y_j\rangle/(2\langle Z_j\rangle_{\rm in})]$, with the argument clipped to $[-1, 1]$, on the programmed small-angle branch. No readout error mitigation is applied to these angle estimates. Each of 4000 bootstrap replicates independently redraws the full outcome multinomial within each preparation and sign at its original number of shots, then repeats pooling and inversion (random seed 20260818). The sample standard deviation gives the angle standard error s_i. For $x_i = \sin\psi_i$, $y_i = \sin\widehat{\psi}_i$, and weights $w_i = (s_i \cos\psi_i)^{-2}$, the reported slope of the weighted fit through the origin and standard error are

$$\widehat{a} = \frac{\sum_i w_i x_i y_i}{\sum_i w_i x_i^2}, \qquad s_a = \left(\sum_i w_i x_i^2\right)^{-1/2}. \tag{N3}$$

The resampling uncertainty is conditional on the physical preparation and fixed device response.

c. Frequency sensitivity. The sensitivity analysis for idle evolution compares all shots with postselected shots, and raw target probabilities with probabilities after readout error mitigation. The time grid, signed periodogram, and frequency search range stay fixed. Figure 5(a) shows the resulting changes in fitted conditional frequencies from the same counts. Relating these changes to a Hamiltonian coefficient requires a trajectory and measurement model.

1. Joint trajectory and calibration check

Write $p = (p_0, p_1)^T$ for control populations and $w = (w_0, w_1)^T$ for unnormalized target coherences, with the convention that their real and imaginary parts give the target X and Y expectations within each control block. Here u and d are the control excitation and relaxation rates, k is the target-coherence decay rate, and ω_s is the target angular frequency conditional on control state s. The model is

$$\dot{p} = \begin{pmatrix} -u & d \\ u & -d \end{pmatrix} p, \tag{N4}$$

$$\dot{w} = \begin{pmatrix} i\omega_0 - k - u & d \\ u & i\omega_1 - k - d \end{pmatrix} w. \tag{N5}$$

TABLE III. Acquisition groups for all 66 injected-angle estimates in Fig. 4(c). Every group uses rotations generated by X_0, X_j and measures Y_0Y_j; the remaining qubits are measured in Z. Each angle is repeated on three devices. A/C and B/E were acquired separately. The nominal preparation polarizations used for normalization are given to ten decimal places. Each sign uses 125,000 shots, allocated over preparations $u = 0, \ldots, 2^n - 1$ in the order below; an angle estimate uses both signs.

Group	n	j	Programmed angles (rad)	$\langle Z_j \rangle_{\text{in}}$	Estimates
A	3	1	$0.1, 0.2, 0.3$	$+0.0546121323$	9
B	4	1	$0.1, 0.2, 0.3$	$+0.0968723995$	9
C	3	1	$0.1, 0.2, 0.3, 0.4$	$+0.0546121323$	12
D	3	2	$0.1, 0.2, 0.3, 0.4$	-0.0152328537	12
E	4	1	$0.1, 0.2, 0.3, 0.4$	$+0.0968723995$	12
F	4	2	$0.1, 0.2, 0.3, 0.4$	$+0.0475325868$	12

$n = 3$ 14148, 20038, 12801, 16576, 17204, 14523, 17396, 12314

$n = 4$ 7450, 10551, 6740, 8728, 9059, 7647, 9160, 6484, 10716, 9252, 7319, 7798, 6001, 4795, 7498, 5802

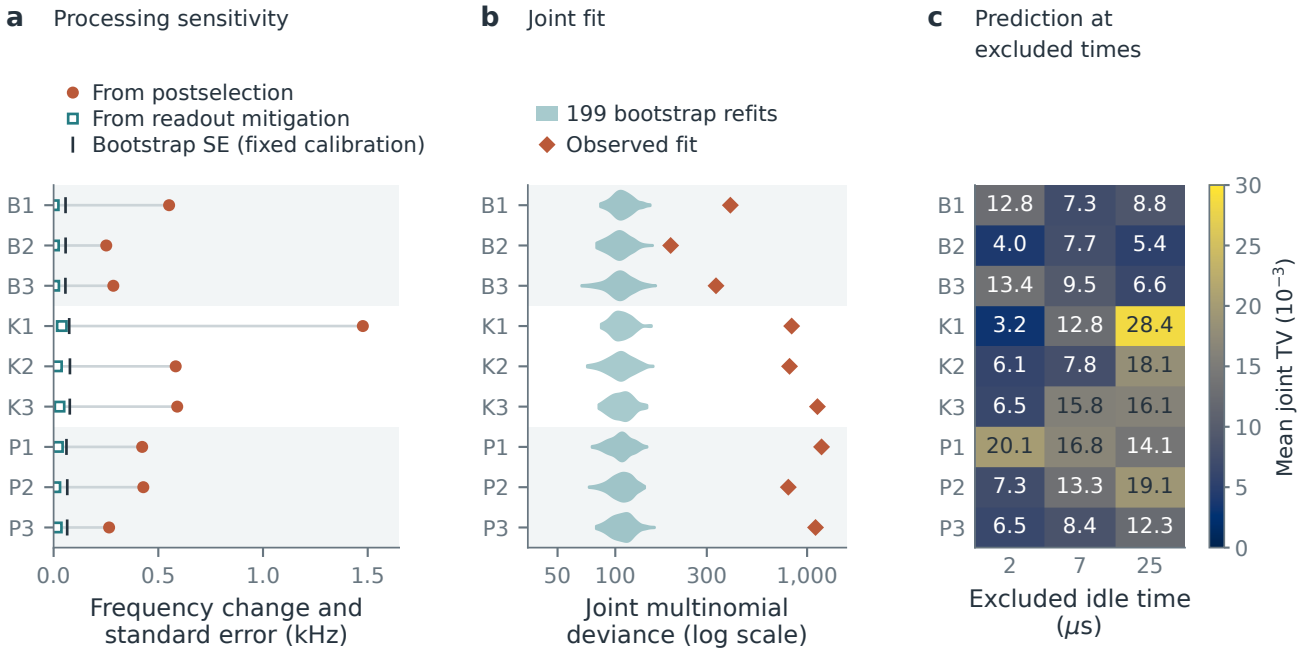


FIG. 5. Processing sensitivity and model diagnostics for Ramsey responses during idle evolution. Pair labels follow Fig. 3. (a) Absolute changes in fitted frequency from postselection on the final control outcome with readout mitigation held fixed (filled circles), and from readout mitigation within postselected data (open squares). Connecting lines pair the two changes, and ticks show the bootstrap standard errors of Fig. 3(b) for scale. (b) Observed deviances from the joint probe and calibration fit (diamonds) and distributions from 199 parametric-bootstrap refits per pair. The axis is logarithmic. (c) Mean total-variation distance (TV) between measured and predicted joint-outcome distributions at three times excluded from fitting, averaged over preparations and quadratures. Cell labels are in units of 10^{-3}. Fits and initial values use the other seven times and calibration counts. The measured outcome frequencies retain shot noise.

For prepared control label c, the initial population is $p_1 = s_c$ and $w_s = a_c e^{i\phi_c} p_s$. Ideal joint outcome probabilities are $(p_s \pm \operatorname{Re} w_s)/2$ for X and $(p_s \pm \operatorname{Im} w_s)/2$ for Y. A column-stochastic 4×4 assignment matrix maps these to measured probabilities. Its twelve free logits are constrained by the four computational-calibration distributions in the same multinomial likelihood, which fits the raw joint counts directly.

We minimize joint multinomial deviance using bounded multistart least squares. Frequency parameters $f_0 = \omega_0/(2\pi)$ and $\Delta f = (\omega_1 - \omega_0)/(2\pi)$ are restricted to $[-260, 260]$ and $[-80, 80]$ kHz. Rates (d, u, k) lie

in $[0, 0.2] \times [0, 0.05] \times [0, 0.2]$ in inverse microseconds; $s_0 \in [0, 0.5]$, $s_1 \in [0.5, 1]$, $a_c \in [0, 1]$, and $\phi_c \in [-\pi, \pi]$. Off-diagonal assignment logits relative to each diagonal entry lie in $[-20, 3]$. These parameter ranges define the tested model.

For each pair, 199 parametric-bootstrap simulations independently sample the probe and calibration multinomials from the fitted model at their original numbers of shots and jointly refit all 23 parameters. The largest simulated deviances range from 142 to 163, below their corresponding observed values. The simulations assume independent multinomial samples, a time- and basis-independent assignment matrix, and the specified preparation model, and calibration circuits constrain the combined preparation and measurement response.

We also fit the model using seven times and the calibration counts, then compare its predictions with measurements at the excluded times $2, 7, 25\,\mu$s. Frequencies in kHz are converted to angular frequencies in rad/μs using $\omega_0 = 2\pi\, 10^{-3} f_0$, with the same conversion for frequency differences.

2. Exact equivalence for inputs diagonal in the control basis

This protocol-specific calculation uses the known distinction between coherent phases and phases from imaginary Kossakowski coefficients [58]. Here tensor factors are ordered control then target. Set $A = ZI$, $B = IZ$, and consider a Hamiltonian that commutes with A and contains $hAB/2$, and a canonical Kossakowski block

$$C_Z = \begin{pmatrix} \gamma_c & a + ib \\ a - ib & \gamma_t \end{pmatrix} \succeq 0 \tag{N6}$$

on (A, B), together with control raising and lowering jumps $\sqrt{u}\,|1\rangle\langle 0| \otimes I$ and $\sqrt{d}\,|0\rangle\langle 1| \otimes I$. Let $\mathcal{S} = \{X : [A, X] = 0\}$, so $X = \sum_s E_s \otimes X_s$ with $E_s = |s\rangle\langle s|$, and write $H = \sum_s E_s \otimes H_s$. Within control block s, $AX = z_s X$ with $z_s = (-1)^s$. Control dephasing and the real off-diagonal Kossakowski term vanish on $\mathcal{S}$, since $AXA = X$ and $AXB + BXA = \{AB, X\}$, while

$$ib(AXB - BXA) = -ibz_s[Z, X_s]. \tag{N7}$$

The raising and lowering jumps transfer whole target blocks, so on $\mathcal{S}$

$$\begin{aligned}(\mathcal{L}X)_s = & -i[H_s + bz_s Z, X_s] + \gamma_t(ZX_sZ - X_s) \\ & - z_s(uX_0 - dX_1).\end{aligned} \tag{N8}$$

The generator preserves $\mathcal{S}$. Its restriction depends on the interaction only through $r = h + 2b$: the term $hAB/2$ contributes $z_s hZ/2$ to H_s, and the other parts of H_s do not involve h or b. Equal restrictions have equal powers on $\mathcal{S}$ and hence equal exponential series. They therefore give equal propagated states from every input in $\mathcal{S}$, including for noncommuting generator components. Any common terminal measurement then gives equal joint probabilities.

For $\gamma_t > 0$, fix r and choose any finite h_*. Taking

$$b_* = (r - h_*)/2, \qquad a_* = 0, \qquad \gamma_c^* = b_*^2/\gamma_t \tag{N9}$$

gives a positive semidefinite rank-one Kossakowski matrix and the same restricted evolution. An explicit jump is $L_* = (b_*/\sqrt{\gamma_t})A - i\sqrt{\gamma_t}B$. For the Hamiltonian $(\omega_c A + \omega_t B + hAB)/2$, $H_s + bz_s Z = \omega_c z_s/2 + (\omega_t + z_s r)Z/2$. Taking traces of the block equation for $X = \rho$ against I and $F = 2|0\rangle\langle 1|$, with $[F, Z] = -2F$ and $ZFZ = -F$, gives the trajectory model of Appendix N 1 with $p_s = \operatorname{Tr}\rho_s$, $w_s = \operatorname{Tr}(F\rho_s)$, $\omega_s = \omega_t + z_s r$, and $k = 2\gamma_t$, so $\gamma_c^* = (r - h_*)^2/(2k)$.

Each constructed model has finite coefficients, whereas the family over all h_* has unbounded control dephasing. If $\gamma_c \le G$ is independently imposed and $a = 0$, the construction satisfies $|h - r| \le \sqrt{2Gk}$. At $k = 0$, positivity forces $b = 0$, so this construction gives $h = r$.

The equivalence applies to actual inputs diagonal in the control basis, common SPAM channels, and intermediate operations that preserve control diagonality. Inputs with the control in a superposition can leave $\mathcal{S}$ and distinguish the generators. The exact data with trusted local controls identify the target exactly: every diagonal Kossakowski coefficient here is local, so $\xi_{ZZ} = 0$ in Eq. (A14). Numerical calculations with the full superoperator verify the record equivalence.

Appendix O: Processor diagnostics and model adequacy

1. Processing sensitivity and joint-model adequacy

For idle evolution, the joint probe counts show how the fitted response depends on postselection on the final control outcome. The selection changes quoted in Sec. VII C [Fig. 5(a)] compare frequencies of different conditional distributions estimated from the same shots. Applying readout error mitigation within the postselected data changes the frequencies by approximately 0.66–39 Hz.

Joint modeling tests the physical interpretation directly. We fit all four outcomes of both probe quadratures using all shots, together with the computational-calibration counts, with the model of Appendix N 1. Across the nine pairs, observed joint deviances range from 194 to 1190, and every value exceeds all 199 corresponding parametric-bootstrap refits, which also resample calibration counts and refit assignment parameters (Fig. 5(b)). These approximate diagnostics identify a mismatch with the tested dynamical and readout model. Panel (c) shows predictions at three held-out times. Appendix N 2 derives the physical equivalence for the protocol with inputs diagonal in the control basis and shows how probes with the control in a superposition distinguish the constructed alternatives.

[1] J. Eisert, D. Hangleiter, N. Walk, I. Roth, D. Markham, R. Parekh, U. Chabaud, and E. Kashefi, Quantum certification and benchmarking, Nat. Rev. Phys. **2**, 382 (2020).

[2] J. Carrasco, A. Elben, C. Kokail, B. Kraus, and P. Zoller, Theoretical and experimental perspectives of quantum verification, PRX Quantum **2**, 010102 (2021).

[3] V. Gebhart, R. Santagati, A. A. Gentile, E. M. Gauger, D. Craig, N. Ares, L. Banchi, F. Marquardt, L. Pezzè, and C. Bonato, Learning quantum systems, Nat. Rev. Phys. **5**, 141 (2023).

[4] F. Yan, P. Krantz, Y. Sung, M. Kjaergaard, D. L. Campbell, T. P. Orlando, S. Gustavsson, and W. D. Oliver, Tunable coupling scheme for implementing high-fidelity two-qubit gates, Phys. Rev. Appl. **10**, 054062 (2018).

[5] B. K. Mitchell, R. K. Naik, A. Morvan, A. Hashim, J. M. Kreikebaum, B. Marinelli, W. Lavrijsen, K. Nowrouzi, D. I. Santiago, and I. Siddiqi, Hardware-efficient microwave-activated tunable coupling between superconducting qubits, Phys. Rev. Lett. **127**, 200502 (2021).

[6] D. M. Zajac, A. J. Sigillito, M. Russ, F. Borjans, J. M. Taylor, G. Burkard, and J. R. Petta, Resonantly driven CNOT gate for electron spins, Science **359**, 439 (2018).

[7] M. Sarovar, T. Proctor, K. Rudinger, K. Young, E. Nielsen, and R. Blume-Kohout, Detecting crosstalk errors in quantum information processors, Quantum **4**, 321 (2020).

[8] K. Rudinger, C. W. Hogle, R. K. Naik, A. Hashim, D. Lobser, D. I. Santiago, M. D. Grace, E. Nielsen, T. Proctor, S. Seritan, S. M. Clark, R. Blume-Kohout, I. Siddiqi, and K. C. Young, Experimental characterization of crosstalk errors with simultaneous gate set tomography, PRX Quantum **2**, 040338 (2021).

[9] X.-L. Qi and D. Ranard, Determining a local Hamiltonian from a single eigenstate, Quantum **3**, 159 (2019).

[10] E. Bairey, I. Arad, and N. H. Lindner, Learning a local Hamiltonian from local measurements, Phys. Rev. Lett. **122**, 020504 (2019).

[11] A. Anshu, S. Arunachalam, T. Kuwahara, and M. Soleimanifar, Sample-efficient learning of interacting quantum systems, Nat. Phys. **17**, 931 (2021).

[12] J. Zhang and M. Sarovar, Quantum Hamiltonian identification from measurement time traces, Phys. Rev. Lett. **113**, 080401 (2014).

[13] A. Zubida, E. Yitzhaki, N. H. Lindner, and E. Bairey, Optimal short-time measurements for Hamiltonian learning (2021), arXiv:2108.08824 [quant-ph].

[14] D. Hangleiter, I. Roth, J. Fuksa, J. Eisert, and P. Roushan, Robustly learning the Hamiltonian dynamics of a superconducting quantum processor, Nat. Commun. **15**, 9595 (2024).

[15] K. Siva, G. Koolstra, J. Steinmetz, W. P. Livingston, D. Das, L. Chen, J. M. Kreikebaum, N. J. Stevenson, C. Jünger, D. I. Santiago, I. Siddiqi, and A. N. Jordan, Time-dependent Hamiltonian reconstruction using continuous weak measurements, PRX Quantum **4**, 040324 (2023).

[16] N. Wiebe, C. Granade, C. Ferrie, and D. G. Cory, Hamiltonian learning and certification using quantum resources, Phys. Rev. Lett. **112**, 190501 (2014).

[17] J. Wang, S. Paesani, R. Santagati, S. Knauer, A. A. Gentile, N. Wiebe, M. Petruzzella, J. L. O'Brien, J. G. Rarity, A. Laing, and M. G. Thompson, Experimental quantum Hamiltonian learning, Nat. Phys. **13**, 551 (2017).

[18] H.-Y. Huang, Y. Tong, D. Fang, and Y. Su, Learning many-body Hamiltonians with Heisenberg-limited scaling, Phys. Rev. Lett. **130**, 200403 (2023).

[19] D. Stilck França, L. A. Markovich, V. V. Dobrovitski, A. H. Werner, and J. Borregaard, Efficient and robust estimation of many-qubit Hamiltonians, Nat. Commun. **15**, 311 (2024).

[20] H.-Y. Hu, M. Ma, W. Gong, Q. Ye, Y. Tong, S. T. Flammia, and S. F. Yelin, Ansatz-free Hamiltonian learning with Heisenberg-limited scaling, PRX Quantum **6**, 040315 (2025).

[21] W. Yu, J. Sun, Z. Han, and X. Yuan, Robust and efficient Hamiltonian learning, Quantum **7**, 1045 (2023).

[22] E. Bairey, C. Guo, D. Poletti, N. H. Lindner, and I. Arad, Learning the dynamics of open quantum systems from their steady states, New J. Phys. **22**, 032001 (2020).

[23] L. Pastori, T. Olsacher, C. Kokail, and P. Zoller, Characterization and verification of Trotterized digital quantum simulation via Hamiltonian and Liouvillian learning, PRX Quantum **3**, 030324 (2022).

[24] T. Olsacher, T. Kraft, C. Kokail, B. Kraus, and P. Zoller, Hamiltonian and Liouvillian learning in weakly-dissipative quantum many-body systems, Quantum Sci. Technol. **10**, 015065 (2025).

[25] S. T. Flammia and J. J. Wallman, Efficient estimation of Pauli channels, ACM Trans. Quantum Comput. **1**, 3 (2020).

[26] A. Erhard, J. J. Wallman, L. Postler, M. Meth, R. Stricker, E. A. Martinez, P. Schindler, T. Monz, J. Emerson, and R. Blatt, Characterizing large-scale quantum computers via cycle benchmarking, Nat. Commun. **10**, 5347 (2019).

[27] R. Harper, S. T. Flammia, and J. J. Wallman, Efficient learning of quantum noise, Nat. Phys. **16**, 1184 (2020).

[28] R. Harper and S. T. Flammia, Learning correlated noise in a 39-qubit quantum processor, PRX Quantum **4**, 040311 (2023).

[29] E. van den Berg, Z. K. Minev, A. Kandala, and K. Temme, Probabilistic error cancellation with sparse Pauli–Lindblad models on noisy quantum processors, Nat. Phys. **19**, 1116 (2023).

[30] E. T. Hockings, A. C. Doherty, and R. Harper, Scalable noise characterization of syndrome-extraction circuits with averaged circuit eigenvalue sampling, PRX Quantum **6**, 010334 (2025).

[31] G. O. Samach, A. Greene, J. Borregaard, M. Christandl, J. Barreto, D. K. Kim, C. M. McNally, A. Melville, B. M. Niedzielski, Y. Sung, D. Rosenberg, M. E. Schwartz, J. L. Yoder, T. P. Orlando, J. I.-J. Wang, S. Gustavsson, M. Kjaergaard, and W. D. Oliver, Lindblad tomography of a superconducting quantum processor, Phys. Rev. Appl. **18**, 064056 (2022).

[32] Y. Liu, J. R. Seddon, T. Kohler, E. Onorati, and T. S. Cubitt, Robust Lindbladian estimation for quantum dynamics (2025), arXiv:2507.07912 [quant-ph].

[33] E. van den Berg, B. Mitchell, K. X. Wei, and M. Malekakhlagh, Large-scale Lindblad learning from time-series data (2025), arXiv:2512.08165 [quant-ph].

[34] S. D. Sinha, Efficient and SPAM-robust ansatz-free Lindbladian learning (2026), B.S. thesis, California Institute of Technology, arXiv:2606.20706 [quant-ph].

[35] D. Burgarth and K. Yuasa, Quantum system identification, Phys. Rev. Lett. **108**, 080502 (2012).

[36] D. Burgarth and K. Yuasa, Identifiability of open quantum systems, Phys. Rev. A **89**, 030302 (2014).

[37] S. T. Merkel, J. M. Gambetta, J. A. Smolin, S. Poletto, A. D. Córcoles, B. R. Johnson, C. A. Ryan, and M. Steffen, Self-consistent quantum process tomography, Phys. Rev. A **87**, 062119 (2013).

[38] R. Blume-Kohout, J. K. Gamble, E. Nielsen, K. Rudinger, J. Mizrahi, K. Fortier, and P. Maunz, Demonstration of qubit operations below a rigorous fault tolerance threshold with gate set tomography, Nat. Commun. **8**, 14485 (2017).

[39] E. Nielsen, J. K. Gamble, K. Rudinger, T. Scholten, K. Young, and R. Blume-Kohout, Gate set tomography, Quantum **5**, 557 (2021).

[40] O. Di Matteo, J. Gamble, C. Granade, K. Rudinger, and N. Wiebe, Operational, gauge-free quantum tomography, Quantum **4**, 364 (2020).

[41] S. Chen, Y. Liu, M. Otten, A. Seif, B. Fefferman, and L. Jiang, The learnability of Pauli noise, Nat. Commun. **14**, 52 (2023).

[42] S. Chen, Z. Zhang, L. Jiang, and S. T. Flammia, Efficient self-consistent learning of gate set Pauli noise, PRX Quantum **7**, 010305 (2026).

[43] E. H. Chen, S. Chen, L. E. Fischer, A. Eddins, L. C. G. Govia, B. Mitchell, A. He, Y. Kim, L. Jiang, and A. Seif, Disambiguating Pauli noise in quantum computers, PRX Quantum **7**, 033045 (2026).

[44] S. T. Flammia, S. D. Sinha, and Y. Tong, Gauge freedom and efficient algorithms for Lindbladian learning (2026), arXiv:2609.35265 [quant-ph].

[45] H. Chernoff, On the distribution of the likelihood ratio, Ann. Math. Stat. **25**, 573 (1954).

[46] S. G. Self and K.-Y. Liang, Asymptotic properties of maximum likelihood estimators and likelihood ratio tests under nonstandard conditions, J. Am. Stat. Assoc. **82**, 605 (1987).

[47] C. J. Geyer, On the asymptotics of constrained M-estimation, Ann. Stat. **22**, 1993 (1994).

[48] A. Rotnitzky, D. R. Cox, M. Bottai, and J. Robins, Likelihood-based inference with singular information matrix, Bernoulli **6**, 243 (2000).

[49] K. O. Ekvall and M. Bottai, Confidence regions near singular information and boundary points with applications to mixed models, Ann. Stat. **50**, 1806 (2022).

[50] K.-C. Li, Honest confidence regions for nonparametric regression, Ann. Stat. **17**, 1001 (1989).

[51] D. L. Donoho and R. C. Liu, Geometrizing rates of convergence, II, Ann. Stat. **19**, 633 (1991).

[52] T. T. Cai and M. G. Low, An adaptation theory for nonparametric confidence intervals, Ann. Stat. **32**, 1805 (2004).

[53] V. Gorini, A. Kossakowski, and E. C. G. Sudarshan, Completely positive dynamical semigroups of N-level systems, J. Math. Phys. **17**, 821 (1976).

[54] G. Lindblad, On the generators of quantum dynamical semigroups, Commun. Math. Phys. **48**, 119 (1976).

[55] R. Blume-Kohout, M. P. da Silva, E. Nielsen, T. Proctor, K. Rudinger, M. Sarovar, and K. Young, A taxonomy of small Markovian errors, PRX Quantum **3**, 020335 (2022).

[56] Á. Rivas, S. F. Huelga, and M. B. Plenio, Quantum non-Markovianity: characterization, quantification and detection, Rep. Prog. Phys. **77**, 094001 (2014).

[57] H.-P. Breuer, E.-M. Laine, J. Piilo, and B. Vacchini, Colloquium: Non-Markovian dynamics in open quantum systems, Rev. Mod. Phys. **88**, 021002 (2016).

[58] A. Seif, M. Hafezi, and Y.-K. Liu, Compressed sensing measurement of long-range correlated noise (2021), arXiv:2105.12589 [quant-ph].

[59] W. Hoeffding, Probability inequalities for sums of bounded random variables, J. Am. Stat. Assoc. **58**, 13 (1963).

[60] S. Sheldon, E. Magesan, J. M. Chow, and J. M. Gambetta, Procedure for systematically tuning up cross-talk in the cross-resonance gate, Phys. Rev. A **93**, 060302 (2016).

[61] A. D. Patterson, J. Rahamim, T. Tsunoda, P. A. Spring, S. Jebari, K. Ratter, M. Mergenthaler, G. Tancredi, B. Vlastakis, M. Esposito, and P. J. Leek, Calibration of a cross-resonance two-qubit gate between directly coupled transmons, Phys. Rev. Appl. **12**, 064013 (2019).

[62] E. Magesan and J. M. Gambetta, Effective Hamiltonian models of the cross-resonance gate, Phys. Rev. A **101**, 052308 (2020).

[63] Y. Pan, M. H. Tsai, W. You, H. Jiang, J. Chen, W. Zhang, I. Lyngaas, Y. Wang, and T. Liu, Identifying the sign of coherent over-rotations with logarithmically many Pauli settings (2026), arXiv:2607.21663 [quant-ph].

[64] P. Szańkowski, M. Trippenbach, and Ł. Cywiński, Spectroscopy of cross correlations of environmental noises with two qubits, Phys. Rev. A **94**, 012109 (2016).

[65] G. A. Paz-Silva, L. M. Norris, and L. Viola, Multiqubit spectroscopy of Gaussian quantum noise, Phys. Rev. A **95**, 022121 (2017).

[66] U. von Lüpke, F. Beaudoin, L. M. Norris, Y. Sung, R. Winik, J. Y. Qiu, M. Kjaergaard, D. Kim, J. Yoder, S. Gustavsson, L. Viola, and W. D. Oliver, Two-qubit spectroscopy of spatiotemporally correlated quantum noise in superconducting qubits, PRX Quantum **1**, 010305 (2020).

[67] B. Gulácsi, J. Kattemölle, and G. Burkard, Characterizing correlated noise with single-qubit operations, Phys. Rev. Res. **7**, L042067 (2025).

[68] C. Dankert, R. Cleve, J. Emerson, and E. Livine, Exact and approximate unitary 2-designs and their application to fidelity estimation, Phys. Rev. A **80**, 012304 (2009).

[69] J. J. Wallman and J. Emerson, Noise tailoring for scalable quantum computation via randomized compiling, Phys. Rev. A **94**, 052325 (2016).

[70] B. Fornberg, Generation of finite difference formulas on arbitrarily spaced grids, Math. Comput. **51**, 699 (1988).